Calculation of Reaction Rate Constants via Instanton Theory in the Canonical and Microcanonical Ensemble

Von der Fakultät Chemie der Universität Stuttgart
zur Erlangung der Würde eines
Doktors der Naturwissenschaften (Dr. rer. nat.)
genehmigte Abhandlung

Vorgelegt von

Andreas Löhle

aus Nagold

Hauptberichter	Prof. Dr. Johannes Kästner
Mitberichter	Prof. Dr. Uwe Manthe
Prüfungsvorsitzender	Prof. Dr. Joris van Slageren
Tag der mündlichen Prüfung	30. Oktober 2018

Institut für Theoretische Chemie
Universität Stuttgart

2018

Danksagung

An dieser Stelle möchte ich mich bei allen herzlich bedanken, die mich beim Schreiben dieser Doktorarbeit unterstützt haben. Mein Dank gilt:

- **Prof. Dr. Johannes Kästner** für die Möglichkeit am Institut für Theoretische Chemie meine Doktorarbeit zu schreiben, sowie für die sehr gute Betreuung und Zusammenarbeit während der gesamten Zeit der Promotion.
- **Prof. Dr. Uwe Manthe** für die Übernahme des Mitberichts.
- **Prof. Dr. Joris van Slageren** für die Übernahme des Prüfungsvorsitzes.
- **Dr. Jan Meisner** und **Max Markmeyer** für die Unterstützung bei der Nutzung von ChemShell und der Hilfe bei verschiedenen chemischen Fragestellungen
- **Dr. Sean McConnell** für hilfreiche Diskussionen bei diversen physikalischen Fragestellungen und für die Implementierung der Näherungsverfahren in den Abschnitten 6.3.2 und 6.4.
- **Alexander Denzel** für seine Hilfe bei diversen Programmierarbeiten.
- **Prof. Dr. Jörg Main** und **PD Dr. Holger Cartarius** für hilfreiche Diskussionen bei Fragen zur Semiklassik.
- Allen übrigen **Mitarbeitern** der Arbeitsgruppe für das kollegiale Miteinander und die immer gute Arbeitsatmosphäre.
- Der **Carl–Zeiss Stiftung** für die finanzielle Förderung dieser Arbeit durch ein Promotionsstipendium.

Abstract

The prediction of rate constants for chemical reactions is one of the principal tasks in the field of theoretical chemistry. It usually relies on the Born–Oppenheimer approximation, which allows to describe the progress of a chemical reaction in configuration space as the movement of a pseudo-particle in an effective $3N$-dimensional potential, with N being the number of nuclei. The treatment of the pseudo particle's dynamics can either be done classically, by using the classical equations of motion, or fully quantum mechanically, which would involve solutions to the time-dependent Schrödinger equation. While the classical treatment is computationally easier to achieve, it cannot account for important quantum effects such as tunneling. However, a full quantum mechanical treatment is usually not feasible for most real-life chemical systems.

This is where instanton theory enters the stage and offers an alternative treatment of the system's dynamics in which tunneling can be treated in a semiclassical fashion. While the fundamental principles of the theory are already known, the practical applicability has been somewhat limited. Particularly in the microcanonical ensemble the use of instanton theory has been restricted to systems in which the vibrational degrees of freedom are separable.

In this thesis new numerical algorithms are presented which allow for the calculation of microcanonical rates for real-life chemical systems in which coupling of vibrational modes appears. Furthermore, it is shown that thermal rates can be obtained from the microcanonical rates in a computationally more efficient manner than currently possible with the use of the determinant method.

In the uni-molecular case the proposed methods are tested for the analytical Müller–Brown potential and for the decay of methylhydroxycarbene to acetaldehyde, for which the electronic energies are obtained via density functional theory (DFT). In either case the obtained results, using the new methods, are in very good

agreement with the results obtained via the conventional determinant method.
For the bi-molecular case the reaction $H_2 + OH \rightarrow H_2O + H$, for which a fitted potential energy surface is available, is investigated. The semiclassical results for the computation of the cumulative reaction probability are compared to a quantum dynamics calculation for which results are provided in the literature. Furthermore, thermal rate constants are obtained from microcanonical rate constants, which show a good agreement with the directly obtained rate constants via canonical instanton theory.
In summary, this thesis proposes a variety of different methods in order to obtain reaction rate constants via instanton theory in the canonical and microcanonical ensemble. The different approaches vary in terms of accuracy and computational effort, yet are all principally applicable to real-life multidimensional chemical systems.

Zusammenfassung

Die Vorhersage von Reaktionsgeschwindigkeitskonstanten ist eine der zentralen Aufgaben im Bereich der theoretischen Chemie. In der Regel geschieht dies auf Basis der Born–Oppenheimer Näherung, die es ermöglicht den Ablauf einer Reaktion als Bewegung eines Pseudoteilchens in einem $3N$-dimensionalen effektiven Potential im Konfigurationsraum zu beschreiben, wobei N die Anzahl der Kerne beschreibt. Die Beschreibung der Dynamik des Pseudoteilchens kann dabei klassisch erfolgen, durch Lösen der klassischen Bewegungsgleichung, oder voll quantenmechanisch, was die Bestimmung der Lösung der zeitabhängigen Schrödingergleichung erfordert. Zwar ist eine klassische Beschreibung in der Regel einfacher, jedoch ist sie nicht in der Lage Quanteneffekte, wie beispielsweise Tunneln, zu berücksichtigen. Andererseits ist eine rein quantenmechanische Beschreibung aufgrund des hohen Rechenaufwands für realistische chemische Systeme in der Regel nicht möglich.

Hier bietet die Instanton-Theorie eine Alternative, die es ermöglicht die Dynamik des Systems und dabei auftretende quantenmechanische Tunneleffekte semiklassisch zu beschreiben. Zwar sind die Grundlagen der Instanton-Theorie im Wesentlichen bereits bekannt, jedoch ist die praktische Anwendbarkeit eher eingeschränkt. Insbesondere im mikrokanonischen Ensemble ist die Verwendung der Instanton-Theorie beschränkt auf Systeme, in denen die Vibrationsfreiheitsgrade separierbar sind.

In dieser Doktorarbeit werden daher verschiedene Algorithmen vorgestellt, die die Berechnung von mikrokanonischen Raten für realistische chemische Systeme, in denen die Vibrationsfreiheitsgrade gekoppelt sind, ermöglicht. Des Weiteren ist es möglich thermische Raten aus mikrokanonischen Raten deutlich effizienter zu berechnen als mit der momentan verwendeten Determinanten-Methode.

Für den unimolekularen Fall werden die vorgestellten Methoden auf das ana-

lytische Müller–Brown Potential und für den Zerfall von Methylhydroxycarben zu Acetaldehyd angewendet. Für diesen Fall stammen die elektronischen Energien aus einer DFT-Rechnung. Für den bimolekularen Fall wird die Reaktion $H_2 + OH \rightarrow H_2O + H$ mit Hilfe einer gefitteten Energiepotentialfläche untersucht. In beiden Fällen wird eine sehr gute Übereinstimmung der Reaktionsgeschwindigkeitskonstanten, beim Vergleich der neuen Methoden mit der konventionellen Determinanten-Methode, erreicht. Die semiklassischen Ergebnisse für die Berechnung der kumulierten Reaktionswahrscheinlichkeit werden mit Literaturergebnissen aus einer Quantendynamik-Rechnung verglichen. Des Weiteren werden thermische Reaktionsgeschwindigkeitskonstanten aus mikrokanonischen Reaktionsgeschwindigkeitskonstanten gewonnen, die eine gute Übereinstimmung mit den direkt bestimmen Ratenkonstanten bei der kanonischen Instanton-Theorie zeigen.

Zusammenfassend werden in dieser Doktorarbeit verschiedene Methoden präsentiert, um Reaktionsgeschwindigkeitskonstanten mithilfe der Instanton-Theorie im kanonischen und mikrokanonischen Ensemble zu berechnen. Die verschiedenen Ansätze variieren dabei in Bezug auf deren Genauigkeit, sowie rechnerischem Aufwand. Sie sind jedoch alle grundsätzlich geeignet, um realistische mehrdimensionale chemische Systeme zu behandeln.

Publications

The content of the following articles is included in this thesis

- Andreas Löhle and Johannes Kästner
  "Calculation of reaction rate constants via instanton theory in the canonical and microcanonical ensemble",
  J. Chem. Theory Comput., (article in press)

- Sean R. McConnel, Andreas Löhle and Johannes Kästner
  "Rate constants from instanton theory via a microcanonical approach",
  J. Chem. Phys., **146**, 074105 (2017)

Contents

1 Introduction

1.1 Motivation

Quantum tunneling is one of the most uncanny phenomena which emerge from the theory of quantum mechanics. The ability of a quantum particle to penetrate a barrier that it could not surmount classically is of crucial importance in a broad variety of different physical processes. It appears in nuclear fusion, which occurs inside the core of stars and is used in modern technology such as the scanning tunneling microscope [1] or the tunneling diode [2], just to name a few.
In the context of chemistry the effects of quantum tunneling are particularly important in chemical reactions that take place at low temperatures or involve the transfer of lightweight atoms such as hydrogen [3–6]. In extremely low-temperature environments, for instance in gas clouds in interstellar space, tunneling can speed up the formation of new species of molecules by several orders of magnitude. This also includes complex organic molecules and therefore might have implications for the origin of life itself.
The simulation of chemical reactions and consequently the prediction of reaction rate constants has been a challenging task for decades in the field of computational chemistry [7–11]. One of the earliest theoretical frameworks that was developed in the 1930's mainly by Henry Eyring, Michael Polanyi and Meredith Evans [12] was transition state theory (TST). It allowed for the first time to derive the Arrhenius law [13] from fundamental mechanistic and statistical considerations rather than from empirical observations. Up to now a variety of different rate theories have been developed over the years which rely on different approximation schemes and as a consequence vary widely in terms of achievable accuracy and required computational effort. Generally the most precise way to determine a reaction rate constant is to calculate the quantum mechanical dynamics of the system. However,

due to the immense numerical computations which are required for a full quantum mechanical treatment, it is to this day only achievable for small systems composed of a few atoms.

A promising and nowadays widespread approach is what is usually referred to as canonical instanton theory. It is in essence a semiclassical theory which has appeared in somewhat different formulations since the 1960's [14–16] and is essentially based on a well known analogy between the Feynman path integral representation of the Schrödinger propagator in quantum mechanics and the calculation of the partition function in statistical physics [17]. The semiclassical treatment of these Feynman path integrals enables to incorporate tunneling contributions by determining the path with the highest tunneling probability at a relatively low computational effort [18]. Instanton theory is usually formulated in the canonical ensemble which requires a system in thermal equilibrium. However, a large number of reactions, which are of interest in the context of astrochemistry, take place in the gas phase at low pressure and therefore do not allow the determination of a well defined temperature. In these cases a rate constant depending on the (collision)-energy rather than temperature is required. This corresponds to a microcanonical formulation of instanton theory. While there have been microcanonical formulations suggested early on [19,20], it is still, due to a lack of reliable numerical methods, hardly used for real chemical systems in which the vibrational modes are not separable.

The key quantity in order to obtain microcanonical rate constants is the so-called cumulative reaction probability $P(E)$. Once $P(E)$ is computed it also is possible to obtain canonical rate constants from microcanonical rate constants in a computationally more efficient manner than via the direct calculation using the current implementation of canonical instanton theory. Therefore the main purpose of this doctoral thesis is to present different numerical algorithms which allow a reliable and efficient calculation of the cumulative reaction probability as well as thermal rate constants for real-life multidimensional chemical systems which naturally includes coupling of vibrational modes.

1.2 Outline

PART I: Literature Review

In **chapter 2** the basic principles of the path integral representation of the Schrödinger propagator and its connection to the calculation of partition functions in statistical physics are introduced. The propagator is then approximated by the action of the classical solution, which gives the dominant contributions to the path integral, and deviations from that classical path.

Chapter 3 introduces the notion of a potential energy surface (PES) and the Born–Oppenheimer approximation it is founded on. Furthermore a formulation of transition state theory in configuration space and the definition of the flux function for classical rate calculations as well as its quantum mechanical analogue, the flux operator, are introduced.

In **chapter 4** canonical instanton theory is derived from the imaginary F-premise, which relates the thermal rate constant to the imaginary part of the system's free energy. The conventional determinant method for calculating the path integral, which is based on the integration of a product of Gaussian integrals is presented.

Chapter 5 deals with the microcanonical analogue of canonical instanton theory which is based on quantum transition state theory. This includes the flux-flux autocorrelation formalism which is introduced in this chapter and from which an expression for the cumulative reaction probability $P(E)$ is derived. The computation of $P(E)$ then requires the calculation of stability parameters which are computed from the eigenvalues of the monodromy matrix.

PART II: New Methods and Applications

In **chapter 6** a variety of different numerical methods are presented in order to calculate the necessary quantities from chapter 5. Three different approximation schemes for coupled high-dimensional systems are presented to calculate the

stability parameters as an alternative to the integration of the linearized equations of motion. Furthermore a fourth algorithm based on the numerical evaluation of the Van Vleck propagator is introduced which allows for the calculation of stability parameters in a reliable, yet numerically more stable way than the equivalent integration of the linearized equation of motion. Additionally a new method is derived for the computation of $dE/d\beta$ which represents the rate at which the instanton's energy changes with respect to its imaginary time period which is given by the inverse temperature

In **chapter 7** the different numerical methods introduced in chapter 6 are applied to different potential energy surfaces (PES). These include analytical systems such as the Müller–Brown potential, a fitted PES for the bi-molecular reaction H_2 + OH $\rightarrow$ H_2O + H and a DFT calculation for the decay of methylhydroxycarbene to acetaldehyde. The results of the different methods are then compared to one another in terms of accuracy and efficiency.

Part I

Literature Review

2 The Feynman Path Integral and Quantum Statistics

The calculation of partition functions via a semiclassical approximation of the path integral representation of the Schrödinger propagator lies at the heart of instanton theory. In this chapter the time-slicing approximation is invoked in order to derive the path integral formalism. Afterwards the basics of statistical quantum mechanics and its connection to the Feynman path integral are briefly reviewed.

2.1 The Feynman Path Integral

In order to obtain the path integral representation of the propagator one starts with the time-slicing approximation of the time evolution amplitude in Eq. (2.1) as it was originally proposed by Feynman [21]. For simplicity one first starts with a particle moving in a one-dimensional potential $V(x)$. The propagator for such a particle moving from x_i to x_f in time $t_\mathrm{f} - t_\mathrm{i}$ is given in the Schrödinger picture as

$$\begin{aligned} \langle x_\mathrm{f}, t_\mathrm{f} | x_\mathrm{i}, t_\mathrm{i} \rangle &= \left\langle x_\mathrm{f} \middle| \mathrm{e}^{-\frac{\mathrm{i}}{\hbar}\hat{H}(t_\mathrm{f}-t_\mathrm{i})} \middle| x_\mathrm{i} \right\rangle \\ &= \left\langle x_\mathrm{f} \middle| \hat{U}(t_\mathrm{f}, t_\mathrm{i}) \middle| x_\mathrm{i} \right\rangle, \quad t_\mathrm{f} > t_\mathrm{i} \end{aligned} \tag{2.1}$$

with $\hat{U}(t_\mathrm{f}, t_\mathrm{i})$ being the time evolution operator and $\hat{H}$ the Hamiltonian of the system. In the first step one slices the time difference $t_\mathrm{f} - t_\mathrm{i}$ into $N+1$ equidistant intervals $\Delta t = \frac{t_\mathrm{f}-t_\mathrm{i}}{N+1}$. Using the composition property of the time-evolution operator

yields

$$\left\langle x_{\mathrm{f}}\middle|\hat{U}(t_{\mathrm{f}},t_{\mathrm{i}})\middle|x_{\mathrm{i}}\right\rangle = \left\langle x_{\mathrm{f}}\middle|\hat{U}(t_{\mathrm{f}},t_N)\ldots\hat{U}(t_n,t_{n-1})\ldots\hat{U}(t_1,t_{\mathrm{i}})\middle|x_{\mathrm{i}}\right\rangle \tag{2.2}$$

$$= \left\langle x_{\mathrm{f}}\middle|\prod_{n=1}^{N+1}\hat{U}(t_n,t_{n-1})\middle|x_{\mathrm{i}}\right\rangle \ , \tag{2.3}$$

with $t_0 = t_{\mathrm{i}}$ and $t_{N+1} = t_{\mathrm{f}}$. In the next step an identity is inserted in between every operator in Eq. (2.3) using a complete set of states in the coordinate representation

$$1 = \int_{-\infty}^{\infty} dx_n \,|x_n\rangle\langle x_n|\,, \quad n = 1,\ldots,N \tag{2.4}$$

such that the propagator becomes a product of N integrals

$$\left\langle x_{\mathrm{f}}\left|\hat{U}(t_{\mathrm{f}},t_{\mathrm{i}})\right|x_{\mathrm{i}}\right\rangle = \left(\prod_{n=1}^{N}\int_{\infty}^{\infty}dx_n\right)\left(\prod_{n=1}^{N+1}\left\langle x_n\left|\hat{U}(t_n,t_{n-1})\right|x_{n-1}\right\rangle\right) \tag{2.5}$$

whereby $x_{N+1} = x_{\mathrm{f}}$ and $x_0 = x_{\mathrm{i}}$. In order to evaluate the term $\left\langle x_n\middle|\hat{U}(t_n,t_{n-1})\middle|x_{n-1}\right\rangle$, a Hamiltonian of the form

$$\hat{H} = \frac{\hat{P}^2}{2M} + \hat{V}(\hat{x}) \tag{2.6}$$

is assumed, where $\hat{P}$ denotes the momentum operator, M the particle mass and $\hat{V}$ the potential energy. Secondly one chooses the number of time slices sufficiently large such that the time evolution operator can be replaced by the series expansion of the exponential function and truncated after terms of the order $\mathcal{O}(\Delta t^2)$ or higher. For an infinitesimal time slice this procedure yields then the following expression

$$\left\langle x_n\middle|\mathrm{e}^{-\frac{\mathrm{i}}{\hbar}\hat{H}\Delta t}\middle|x_{n-1}\right\rangle = \langle x_n|\mathbf{1}|x_{n-1}\rangle - \left\langle x_n\middle|\frac{\mathrm{i}}{\hbar}\hat{H}\Delta t\middle|x_{n-1}\right\rangle + \mathcal{O}(\Delta t^2)\ . \tag{2.7}$$

Eq. (2.7) leaves us then with three different terms that need to be evaluated in the coordinate representation:

$$\langle x_n | x_{n-1} \rangle = \delta(x_n - x_{n-1}) \tag{2.8}$$

$$\left\langle x_n \left| \frac{\hat{P}^2}{2M} \right| x_{n-1} \right\rangle = \frac{1}{2M} \left\langle x_n \left| \hat{P}^2 \right| x_{n-1} \right\rangle \tag{2.9}$$

$$\left\langle x_n \left| \hat{V} \right| x_{n-1} \right\rangle = V(x_n)\delta(x_n - x_{n-1}) \tag{2.10}$$

While the coordinate representations of Eq. (2.8) and Eq. (2.10) can immediately be seen, the expression in Eq. (2.9) requires a bit more work. First a unity is inserted using the momentum operator's eigenbasis

$$\left\langle x_n \left| \hat{P}^2 \right| x_{n-1} \right\rangle = \int_{-\infty}^{\infty} \left\langle x_n \left| \hat{P}^2 \right| p_n \right\rangle \langle p_n | x_{n-1} \rangle \, dp_n \tag{2.11}$$

$$= \int p_n^2 \langle x_n | p_n \rangle \langle p_n | x_{n-1} \rangle \, dp_n \ . \tag{2.12}$$

Using the coordinate representation of the momentum eigenstates

$$\langle x | p \rangle = \frac{1}{\sqrt{2\pi\hbar}} \mathrm{e}^{\frac{\mathrm{i}}{\hbar} px} \ , \tag{2.13}$$

Eq. (2.12) can be rewritten as

$$\left\langle x_n \left| \hat{P}^2 \right| x_{n-1} \right\rangle = \frac{1}{2\pi\hbar} \int \ p_n^2 e^{\frac{\mathrm{i}}{\hbar} p_n (x_n - x_{n-1})} dp_n \ . \tag{2.14}$$

In the next step one uses the Fourier representation of the delta distribution

$$\delta(x - x') = \frac{1}{2\pi\hbar} \int dp e^{\frac{\mathrm{i}}{\hbar} p(x - x')} \ , \tag{2.15}$$

applies it to Eq. (2.8) and Eq. (2.10) and uses it in Eq. (2.7) and the following expression

$$\left\langle x_n \middle| \mathrm{e}^{-\frac{\mathrm{i}}{\hbar}\hat{H}\Delta t} \middle| x_{n-1} \right\rangle = \frac{1}{2\pi\hbar} \int dp_n \left(1 - \left(\frac{p_n^2}{2} + V(x_n)\right) \frac{\mathrm{i}}{\hbar}\Delta t\right) e^{\frac{\mathrm{i}}{\hbar}p(x_n - x_{n-1})} \tag{2.16}$$

$$= \frac{1}{2\pi\hbar} \int dp_n e^{\frac{\mathrm{i}}{\hbar}\left(p_n(x_n - x_{n-1}) - \left(\frac{p_n^2}{2} + V(x_n)\right)\Delta t\right)} \tag{2.17}$$

is obtained. The propagator in Eq. (2.1) can therefore be written as

$$\langle x_\mathrm{f}, t_\mathrm{f} | x_\mathrm{i}, t_\mathrm{i} \rangle \approx \left(\prod_{n=1}^{N} \int_{-\infty}^{\infty} dx_n\right) \left(\prod_{n=1}^{N+1} \int_{-\infty}^{\infty} \frac{dp_n}{2\pi\hbar}\right) \exp\left(\frac{\mathrm{i}}{\hbar}\mathcal{S}_N\right) \tag{2.18}$$

with $\mathcal{S}_N$ defined as

$$\mathcal{S}_N = \sum_{n=1}^{N+1} \left[p_n(x_n - x_{n-1}) - \left(\frac{p_n^2}{2} + V(x_n)\right)\Delta t\right] . \tag{2.19}$$

The symbol $\approx$ in Eq. (2.18) accounts for the fact that the continuum limit of $N \to \infty$ and $\Delta t \to 0$ has not been taken yet. In order to get an equivalent formulation for the propagator the continuum limit in Eq. (2.18) needs to be performed. This leads to the Feynman path integral in phase space

$$\begin{aligned} \langle x_\mathrm{f}, t_\mathrm{f} | x_\mathrm{i}, t_\mathrm{i} \rangle &= \lim_{\substack{N\to\infty \\ \Delta t\to 0}} \left(\prod_{n=1}^{N} \int_{-\infty}^{\infty} dx_n\right) \left(\prod_{n=1}^{N+1} \int_{-\infty}^{\infty} \frac{dp_n}{2\pi\hbar}\right) \exp\left(\frac{\mathrm{i}}{\hbar}\mathcal{S}_N\right) \\ &= \int \mathcal{D}p \int \mathcal{D}x e^{\frac{\mathrm{i}}{\hbar}\mathcal{S}[x(t),p(t)]} , \end{aligned} \tag{2.20}$$

whereby the action $\mathcal{S}$ in phase space becomes in the continuum limit a functional of the following form:

$$\mathcal{S}[x(t), p(t)] = \int_{t_\mathrm{i}}^{t_\mathrm{f}} dt \left(p(t)\frac{dx}{dt} - \frac{1}{2}p(t)^2 - V(x(t))\right) \tag{2.21}$$

Now there is one p_n-integral more than for the integration over x_n. This is a consequence of the fact that the endpoints of the paths are kept fixed in position space but no restrictions on p_i or p_f appear in the derivation. However, one can

further simplify the expression in Eq. (2.20) by integrating out the momenta. Before taking the continuum limit one first has to complete the squares for $\mathcal{S}_N$ in Eq. (2.19). This yields

$$\mathcal{S}_N = \sum_{n=1}^{N+1} \left[-\frac{\Delta t}{2M} \left(p_n - \frac{x_n - x_{n-1}}{\Delta t} \right)^2 + \frac{M\Delta t}{2} \left(\frac{x_n - x_{n-1}}{\Delta t} \right)^2 - \Delta t V(x_n) \right] \tag{2.22}$$

The integration over the momenta in Eq. (2.18) can now be performed using Fresnel formulas [22]. This gives

$$\frac{1}{2\pi\hbar} \int_{-\infty}^{\infty} dp_n \exp\left(-\frac{\mathrm{i}\Delta t}{2M\hbar} \left(p_n - \frac{x_n - x_{n-1}}{\Delta t} \right)^2 \right) = \sqrt{\frac{M}{2\pi\hbar \mathrm{i}\Delta t}} \,. \tag{2.23}$$

Using this result the final expression for the path integral in configuration space yields

$$\langle x_\mathrm{f}, t_\mathrm{f} | x_\mathrm{i}, t_\mathrm{i} \rangle \approx \left(\frac{M}{2\pi \mathrm{i}\hbar \Delta T} \right)^{\frac{N+1}{2}} \prod_{n=1}^{N} \int_{-\infty}^{\infty} \mathrm{e}^{\frac{\mathrm{i}}{\hbar}\mathcal{S}_N} dx_n \,, \tag{2.24}$$

where $\mathcal{S}_N$ is now the remaining sum

$$\mathcal{S}_N = \sum_{n=1}^{N+1} \left[\frac{M\Delta t}{2} \left(\frac{x_n - x_{n-1}}{\Delta t} \right)^2 - \Delta t V(x_n) \right] \,. \tag{2.25}$$

In the continuum limit the path integral can now be written as

$$\langle \mathbf{x}_\mathrm{f}, t_\mathrm{f} | \mathbf{x}_\mathrm{i}, t_\mathrm{i} \rangle = \int_{x(t_\mathrm{i})=\mathbf{x}_\mathrm{i}}^{x(t_\mathrm{f})=\mathbf{x}_\mathrm{f}} \mathcal{D}x(t) e^{\frac{\mathrm{i}}{\hbar} S[x(t)]} \tag{2.26}$$

whereby the integration symbol $\mathcal{D}x$ is defined as

$$\int \mathcal{D}x(t) \equiv \lim_{\substack{N\to\infty \\ \Delta t \to 0}} \left(\frac{M}{2\pi \mathrm{i}\hbar \Delta t} \right)^{\frac{N+1}{2}} \left(\prod_{n=1}^{N} \int_{-\infty}^{\infty} dx_n \right) \tag{2.27}$$

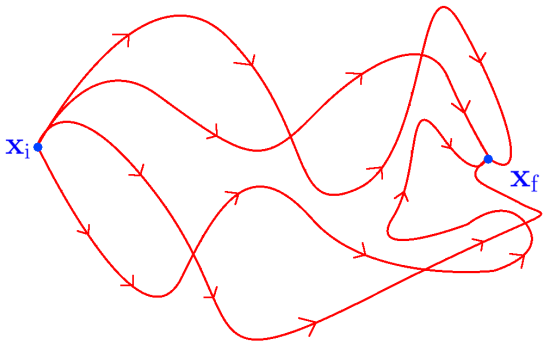

Figure 2.1: The red lines represent the possible paths in configuration space with a fixed beginning and end point $\mathbf{x}_\mathrm{f}$ and $\mathbf{x}_\mathrm{i}$. Each path is weighted by a phase factor which is given by the path's action $\mathcal{S}[x(t)]$.

and $\mathcal{S}_N$ becomes in the continuum limit the familiar action functional that appears in the Langrangian formulation of classical mechanics,

$$\mathcal{S}[x(t)] = \int_{t_\mathrm{i}}^{t_\mathrm{f}} \left[\frac{1}{2} m\dot{x}(t)^2 - V(x(t))\right] dt \ , \tag{2.28}$$

with $x(t_\mathrm{i}) = x_\mathrm{i}$ and $x(t_\mathrm{f}) = x_\mathrm{f}$. So in order to get the probability amplitude of a particle going from x_i to x_f in time $t_\mathrm{f} - t_\mathrm{i}$ one has to sum of over all possible paths in configuration space, while the amplitude $\exp(\mathrm{i}/\hbar\mathcal{S})$ of each path is given by its action $\mathcal{S}$ as illustrated in Figure 2.1. The Feynman path integral expression in Eq. (2.26) is essentially a generalization of the action principle from classical mechanics to quantum theory. It is important to emphasize that this path integral representation of the quantum mechanical propagator is completely equivalent to the description of quantum mechanics in the Schrödinger picture. Even though the Feynman path integral formalism reveals its biggest advantages in the context of quantum field theory one can still choose to use it as a representation for the non-relativistic propagator because it allows for a semiclassical approximation in a natural and much easier fashion than otherwise possible in the Schrödinger picture.

2.2 Semiclassical Approximation

In the previous section the path integral representation of the non-relativistic Schrödinger propagator has been introduced. However, there exist only a few physical systems for which the path integral can be computed exactly. In the most general case this is only possible for systems with a Lagrangian up to quadratic order. Higher order terms in the Lagrangian are usually treated perturbatively as in the case of quantum electrodynamics [23]. However, this thesis focuses on the semiclassical treatment of the path integral expression in Eq. (2.29) via a saddle point approximation and neglects terms which go beyond second order. Extending the one-dimensional formulation of the previous section to an arbitrary D-dimensional system gives

$$\langle \mathbf{x}_\mathrm{f}, t_\mathrm{f} | \mathbf{x}_\mathrm{i}, t_\mathrm{i} \rangle = \int \mathcal{D}\mathbf{x}\ \mathrm{e}^{\frac{\mathrm{i}}{\hbar}\mathcal{S}[\mathbf{x}(t)]}\ , \tag{2.29}$$

with $\mathbf{x}(t)$ containing the D coordinates of an arbitrary path at time t. Let's first recall the classical limit of $\hbar \to 0$ in order to get an intuitive understanding of the procedure. It is known from the correspondence principle that the classical behavior of a quantum system should resurface if one looked at it on a macroscopic length or energy scale. In the context of the path integral this means that as one moves to larger and larger length scales, $\hbar$ appears to be smaller and smaller and in the limit of $\hbar \to 0$ the amplitudes are heavily oscillating and canceling each other by interference. Only paths with a slowly varying phase $\mathcal{S}/\hbar$ are still contributing to the integral in that limit. Thus the paths which leave the action functional stationary describe the classical behavior. This gives the following condition

$$\delta\mathcal{S} = 0 \tag{2.30}$$

$$\Rightarrow \frac{\partial\mathcal{L}}{\partial\mathbf{x}} - \frac{d}{dt}\frac{\partial\mathcal{L}}{\partial\dot{\mathbf{x}}} = 0 \tag{2.31}$$

$$\Rightarrow\ M\ddot{\mathbf{x}} = -\nabla V(\mathbf{x})\ . \tag{2.32}$$

The variation of $\mathcal{S}$ gives the Euler–Lagrange equations and if a Lagrangian of the form $\mathcal{L} = (1/2)M\dot{\mathbf{x}}^2 - V(\mathbf{x})$ is assumed one gets, as expected, Newton's equation of motion in Eq. (2.32). If quantum corrections to the classical behavior ought to

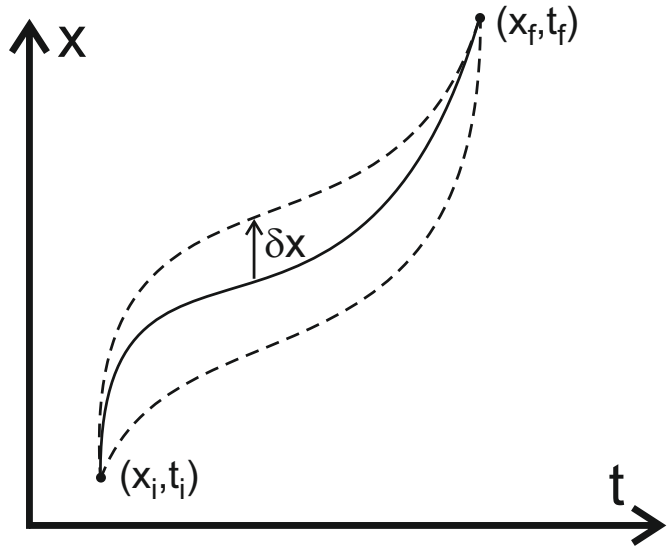

Figure 2.2: All possible paths are parameterized as deviations from the classical solution $\mathbf{x}(t) = \mathbf{x}_{\rm cl}(t) + \delta\mathbf{x}(t)$.

be included one first parameterizes the path as

$$\mathbf{x}(t) = \mathbf{x}_{\rm cl}(t) + \delta\mathbf{x}(t) \ , \tag{2.33}$$

with $\mathbf{x}_{\rm cl}(t)$ being the solution to Eq. (2.32) and $\delta\mathbf{x}$ deviations from the classical path which satisfy the boundary conditions $\delta\mathbf{x}(t_{\rm i}) = \delta\mathbf{x}(t_{\rm f}) = 0$ as depicted in Figure 2.2. In a next step $\mathcal{S}$ is expanded in powers of these fluctuations which yields

$$\mathcal{S} = \mathcal{S}_{\rm cl} + \int_{t_{\rm i}}^{t_{\rm f}} \frac{\delta\mathcal{S}}{\delta\mathbf{x}(t)}\delta\mathbf{x}(t)dt + \frac{1}{2}\int_{t_{\rm i}}^{t_{\rm f}} \frac{\delta^2\mathcal{S}}{\delta\mathbf{x}(t)\delta\mathbf{x}(t')}\delta\mathbf{x}(t)\delta\mathbf{x}(t')dt + \mathcal{O}(\delta x(t)^3) \ . \tag{2.34}$$

Since possible paths are expanded around the classical solution the functional derivative in the second term of Eq. (2.34) vanishes. If one truncates after the quadratic term and assumes again the standard form for the Lagrangian $\mathcal{L} =$

$1/2M\dot{\mathbf{x}}^2 - V(\mathbf{x})$ one obtains for the quadratic term

$$\frac{1}{2}\int_{t_\mathrm{i}}^{t_\mathrm{f}} \frac{\delta^2\mathcal{S}}{\delta\mathbf{x}(t)\delta\mathbf{x}(t')}\delta\mathbf{x}(t)\delta\mathbf{x}(t')dt = \int_{t_\mathrm{i}}^{t_\mathrm{f}} \left(\frac{M}{2}\left(\frac{\partial\delta\mathbf{x}}{\partial t}\right)^2 - \delta\mathbf{x}(t)\mathbf{V}''(\mathbf{x}_\mathrm{cl}(t))\delta\mathbf{x}(t)\right) dt \ . \tag{2.35}$$

Given this result one can now move from an integration over all possible paths $\mathcal{D}\mathbf{x}$ to an integration over all deviations from the classical path such that the path integral in Eq. (2.29) can be written as

$$\langle \mathbf{x}_\mathrm{f}, t_\mathrm{f}|\mathbf{x}_\mathrm{i}, t_\mathrm{i}\rangle \approx \mathrm{e}^{\frac{\mathrm{i}}{\hbar}\mathcal{S}_\mathrm{cl}} \int \mathcal{D}\delta\mathbf{x}(t)\mathrm{e}^{\frac{\mathrm{i}}{\hbar}\int_{t_\mathrm{i}}^{t_\mathrm{f}}\left(\frac{M}{2}\left(\frac{d\delta\mathbf{x}}{dt}\right)^2 - \frac{1}{2}\delta\mathbf{x}(t)\mathbf{V}''(\mathbf{x}_\mathrm{cl}(t))\delta\mathbf{x}(t)\right)dt} \tag{2.36}$$

$$= \mathrm{e}^{\frac{\mathrm{i}}{\hbar}\mathcal{S}_\mathrm{cl}} \ F_\mathrm{SC}(\mathbf{x}_\mathrm{f}, \mathbf{x}_\mathrm{i}, t_\mathrm{f} - t_\mathrm{i}) \ . \tag{2.37}$$

So in order to evaluate the semiclassically approximated propagator, the classical solution and the second derivatives of the potential along the classical path have to be determined. The first term of Eq. (2.37) describes the classical contribution to the transition amplitude while the second term F_SC describes quantum corrections up to second order to the classical solution. From now on these corrections will be referred to as quantum fluctuations and F_SC is called the fluctuation factor. Since the evaluation of F_SC is principally one of the main objectives of this thesis it is skipped in this section as it will be dealt with in much greater detail in subsequent chapters. It is important to notice however, that no matter which method is chosen the required information stays unaltered, meaning every approach to evaluate F_SC always requires at least the second derivatives of the potential along the classical solution.

2.3 The Path Integral and Quantum Statistics

One of the key benefits of the Feynman path integral formulation of quantum mechanics is, that it has not only an interesting but also very helpful connection to statistical physics. Throughout this thesis the relationship between the partition function in the canonical ensemble and the path integral representation of the non-relativistic Schrödinger propagator in imaginary time will be continuously used.

This unified view of quantum theory and statistical mechanics allows to apply various methods which emerged in the context of quantum field theory and apply them to the computation of partition functions. For these reasons the basics of the different statistical ensembles and the description of mixed quantum states are briefly reviewed.

2.3.1 The Microcanonical Ensemble

The microcanonical ensemble describes a system which is completely isolated from the surrounding environment. Hence there is no exchange of energy or particles possible. It is often referred to as the NVE ensemble since the macroscopic properties of the system, namely the number of particles N, the volume V and the energy E are kept constant. Since the occupation of microstates of the same energy is assumed to be uniform in the microcanonical ensemble, the probability $\rho(E_n)$ of finding the system in a particular state for a given energy E_n is given by

$$\rho(E_n) = \frac{1}{\nu(E_n)} \ , \tag{2.38}$$

whereby $\nu(E)$ describes the number of states that share the same energy and therefore is called microcanonical partition function or density of states. In mathematical terms this means $\nu(E)$ is given by the following expression

$$\nu(E_n) = \sum_{E_n \leq E \leq E_n + \Delta E} 1 \ . \tag{2.39}$$

Eq. (2.39) counts all the system's microstates which have an energy E_n that lies within the interval $[E_n, E_n + \Delta E]$ with ΔE being an infinitesimal energy shift.

2.3.2 The Canonical Ensemble

The canonical ensemble describes a physical system which is in thermal equilibrium with its surrounding environment. Since it is not an isolated system it can exchange heat and the total energy of the system is not conserved any longer. This ensemble is also called the NVT ensemble since the macroscopic properties of the system namely the number of particles N, volume V and the temperature T are constant.

For such a system the probability of finding a microstate at an energy E_n is given by

$$\rho(E_n) = \frac{e^{-\beta E_n}}{\sum_j \nu(E_j) e^{-\beta E_j}} \ , \tag{2.40}$$

where $\beta = \frac{1}{k_B T}$ with k_B being the Boltzmann constant and $\nu(E)$ is the microcanonical partition function or density of states from Eq. (2.39). The expression in the denominator in Eq. (2.40) which acts as normalization is called the canonical partition function $\mathcal{Q}$.

$$\mathcal{Q} = \sum_{j=0}^{\infty} \nu(E_j) e^{-\beta E_j} \tag{2.41}$$

The microcanonical partition function can can be written in a continuous form for $\nu(E) = \sum_j \delta(E - E_j)$ such that the canonical partition function

$$\mathcal{Q} = \int_{-\infty}^{\infty} \nu(E) e^{-\beta E} dE \ , \tag{2.42}$$

appears as the Laplace transform of the microcanonical parition function. The fact that one can switch from microcanonical to the canonical ensemble via a Laplace transform is an important result which will be used repeatedly in subsequent chapters.

2.3.3 The Grand Canonical Ensemble

The grand canonical ensemble is like the canonical ensemble in thermal equilibrium but it allows in addition to the exchange of heat the exchange of particles with the environment. It is often referred to as the μVT ensemble as instead of the number of particles the chemical potential μ is conserved. The chemical potential describes the amount of energy that is released or absorbed due to a change of the particle number N. The grand canonical partition function is given as

$$\mathcal{Q}_G = \sum_i \nu(E_i) \mathrm{e}^{-\beta(E_i - \mu N_i)} \ . \tag{2.43}$$

The grand canonical ensemble is mentioned here for completeness but it is of no significance for the remaining part of the thesis and will therefore not be discussed any further.

2.3.4 Quantum Statistics

In order to describe a quantum system in a specific ensemble one has to apply the fundamental rules of statistical physics to quantum mechanics. The combination of both can be called statistical quantum mechanics. The combination of both theories can be illustrated by the following example. Let's say a quantum system is prepared to be in the quantum state $|\Psi_\mathrm{i}\rangle$ at time t_i and one wants to calculate the probability amplitude $A_{\mathrm{i}\to\mathrm{j}}$ of finding the system in another quantum state $|\Psi_\mathrm{j}\rangle$ at a later time t_j. Then $A_{\mathrm{i}\to\mathrm{j}}$ is given by

$$A_{\mathrm{i}\to\mathrm{j}} = \left\langle \Psi_\mathrm{j} \middle| \exp\left(-\frac{\mathrm{i}}{\hbar}\hat{H}(t_\mathrm{j}-t_\mathrm{i})\right) \middle| \Psi_\mathrm{i} \right\rangle \ . \tag{2.44}$$

But what if one does not know in which quantum state the system is in at t_i. In that case one first has to choose a statistical ensemble which then provides the probability of finding the system in a certain state. So there is the inherent probabilistic nature of quantum mechanics that follows from the Copenhagen interpretation and in addition to that the classical probability of finding a quantum system in a certain initial state which is given by the corresponding statistical ensemble. This leads to the definition of the density operator [24]

$$\hat{\rho} = \sum_i \omega_i \left|\Psi_i\right\rangle \left\langle\Psi_i\right| , \quad 0 \le \omega_i \le 1 \ . \tag{2.45}$$

The density operator, also called the density matrix, contains the probability ω_i of finding the system in the pure state $|\Psi_i\rangle$. Therefore the sum of those probabilities must be equal to 1, $\sum_i \omega_i = 1$. In the formalism of quantum statistics the expectation value of an operator $\hat{A}$ is then given by

$$\left\langle \hat{A} \right\rangle = \frac{1}{\mathcal{Q}} \mathrm{tr}\left(\hat{A}\hat{\rho}\right) \ , \tag{2.46}$$

and the partition function of a system is given by the trace of the corresponding density operator $\hat{\rho}$

$$\mathcal{Q} = \mathrm{tr}\,(\hat{\rho}) \tag{2.47}$$

Given the previous definitions in subsections 2.3.1 to 2.3.3 the different density operators for the three different ensemble are defined in the following way:

- Microcanonical ensemble

$$\hat{\rho}_M = \delta(E - \hat{H}) \tag{2.48}$$

- Canonical ensemble

$$\hat{\rho}_C = \mathrm{e}^{-\beta\hat{H}} \tag{2.49}$$

- Grand canonical ensemble

$$\hat{\rho}_G = \mathrm{e}^{-\beta(\hat{H}-\mu\hat{N})} \tag{2.50}$$

2.4 Path Integral Representation of the Partition Function

The definition of the density operator in section 2.3.4 makes it easy to find a path integral representation of the partition function. First one starts with the partition function in the canonical ensemble. Following Eq. (2.47) one gets

$$\mathcal{Q} = \mathrm{tr}\left(\mathrm{e}^{-\beta\hat{H}}\right) \ . \tag{2.51}$$

Now if the trace was taken in the eigenbasis of $\hat{H}$ such that $\hat{H}\,|n\rangle = E_n\,|n\rangle$ one would get the familiar result

$$\mathcal{Q} = \sum_n \left\langle n \middle| \mathrm{e}^{-\beta\hat{H}} \middle| n \right\rangle \tag{2.52}$$

$$= \sum_n \mathrm{e}^{-\beta E_n} \ . \tag{2.53}$$

However, this requires knowledge of the full spectrum of the Hamiltonian. In order to obtain a path integral expression the trace has to be taken in the position representation such that

$$\mathcal{Q} = \int \left\langle \mathbf{x} \middle| \mathrm{e}^{-\beta\hat{H}} \middle| \mathbf{x} \right\rangle d\mathbf{x} \ . \tag{2.54}$$

The expression in Eq. (2.54) looks similar to the Schrödinger propagator for a quantum particle starting and ending at the same position $|\mathbf{x}\rangle$. In fact it is equal, if β is replaced with $\mathrm{i}(t_\mathrm{f} - t_\mathrm{i})/\hbar$ such that

$$\left\langle \mathbf{x} \middle| \mathrm{e}^{-\beta\hat{H}} \middle| \mathbf{x} \right\rangle = \left\langle \mathbf{x} \middle| \mathrm{e}^{-\frac{\mathrm{i}}{\hbar}\hat{H}(t_\mathrm{f}-t_\mathrm{i})} \middle| \mathbf{x} \right\rangle \Big|_{(t_\mathrm{f}-t_\mathrm{i})=-\mathrm{i}\hbar\beta} \tag{2.55}$$

So if one takes the Schrödinger propagator and performs a transformation from real time t to imaginary time $\tau = -\mathrm{i}\hbar t$ one obtains an expression for the canonical partition function for which then the path integral expression for the propagator in Eq. (2.26) can be used. This yields

$$\mathcal{Q}_k = \int d\mathbf{x} \left\langle \mathbf{x} \middle| \mathrm{e}^{-\frac{\mathrm{i}}{\hbar}\hat{H}(t_\mathrm{f}-t_\mathrm{i})} \middle| \mathbf{x} \right\rangle \Big|_{(t_\mathrm{f}-t_\mathrm{i})=-\mathrm{i}\hbar\beta} \tag{2.56}$$

$$= \int d\mathbf{x} \int \mathcal{D}\mathbf{x}(\tau) \mathrm{e}^{-\mathcal{S}_E[x(\tau)]} \ . \tag{2.57}$$

The transformation from real to imaginary time is called a Wick rotation [25]. By moving the time axis to the complex plane one first has to realize the changes to

the action functional $\mathcal{S}$. Under a Wick rotation it becomes

$$\frac{\mathrm{i}}{\hbar}\mathcal{S}\Big|_{(t_\mathrm{f}-ti)-\mathrm{i}\hbar\beta} = -\underbrace{\int_0^{\beta\hbar}\left(\frac{M}{2}\frac{d\mathbf{x}^2}{d\tau}+V(\mathbf{x}(\tau))\right)d\tau}_{\mathcal{S}_E} \ . \tag{2.58}$$

The change from real to imaginary time has two crucial consequences. First the new action functional $\mathcal{S}_E$, called the Euclidean action, has a change in the sign of the potential energy. Secondly $\mathcal{S}$ becomes entirely imaginary which leads to an entirely real exponential factor with which each path is weighted. It is also worth mentioning that unlike the path integral in real time, the Euclidean path integral has a rigorous mathematical definition as integration against a Wiener measure [26]. The term Euclidean has it origins in the context of quantum field theory where switching from real to imaginary time changes the space-time geometry from a Minkowski to a Euclidean metric. This can simply be illustrated in the following way. If the path is generalized to be a function of a set of independent parameters x^μ one gets

$$\int \mathcal{D}\Phi(x^\mu)\mathrm{e}^{\frac{\mathrm{i}}{\hbar}S[\Phi(x^\mu)]} \ , \ S=\int \mathcal{L}(\Phi,\partial_\mu\Phi,x^\mu)\ dx^\mu \ , \tag{2.59}$$

with the action functional $\mathcal{S}$ now being a μ-dimensional integral over the Lagrangian density $\mathcal{L}$. The integral in Eq. (2.59) is an integration over all possible configurations of the field Φ. Since quantum field theory is a relativistic theory one has a 4-dimensional space time with the following Minkowski metric

$$ds^2 = -(cdt)^2+dx^2+dy^2+dz^2 \ . \tag{2.60}$$

Due to the Wick rotation the real time increment becomes $dt = -\mathrm{i}d\tau$ and the Minkowski metric is turned into a Euclidean metric

$$ds^2 = c^2d\tau^2+dx^2+dy^2+dz^2 \ . \tag{2.61}$$

The path integral in Eq. (2.57) is therefore simply a special case of a one-dimensional field theory in which $\Phi(x^0=\tau)=\mathbf{x}(\tau)$ is parameterized by one independent variable τ. This is the reason why quantum mechanics is often referred to as a field

theory in 0 + 1 dimension. This admittedly rather abstract view of quantum mechanics will become very useful later on as one can use techniques which were developed in the context of a 3 + 1 dimensional quantum field theory in order to render divergent partition functions finite.

In the case of the microcanonical partition function $\nu(E)$ one has to take the trace of the density operator $\hat{\rho}_m$ which gives

$$\nu(E) = \int \left\langle \mathbf{x} \middle| \delta\Big(E - \hat{H}\Big) \middle| \mathbf{x} \right\rangle d\mathbf{x} \; . \tag{2.62}$$

Now in order to get a path integral expression for Eq. (2.62) one uses the Fourier representation of the delta distribution such that

$$\begin{aligned} \nu(E) =& \int \left\langle \mathbf{x} \middle| \frac{1}{2\pi\hbar} \int_{-\infty}^{\infty} \mathrm{e}^{-\frac{\mathrm{i}}{\hbar}(\hat{H}-E)} dT \middle| \mathbf{x} \right\rangle d\mathbf{x} && (2.63)\\ =& \frac{1}{2\pi\hbar} \int \mathrm{e}^{\frac{\mathrm{i}}{\hbar}ET} \int \left\langle \mathbf{x} \middle| \mathrm{e}^{-\frac{\mathrm{i}}{\hbar}\hat{H}T} \middle| \mathbf{x} \right\rangle d\mathbf{x} dT && (2.64)\\ =& \frac{1}{2\pi\hbar} \int dT \oint \mathcal{D}\mathbf{x} \; \mathrm{e}^{\frac{\mathrm{i}}{\hbar}\mathcal{W}} \; . && (2.65) \end{aligned}$$

The expression for $\nu(E)$ in Eq. (2.65) is an integral over all closed paths with a real time period T where each path has a phase factor which is given by the so-called Hamilton–Jacobi or shortened action $\mathcal{W}$ [27]

$$\begin{aligned} \mathcal{W} =& \int_0^T \left(\frac{M}{2}\dot{\mathbf{x}}^2 - V(\mathbf{x}) + E \right) dt && (2.66)\\ =& \int_0^T \left(\frac{M}{2}\dot{\mathbf{x}}^2 - V(\mathbf{x}) + \frac{M}{2}\dot{\mathbf{x}}^2 + V(\mathbf{x}) \right) dt && (2.67)\\ =& \int_0^T M\dot{\mathbf{x}}^2 dt = \int \mathbf{p}(\mathbf{x}) \; d\mathbf{x} \; , && (2.68) \end{aligned}$$

which is simply given by the momentum integrated along the path. Unlike in the canonical case where only paths are considered that have the same imaginary period $T = -\mathrm{i}\hbar\beta$ but can vary in E, in this case E is kept fixed and the real time period of the paths is unrestricted. The expressions for the microcanonical partition function in Eq. (2.65) as well the canonical partition function in Eq. (2.57)

are exact. The semiclassical approximations can principally be done as explained in section 2.2 and will be dealt with extensively in chapters 4 and 5.

2.5 Summary

The Feynman path integral representation of the Schrödinger propagator can be derived using the time slicing approximation. The exact evaluation of the path integral is generally only possible in systems with a Lagrangian that contains no terms higher than second order. Therefore a semiclassical approximation scheme is used in which the path integral is approximated via a steepest descent integration which only takes into account contributions from the classical path and their quantum corrections up to second order. Through the use of the density operator from statistical quantum mechanics and the transformation from real to imaginary time an expression for the canonical partition function in terms of the Schrödinger propagator and consequently a path integral representation can be found. Analogously a path integral representation for the microcanonical partition function can be defined by using the Fourier representation of the microcanonical density operator. These provide the basic tools which are needed in order to formulate a canonical and microcanonical instanton theory which is done in chapters 4 and 5.

3 Transition State Theory

Transition state theory (TST) is one of earliest theoretical frameworks that was developed in the 1930's mainly by Henry Eyring, Michael Polanyi and Meredith Evans [12] in order to compute chemical reaction rate constants. A widely used expression to determine rate constants is the Arrhenius equation [13]

$$k(\beta) = A\mathrm{e}^{-\beta E_a} \ , \tag{3.1}$$

where E_a is the activation energy of the reaction and A is a pre-factor which is specific to each individual reaction. However, before the advent of TST, A and E_a had to be determined empirically. TST allowed for the first time to determine these two factors from fundamental mechanistic and statistical considerations. Fundamentally TST provides a conceptual framework in order to understand chemical reactivity qualitatively as well as quantitatively. The concepts used in TST, like the notion of a potential energy surface (PES) or a dividing surface are also the basis of instanton theory. Therfore in this chapter the basic concepts of TST are reviewed. The focus lies on a formulation of TST in configuration space since throughout this thesis only systems with Hamiltonians of the form $H = T + V$ with T being the kinetic energy and V the potential energy are investigated. Only in these cases the first-order saddle point of the Hamiltonian is related to the first-order saddle point of the potential. This would not be the case for example if magnetic interactions were taken into account [28].

3.1 Potential Energy Surface

One of the key concepts used in TST is the notion of a potential energy surface (PES). It describes the energy of the system dependent on the position of the

system's atoms. It was first proposed by Ren Marcelin in 1913 [29] and is to this day one of the key tools which enable the analysis of molecular geometries and chemical reaction dynamics. The concept of the PES is tightly linked to the Born–Oppenheimer approximation. In order to obtain the energy function $E(\mathbf{R})$, whereby $\mathbf{R}$ is a vector that contains the positions of the nuclei, one has to solve the molecular Schrödinger equation

$$\hat{H}_{\mathrm{m}}\ \Psi(\tilde{\mathbf{r}}, \mathbf{R}) = E\ \Psi(\tilde{\mathbf{r}}, \mathbf{R})\ . \tag{3.2}$$

The wave function $\Psi(\tilde{\mathbf{r}}, \mathbf{R})$ describes the molecule's quantum state dependent on the position of the nuclei as well as the position of the electrons $\tilde{\mathbf{r}}$. The molecular Hamiltonian for a system with N nuclei and n electrons is given by

$$\hat{H}_{\mathrm{m}} = \hat{T}_{\mathrm{nuc}} + \hat{T}_{\mathrm{el}} + \hat{V}_{\mathrm{ee}} + \hat{V}_{\mathrm{NN}} + \hat{V}_{\mathrm{en}} \tag{3.3}$$

whereby the terms

$$\hat{T}_{\mathrm{nuc}} = -\sum_{j=1}^{N} \frac{\hbar^2}{2M_j} \nabla_j^2\ , \quad \hat{T}_{\mathrm{el}} = -\sum_{i=1}^{n} \frac{\hbar^2}{2m_e} \nabla_i^2 \tag{3.4}$$

describe the kinetic energy of the nuclei and electrons and the terms

$$\hat{V}_{\mathrm{NN}} = \frac{q_0}{4\pi\varepsilon_0} \sum_{j<J} \frac{Z_j Z_J}{|\vec{R}_j - \vec{R}_J|}\ , \quad \hat{V}_{\mathrm{ee}} = \frac{q_0}{4\pi\varepsilon_0} \sum_{i<I} \frac{1}{|\vec{r}_i - \vec{r}_I|} \tag{3.5}$$

the interaction of the nuclei and the electrons among themselves. The final term describes the interaction of the electrons with the nuclei

$$\hat{V}_{\mathrm{en}} = -\frac{q_0}{4\pi\varepsilon_0} \sum_{i,j} \frac{Z_j}{|\vec{r}_i - \vec{R}_j|}\ , \tag{3.6}$$

where Z is the atomic number of the j^{th}- atom, q_0 the elementary charge and ϵ_0 the constant for electric vacuum permittivity. Since a solution to Eq. (3.2) becomes increasingly difficult for higher dimensional systems due to an exponential increase in computational effort the Born–Oppenheimer approximation [30] is used, which separates the movement of the electrons from the movement of the nuclei. This is

possible since the mass of a proton is much larger than the mass of an electron, yet the electromagnetic force acts equally on both. This leads to a relatively large inertia of the nuclei in comparison to the electrons. The separation leads to the following ansatz for the molecular wave function

$$\Psi(\tilde{\mathbf{r}}, \mathbf{R}) = \phi(\tilde{\mathbf{r}}, \mathbf{R})\chi(\mathbf{R}) \ , \tag{3.7}$$

which leads to different equations. One Schrödinger equation for the electronic energies $E(\mathbf{R})$

$$\left(\hat{T}_{\text{el}} + \hat{V}_{ee} + \hat{V}_{NN} + \hat{V}_{en}\right) \phi(\tilde{\mathbf{r}}, \mathbf{R}) = E(\mathbf{R})\phi(\tilde{\mathbf{r}}, \mathbf{R}) \tag{3.8}$$

and the corresponding Schrödinger equation for the energies E_{nuc} of the nuclei

$$\left(\hat{T}_{NN} + E(\mathbf{R})\right) \chi(\mathbf{R}) = E_{\text{nuc}}\chi(\mathbf{R}) \ . \tag{3.9}$$

Eq. (3.8) is then solved for different sets of the nuclei positions $\mathbf{R}$ and consequently a energy surfaces $E(\mathbf{R})$ for the electronic energies can be obtained. In the case of a reaction of N atoms one obtains a $3N$-dimensional surface in which every point on the PES represents a specific configuration of the molecule's nuclei. This is a key result since a fundamental principle of TST is to describe the progress of a chemical reaction as the movement of a single pseudoparticle in this $3N$-dimensional configuration space which is equivalent to the movement of N particles in 3-dimensional real space.

3.2 Transition State Theory in Configuration Space

As mentioned in section 3.1 one can describe the progress of a chemical reaction as the movement of a pseudoparticle on a multidimensional PES. The question of whether a reaction is likely to happen can therefore theoretically be answered by directly calculating the dynamics of the system. First an initial state is chosen then the dynamics of the system starting from that initial state is calculated and the time is determined after which it ends up in the region of the PES, which represents the possible reaction products. This process then needs to be repeated

for all possible initial states and the reaction rate constant k can then be obtained from the sum of all inverse times t_i^{-1}

$$k = \sum_{i=1}^{N} \frac{1}{t_i} \ , \tag{3.10}$$

where N is the number of possible initial states and t_i the time until it reaches the product region. However, since the number of initial states can be infinitely large and the calculation of the dynamics (classical or quantum) is computationally very demanding, TST offers an alternative and very efficient way. In configuration space one can write the system's Hamiltonian in mass weighted coordinates in the following way

$$H(\mathbf{r}, \mathbf{p}) = \frac{\mathbf{p}^2}{2} + V(\mathbf{r}) \ , \tag{3.11}$$

where $\mathbf{r}$ describes the position of the pseudoparticle in mass weighted coordinates, $\mathbf{p}$ its momentum in mass weighted coordinates and $V(\mathbf{r})$ is the electronic potential obtained from Eq. (3.8). The next step is to define a so-called dividing surface which separates the reactant side from the product side. In case of a D-dimensional configuration space the dividing surface is a $D-1$-dimensional hyper surface. Furthermore one can define a function $s(\mathbf{r})$ which has to fulfill the following requirements:

$$s(\mathbf{r}) = \begin{cases} s(\mathbf{r}) < 0 & \text{On the reactand side} \\ s(\mathbf{r}) = 0 & \text{On the dividing surface} \\ s(\mathbf{r}) > 0 & \text{On the product side} \end{cases} \tag{3.12}$$

Using $s(\mathbf{r})$ one can now construct a flux-function $\mathcal{F}$ [31]

$$\mathcal{F}(\mathbf{r}, \mathbf{p}) := \frac{d}{dt}\Theta(s(\mathbf{r})) = \delta\left(s(\mathbf{r})\right) \frac{\partial s}{\partial \mathbf{r}} \ \mathbf{p} \tag{3.13}$$

where Θ is the Heaviside step function. The definition in Eq (3.13) begins to make sense if $\mathcal{F}$ is integrated for a given particle trajectory $\mathbf{r}(t)$ which yields [31]

$$\int_{-\infty}^{\infty} \mathcal{F}(\mathbf{r},\mathbf{p})dt = \int_{\text{initial}}^{\text{final}} d\Theta(s(\mathbf{r})) \tag{3.14}$$
$$= \begin{cases} +1 & \text{Reaction from reactant to product} \\ -1 & \text{Reaction from product to reactant} \\ 0 & \text{Otherwise} \end{cases}$$

So the time integral over the flux function gives either a positive contribution of $+1$ if the trajectory $\mathbf{r}(t)$ ends up on the products side at $t \to \infty$, a negative contribution of -1 if it starts on the product side and ends up on the reactant side or no contribution at all if the initial and final state are on the same side of the dividing surface. It therefore counts the number of elementary reactions from reactant to product and backwards. Now it is important to mention that a formulation of transition state theory in configuration space does not allow for the construction of a dividing surface in higher dimension which is completely free of recrossing and only based on the PES [32]. Such a dividing surface has principally to be constructed in full phase space.

3.3 Classical Rate Calculation

If one is interested in a thermal rate constant the thermal average of the flux function in Eq. (3.13) has to be calculated. If the reaction coordinate is assumed to be r_1 the rate constant $k(\beta)$ is given by [33]

$$k(\beta) = \frac{\iint_{p_1>0} \mathcal{F}(\mathbf{r},\mathbf{p}) \mathrm{e}^{-\beta H(\mathbf{r},\mathbf{p})} d\mathbf{p}\, d\mathbf{r}}{\iint \mathrm{e}^{-\beta H(\mathbf{r},\mathbf{p})} d\mathbf{p}\, d\mathbf{r}} \tag{3.15}$$
$$= \frac{\iint_{p_1>0} \delta(s(\mathbf{r})) s'(\mathbf{r}) p_1 \mathrm{e}^{-\beta H(\mathbf{r},\mathbf{p})} d\mathbf{p}\, d\mathbf{r}}{\iint \mathrm{e}^{-\beta H(\mathbf{r},\mathbf{p})} d\mathbf{p}\, d\mathbf{r}} \tag{3.16}$$

Without loss of generality the coordinates are chosen such that the saddle point of the system is situated at $r_1 = 0$. A practical choice for $s(\mathbf{r})$ is $s = r_1$ such

that $s'(\mathbf{r}) = 1$. Since the Hamiltonian in mass weighted coordinates is given by Eq. (3.11) the integration over p_1 simply gives $1/\beta$. Furthermore there is only a contribution from r_1 due to the delta distribution in the integral such that the thermal rate constant can be calculated as

$$k(\beta) = \frac{1}{\beta} \frac{\iint \mathrm{e}^{-\beta H(\mathbf{r},\mathbf{p})\big|_{r_1=0}} \, dp_2 \ldots dp_D \; dr_2 \ldots dr_D}{\iint \mathrm{e}^{-\beta H(\mathbf{r},\mathbf{p})} \, dp_1 \ldots dp_D \; dr_1 \ldots dr_D} \; , \tag{3.17}$$

where the denominator is simply the classical partition function in the canonical ensemble.

In the microcanonical case the energy of the system is kept fixed and a rate constant, dependent on energy rather than temperature is computed. The microcanonical rate constant can be obtained via the same principle as in the canonical case. The expectation value of the flux in the microcanonical ensemble is given by

$$k(E) = \frac{\iint \mathcal{F}(\mathbf{r},\mathbf{p}) \delta(E - H(\mathbf{r},\mathbf{p})) d\mathbf{r} \; d\mathbf{p}}{\iint \delta(E - H(\mathbf{r},\mathbf{p})) d\mathbf{r} \; d\mathbf{p}} \tag{3.18}$$

The delta distribution can be represented as

$$\delta(E - H(\mathbf{r},\mathbf{p})) = \lim_{\epsilon \to 0} \frac{1}{\sqrt{2\pi\epsilon}} \mathrm{e}^{\frac{-(E-H(\mathbf{r},\mathbf{p}))^2}{2\epsilon}} \; . \tag{3.19}$$

In practice one might choose a small but finite value to be able to compute the expression in Eq. (3.19). Using this definition one obtains for $k(E)$

$$k(E) = \frac{\lim_{\epsilon \to 0} \iint \mathcal{F}(\mathbf{r},\mathbf{p}) \mathrm{e}^{\frac{-(E-H(\mathbf{r},\mathbf{p}))^2}{2\epsilon}} d\mathbf{r} \; d\mathbf{p}}{\lim_{\epsilon \to 0} \iint \mathrm{e}^{\frac{-(E-H(\mathbf{r},\mathbf{p}))^2}{2\epsilon}} d\mathbf{r} \; d\mathbf{p}} \; , \tag{3.20}$$

whereby the denominator is the partition function in the microcanonical ensemble. So in summary, the rate constant of the reaction is simply the expectation value of the flux function defined in Eq. (3.13).

$$k = \langle \mathcal{F} \rangle \; . \tag{3.21}$$

The expression in Eq. (3.21) is of special interest since it will allow for the formulation of a quantum mechanical version of transition state theory.

3.4 Quantum Transition State Theory

So far the movement of the pseudoparticle has been treated solely classically. If the particle starting in the reactant has not enough energy, it is not able to reach the transition state and move on to the reactant side. However, it is known, particularly in the case of light atoms, that tunneling can have significant effects and even be dominating at low energies. In these cases it is therefore necessary to formulate a quantum mechanical analogue of transition state theory.

3.4.1 S-Matrix

Instead of treating the movement of the pseudoparticle classically one can switch to a completely quantum mechanical treatment. This can easily be illustrated by looking at a very simple example of a one-dimensional potential energy barrier as shown in Figure 3.1. In order to calculate a rate one first needs to calculate the transmission coefficient. In this simple case it can be achieved easily by using the following ansatz for the wave functions outside the potential barrier

$$\begin{aligned} \Psi_{\mathrm{L}}(x) &= Ae^{ikx} + Be^{-ikx} \\ \Psi_{\mathrm{R}}(x) &= Ce^{ikx} + De^{-ikx} \ , \end{aligned} \tag{3.22}$$

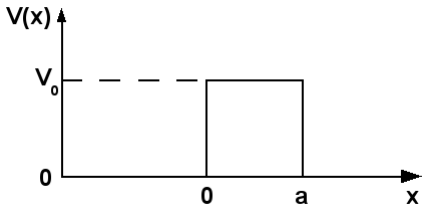

Figure 3.1: Rectangular barrier in one dimension of width a and height V_0

with $k = \sqrt{2mE/\hbar^2}$ and $\Psi_{\mathrm{R}}(x)$ being the wave function for the pseudoparticle coming from the right and $\Psi_{\mathrm{L}}(x)$ the wave function coming from the left. The transition overlap of the outgoing waves with the incoming waves can be written as

$$\underbrace{\begin{pmatrix} B \\ C \end{pmatrix}}_{\Psi_{\mathrm{out}}} = \underbrace{\begin{pmatrix} S_{11} & S_{12} \\ S_{21} & S_{22} \end{pmatrix}}_{\mathbf{S}} \underbrace{\begin{pmatrix} A \\ D \end{pmatrix}}_{\Psi_{\mathrm{in}}} . \tag{3.23}$$

Eq. (3.23) shows that the transition overlap of the outgoing wave function Ψ_{out} with the incoming wave function Ψ_{in} is described by a linear relationship in which the S-Matrix completely describes the scattering properties of the potential [34]. In the simple case of a one-dimensional rectangular barrier the same ansatz for the wave function in Eq. (3.22) can be chosen with the boundary conditions $D = 0$, $A = 1$. By making use of the continuity requirement of the wave function and its derivatives at the respective boundaries of the potential one can determine the transmission and reflection coefficients analytically. A thermal rate constant can then be calculated by thermally averaging the transmission coefficient such that

$$k(\beta) = \frac{1}{2\hbar\mathcal{Q}} \int T_L(E) \mathrm{e}^{-\beta E} \, dE \tag{3.24}$$

$$= \frac{1}{2\hbar\mathcal{Q}} \int |S_{21}|^2 \, \mathrm{e}^{-\beta E} \, dE \ , \tag{3.25}$$

with $\mathcal{Q}$ being the canonical partition function of the reactant and $T_L(E)$ the transmission coefficient for the particle going from left to right. In order to extend the expression in Eq. (3.25) to a general multidimensional case the so-called cumulative reaction probability $P(E)$ is introduced [19]

$$P(E) = \sum_J (2J+1) \sum_{n_p, n_r} \left| \mathbf{S}_{n_p, n_r}(E, J) \right|^2 \tag{3.26}$$

which is the result of averaging all cross sections where n_r denotes the quantum number of the reactant state, n_p the quantum number of the product sate and J denotes the values of the total angular momentum. Since Eq. (3.26) is a cumulative probability it can in principle be bigger than one in the case of degenerate states.

Once $P(E)$ is obtained an expression for the microcanonical rate constant can be defined which is given by [35]

$$k(E) = \frac{1}{2\pi\hbar}\frac{P(E)}{\nu_{\mathrm{r}}(E)} \ , \tag{3.27}$$

where $\nu_{\mathrm{r}}(E)$ is the reactant's density of states. The thermal rate constant can then easily be obtained by thermally averaging $K(E)$ such that

$$k(\beta) = \frac{\int k(E)\nu_{\mathrm{r}}(E)\mathrm{e}^{-\beta E}dE}{\int \nu_{\mathrm{r}}(E)\mathrm{e}^{-\beta E}dE} \tag{3.28}$$

$$= \frac{1}{2\pi\hbar\mathcal{Q}_{RS}}\int_{-\infty}^{\infty} P(E)\mathrm{e}^{-\beta E}dE \ , \tag{3.29}$$

with $\mathcal{Q}_{\mathcal{RS}}$ being the partition function of the reactant.

3.4.2 Flux Operator

If Eq. (3.26) is used to calculate $P(E)$ one would have to solve the Schrödinger equation with the correct boundary conditions in order to obtain the full S-matrix first. However, since one is usually only interested in the rate constant rather than all the detailed information of each state to state interaction contained in the S-matrix, it should be possible to find a more efficient way of calculating $P(E)$. In fact this can be achieved by using the quantum mechanical analogue of the classical formulation of transition state theory which is also referred to as the quantum-flux-flux autocorrelation formalism [31]. Let's first introduce the classical expression for $P(E)$ and then transform it to its quantum mechanical form. The classical expression is as follows [36]

$$P_{\mathrm{cl}}(E) = \frac{1}{(2\pi\hbar)^{D-1}}\int\int \delta(E-H)\mathcal{F}(\mathbf{x},\mathbf{p})\ \xi(\mathbf{x},\mathbf{p})d\mathbf{p}d\mathbf{x} \ , \tag{3.30}$$

where $\mathcal{F}(\mathbf{x},\mathbf{p})$ is the classical flux function from Eq. (3.13) and $\xi(\mathbf{x},\mathbf{p})$ is the characteristic function which is supposed to ensure that there is only a contribution to the integral in Eq. (3.30) if the trajectory of the pseudoparticle crossing the dividing surface from reactant to the product side stays there at $t \to \infty$. So the

easiest choice for $\xi(\mathbf{x}, \mathbf{p})$ would be a function that is equal to 1 if the particle stays on the product site infinitely long and is equal to 0 else. Now in order to find a quantum mechanical expression for Eq. (3.30) a quantum mechanical analogue of the flux operator $\hat{\mathcal{F}}$ has to be constructed first. Let's start by remembering that in the Heisenberg picture the time derivative of an arbitrary operator $\hat{A}$ is given by

$$\frac{d}{dt}\hat{A} = \frac{\mathrm{i}}{\hbar}\left[\hat{H}, \hat{A}\right] + \frac{\partial \hat{A}}{\partial t} \ . \tag{3.31}$$

Taking the flux function $\mathcal{F}$ in Eq. (3.13) and turning it into an operator by using Eq. (3.31) yields

$$\hat{F} = \frac{d}{dt}\hat{\theta}(s(\hat{\mathbf{x}})) = \frac{\mathrm{i}}{\hbar}\left[\hat{H}, \hat{\theta}(s(\hat{\mathbf{x}}))\right] \ . \tag{3.32}$$

Furthermore the characteristic function can be written as [19]

$$\hat{\xi}(\mathbf{x}, \mathbf{p}) = \int_0^\infty \frac{d\hat{\theta}(s(\hat{\mathbf{x}})}{dt} dt = \int_0^\infty \hat{F}(t)\ dt \ . \tag{3.33}$$

Now using Eq. (3.33), remembering that the quantum mechanical analogue to the phase space integration is taking the trace $(2\pi\hbar)^D \int\int d\mathbf{x} d\mathbf{p} \rightarrow \mathrm{Tr}$ and applying it to Eq. (3.30) yields the following expression

$$P(E) = 2\pi\hbar \mathrm{Tr}\left[\delta(E - \hat{H})\hat{F}\int_0^\infty \hat{F}(t) dt\right] \ . \tag{3.34}$$

Since taking the trace is a linear operation and the time evolution of the flux operator in the Heisenberg picture is given by

$$\hat{F}(t) = \mathrm{e}^{\frac{\mathrm{i}}{\hbar}\hat{H}t}\hat{F}\mathrm{e}^{-\frac{\mathrm{i}}{\hbar}\hat{H}t} \tag{3.35}$$

one obtains

$$P(E) = \frac{1}{2}(2\pi\hbar)\int_{-\infty}^{\infty} \mathrm{Tr}\left[\delta(E - \hat{H})\hat{F}\mathrm{e}^{\frac{\mathrm{i}}{\hbar}\hat{H}t}\hat{F}\mathrm{e}^{-\frac{\mathrm{i}}{\hbar}\hat{H}t}\right] dt \ . \tag{3.36}$$

Since the operator $\mathrm{e}^{-\frac{\mathrm{i}}{\hbar}\hat{H}t}$ can be replaced with $\mathrm{e}^{-\frac{\mathrm{i}}{\hbar}Et}$ and the time integral

$$\int_{-\infty}^{\infty} \mathrm{e}^{\mathrm{i}(\hat{H}-E)t}\, dt = 2\pi\hbar\delta(E-\hat{H}) \;, \tag{3.37}$$

is the Fourier representation of the delta distribution, one arrives at the final expression for the cumulative reaction probability which was proposed by Miller in 1975 [19]:

$$P(E) = \frac{1}{2}(2\pi\hbar)^2 \mathrm{Tr}\left[\delta(E-\hat{H})\hat{F}\delta(E-\hat{H})\hat{F}\right] \;. \tag{3.38}$$

Notice that the expression Eq. (3.38) is in principle exact. It yields exactly the same result as Eq. (3.26) yet it does not require the calculation of the full S-Matrix.

3.5 Quantum Rate Calculation

If the flux operator $\hat{\mathcal{F}}$ is defined as

$$\hat{\mathcal{F}} = \hat{F}\int_0^{\infty} \mathrm{e}^{\frac{\mathrm{i}}{\hbar}\hat{H}t}\hat{F}\mathrm{e}^{-\frac{\mathrm{i}}{\hbar}\hat{H}t}\, dt \tag{3.39}$$

the microcanoncical rate constant can be written analogously to Eq. (3.21) as the expectation value of $\hat{\mathcal{F}}$ in the microcanonical ensemble

$$k(E) = \frac{1}{2\pi\hbar}\frac{P(E)}{\Gamma(E)} \tag{3.40}$$

$$= \frac{\mathrm{Tr}\left(\delta(E-\hat{H})\hat{\mathcal{F}}\right)}{\mathrm{Tr}\left(\delta(E-\hat{H})\right)} \tag{3.41}$$

$$= \langle\hat{\mathcal{F}}\rangle \;. \tag{3.42}$$

In order to obtain a thermal rate constant one can either Laplace transform $k(E)$ as in Eq. (3.25) or calculate the expectation value of $\hat{\mathcal{F}}$ directly in the canonical

ensemble

$$k(\beta) = \langle \hat{\mathcal{F}} \rangle \tag{3.43}$$

$$= \frac{\mathrm{Tr}\left(\mathrm{e}^{-\beta \hat{H}} \hat{\mathcal{F}}\right)}{\mathrm{Tr}\left(\mathrm{e}^{-\beta \hat{H}}\right)} \,. \tag{3.44}$$

However, the calculation of the trace of the operator $\hat{\mathcal{F}}$ remains computationally very demanding if it is treated fully quantum mechanically. One alternative is the use of instanton theory in order to compute a semiclassical approximation of the trace. Especially in chapter 5 when a microcanonical version of instanton theory is introduced the flux formalism becomes indispensable.

3.6 Summary

Transition sate theory offers a fundamental and conceptually very useful framework to understand chemical reactions from a microscopic and statistical perspective. It is mainly based on the Born-Oppenheimer approximation in which the movement of the nuclei is separated from the movement of the electrons and consequently a potential energy surface can be constructed which gives the electronic energies dependent on the positions of the nuclei. The progress of a reaction is then described as the movement of a pseudoparticle in that multidimensional effective potential. Rather then calculating the full dynamics of the system, a formulation of TST in configuration space allows for a rate constant calculation by defining a dividing surface which is related to the first order saddle point of the PES and the flux through it. In the classical formulation of TST the pseudoparticle is treated classically and therefore no quantum effects such as tunneling can be included. If the pseudoparticle is treated as a quantum particle it is possible to construct a quantum mechanical analogue of the flux function which in theory allows one to calculate an exact rate constant by calculating the expectation value of the flux operator without going through the hassle of obtaining the full S-Matrix. However, since an exact calculation of the quantum mechanical trace is computationally very demanding an approximation scheme, e.g. instanton theory, is usually required to

evaluate the trace and hence approximate the reaction rate constant.

4 Canonical Instanton Theory

The term instanton first appeared in the context of quantum field theory where it is used to describe tunneling phenomena such as the semiclassical analysis of the decay of the false vacuum state [15]. In the most general definition an instanton is a solution to the classical equations of motion of a field theory on Euclidean space time with a non-zero and finite action [37]. In the context of reaction rate theory an instanton describes the dynamics of a chemical reaction at low temperature or low energy when tunneling is the dominant contributor to the rate constants. In this chapter the canonical formulation of instanton theory is introduced and the determinant method, which is currently the prevalent algorithm to compute the necessary quantities for the calculation of the rate constant, is presented.

4.1 Decay Rates and Complex Energies

The decay of a quantum state is fundamentally a time dependent phenomenon for which the calculation of a rate usually involves finding a solution to the time dependent Schrödinger equation $\mathrm{i}\hbar\partial_t |\Psi\rangle = \hat{H} |\Psi\rangle$ with the correct initial conditions. Another widely applied method is to describe the decay of such quasi-bound states by solving the stationary Schrödinger equation

$$\hat{H}^{\mathrm{eff}} |\Psi\rangle = E |\Psi\rangle , \quad E \in \mathbb{C} \tag{4.1}$$

with a non-hermitian effective Hamiltonian $\hat{H}^{\mathrm{eff}}$ which in principle allows for complex energies. The standard approach in this case would be to use a Hamiltonian of the following form [38]

$$\hat{H}^{\mathrm{eff}}_{n,n'} = \hat{H}_{n,n'} - \mathrm{i}\frac{1}{2}\Gamma_{n,n'} \tag{4.2}$$

whereby $\hat{H}_{n,n'}$ describes coupling among the 0^{th} order basis states in the reactant $|n\rangle$. The imaginary part $\Gamma_{n,n'}$ is a small perturbation which describes the coupling to dissociative states. Using this approach one obtains the following energy eigenvalues

$$\hat{H}^{\text{eff}}|n\rangle = \left(E_n^r - \mathrm{i}\frac{\hbar}{2}\gamma_n\right)|n\rangle \ . \tag{4.3}$$

The real part E_n^r describes the energy of the quasi-bound state in the reactant whereby γ_n describes its decay rate. This can easily bee seen if one looks at the time evolved solution in the position representation

$$\Psi_n(x,t) = \Phi_n(x)e^{-\frac{\mathrm{i}}{\hbar}E_n t} \tag{4.4}$$

with $\Phi_n(x) = \langle x|n\rangle$ and calculates its probability density

$$|\Psi(x,t)|^2 = \Phi(x)\Phi^*(x)\mathrm{e}^{-\frac{\mathrm{i}}{\hbar}\left(E_n^r - \mathrm{i}\frac{\hbar}{2}\gamma_n\right)t}e^{\frac{\mathrm{i}}{\hbar}\left(E_n^r + \mathrm{i}\frac{\hbar}{2}\gamma_n\right)t} \tag{4.5}$$

$$= |\Phi(x)|^2 e^{-\gamma_n t} \ . \tag{4.6}$$

The thermal rate constant can then simply be calculated by thermally averaging the different γ_n and one arrives at

$$k(\beta) = \frac{\sum_n \gamma_n \mathrm{e}^{-\beta E_n}}{\sum_n \mathrm{e}^{-\beta E_n}} \ . \tag{4.7}$$

Instead of determining each individual decay rate first and then thermally average them later one can directly calculate the thermal rate constant by invoking the imaginary F premise. It relates the imaginary part of the system's free energy F to the thermal reaction rate constant [16, 39, 40] as

$$k(\beta) = -\frac{2}{\hbar}\mathrm{Im}F = -\frac{2}{\hbar}\mathrm{Im}\left(-\frac{1}{\beta}\ln\mathcal{Q}\right) \tag{4.8}$$

$$= \frac{2}{\hbar\beta}\arctan\left(\frac{\mathrm{Im}\mathcal{Q}}{\mathrm{Re}\mathcal{Q}}\right) \tag{4.9}$$

$$\approx \frac{2}{\hbar\beta}\frac{\mathrm{Im}\mathcal{Q}}{\mathrm{Re}\mathcal{Q}} \quad \text{for } \mathrm{Im}\mathcal{Q} \ll \mathrm{Re}\mathcal{Q} \tag{4.10}$$

whereby $\mathcal{Q}$ is the system's canonical partition function. The task of calculating $k(\beta)$ is therefore reduced to finding the real and imaginary part of the partition function where the real part represents the partition function of the reactant state and the imaginary part the partition function of the transition state, respectively.

4.2 Semiclassical Approximation and the Instanton

The result in Eq. (4.10) is very useful because one can now easily find a path integral representation by applying the relationship between quantum mechanics and statistics as outlined in section 2.3. Taking the trace of the Boltzmann operator in the canonical ensemble gives

$$\mathcal{Q} = \int d\mathbf{x} \left\langle \mathbf{x} \middle| \mathrm{e}^{-\beta \hat{H}} \middle| \mathbf{x} \right\rangle \tag{4.11}$$

$$= \int d\mathbf{x} \int \mathcal{D}\mathbf{x}(\tau) \mathrm{e}^{-S_E/\hbar} \tag{4.12}$$

where S_E is the Euclidean action for a D- dimensional system in mass weighted coordinates

$$\mathcal{S}_E = \int_0^{\beta\hbar} \left(\frac{1}{2} \dot{\mathbf{x}}(\tau)^2 + V(\mathbf{x}(\tau)) \right) d\tau \ . \tag{4.13}$$

If the semiclassical approximation in section 2.2 is applied, the partition function becomes

$$\mathcal{Q}_{\mathrm{SC}}(\beta) = \sum_i \ F^i_{\mathrm{SC}}(\mathbf{x}, \mathbf{x}, \beta) \ \mathrm{e}^{-S^i_{\mathrm{cl}}[\mathbf{x}]/\hbar} \ , \tag{4.14}$$

where $F^i_{\mathrm{SC}}(\mathbf{x}, \mathbf{x}, \beta)$ is the fluctuation factor of the i^{th} solution that fulfils the classical equation of motion

$$\frac{d^2\mathbf{x}}{d\tau^2} = \nabla V(\mathbf{x}(\tau)). \tag{4.15}$$

Using Eq. (2.37) in imaginary time and mass weighted coordinates one gets

$$F^i_{\mathrm{SC}}(\mathbf{x},\mathbf{x},\beta) = \int \mathcal{D}\delta\mathbf{x}(\tau)\mathrm{e}^{-\frac{1}{\hbar}\int_0^{\beta\hbar}\left(\frac{1}{2}\left(\frac{d\delta\mathbf{x}}{d\tau}\right)^2+\frac{1}{2}\delta\mathbf{x}(\tau)\mathbf{V}''(\mathbf{x}^i_{\mathrm{cl}}(\tau))\delta\mathbf{x}(\tau)\right)d\tau} \tag{4.16}$$

with S^i_{cl} being the corresponding Euclidean action of the i^{th} solution. Due to the sign change in front of the potential the differential equation describes now the movement of the pseudoparticle in the upside down potential $-V(\mathbf{x})$ as depicted in Figure 4.1. Usually there can be two classical solutions found in the upside-down potential which fulfill Eq. (4.15). The trivial solution of a particle at rest for the time $\beta\hbar$, thus fulfilling $\ddot{\mathbf{x}} = 0$ and a periodic solution moving back and forth as depicted in Figure 4.1. This periodic instanton solution is also referred to as the bounce trajectory. In this thesis the term instanton always refers to this bounce trajectory.

4.2.1 Evaluation of the Fluctuation Factor

Once an instanton has been located, Eq. (4.16) can be evaluated in the following way. First the kinetic term in the argument of the exponential function of the fluctuation factor in Eq. (4.16) can be partially integrated which yields

$$\int_0^{\beta\hbar}\frac{1}{2}\left(\delta\dot{\mathbf{x}}\right)^2 d\tau = \frac{1}{2}\delta\mathbf{x}\delta\dot{\mathbf{x}}\Big|_0^{\beta\hbar} - \int_0^{\beta\hbar}\frac{1}{2}\delta\ddot{\mathbf{x}}\delta\mathbf{x}\; dt\;. \tag{4.17}$$

Since $\delta\mathbf{x}$ vanishes at $\tau = 0$ and $\tau = \beta\hbar$ the action $\mathcal{S}_E$ in the exponential can be written as

$$\mathcal{S}_E = \int_0^{\beta\hbar}\frac{1}{2}\delta\mathbf{x}\left[-\frac{d^2}{d\tau^2} + V''(\mathbf{x}(\tau))\right]\delta\mathbf{x}\; dt\;. \tag{4.18}$$

In a second step the Euclidean action is represented in a normal mode expansion [22]. This is done be expressing the deviations $\delta\mathbf{x}$ as a linear combination of $y_n(\tau)$

$$\delta\mathbf{x}(\tau) = \sum_{n=0}^{\infty}\alpha_n y_n(\tau) \tag{4.19}$$

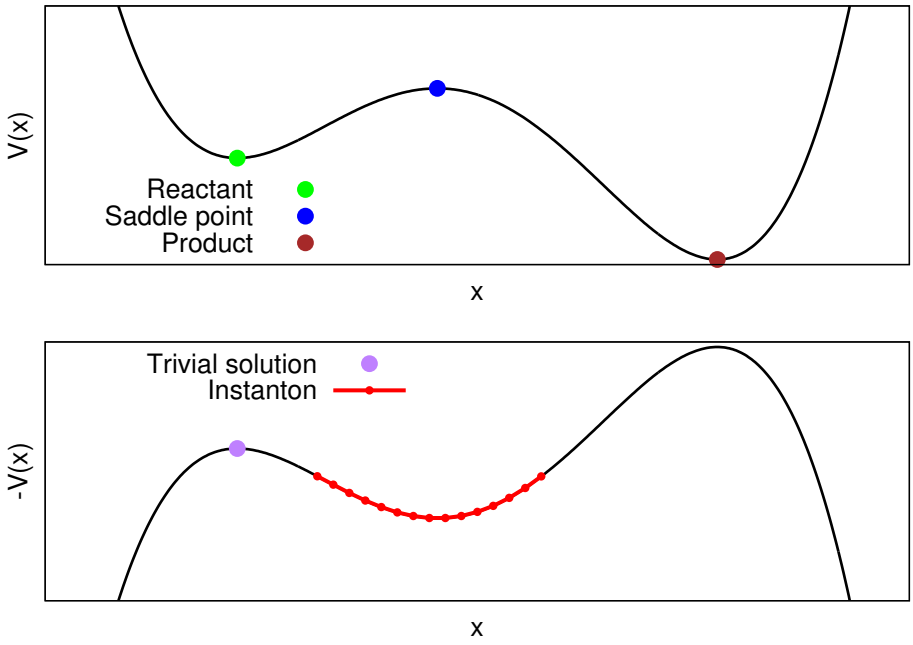

Figure 4.1: The upper graph shows the original potential energy surface. The lower graph shows the upside-down potential in which the classical solutions have to be determined. The red line marks the instanton solution with period $\beta\hbar$ and the purple dot marks the trivial solution which is at rest during that time period.

whereby $y_n(\tau)$ are the normalized and orthogonal eigenfunctions of the differential equation

$$\left(-\frac{d^2}{d\tau^2} + V''(\mathbf{x}_{\mathrm{cl}})\right) y_n(\tau) = \lambda_n y_n(\tau) \tag{4.20}$$

such that $\mathcal{S}_E$ becomes

$$\mathcal{S}_E = \frac{1}{2}\sum_{n=0}^{\infty} \lambda_n \alpha_n^2 \ . \tag{4.21}$$

This yields for the path integral expression for the fluctuation factor

$$\begin{aligned} F_{\mathrm{SC}}(\mathbf{x},\mathbf{x},\beta) &= \int \mathcal{D}\delta\mathbf{x}(\tau) \exp\left(-\frac{1}{\hbar}\int_0^{\beta\hbar} \frac{1}{2}\delta\mathbf{x}\left[-\frac{d^2}{d\tau^2} + V''(\mathbf{x}(\tau))\right]\delta\mathbf{x}dt\right) \\ &= \mathcal{N}\left(\prod_{n=0}^{\infty}\frac{1}{\sqrt{2\pi\hbar}}\right)\int \ \mathrm{e}^{-\frac{1}{\hbar}\frac{1}{2}\sum_{n=0}^{\infty}\lambda_n\alpha_n^2}\ d^n\alpha \qquad (4.22) \\ &= \mathcal{N}\prod_{n=0}^{\infty}\frac{1}{\sqrt{\lambda_n}}\ , \qquad (4.23) \end{aligned}$$

where $\mathcal{N}$ is a factor which stems from the Jacobian which relates the normal mode measure to the integration measure over $\delta\mathbf{x}$. Explicit knowledge of the value of $\mathcal{N}$ is not necessary since usually only the ratios of fluctuation factors in which the term $\mathcal{N}$ cancels out are of interest. It is important to keep in mind that the integrals in Eq. (4.23) only converge for $\lambda_n > 0$, $\forall n$. However, in general the eigenvalue spectrum is not positive definite. Since the instanton is a saddle point of the Euclidean action it has one negative eigenvalue. Furthermore, there are additional zero- valued eigenvalues which are connected to symmetries of the system. However, one can handle these potentially divergent contributions in a physically sensible manner, if the following methods are applied

4.2.2 Treatment of the Zero Eigenvalue Mode

If Eq. (4.23) is supposed to be used in order to calculate F_{SC} for the instanton one inevitably encounters the following divergent integral

$$\int_{-\infty}^{\infty} \mathrm{e}^{-\frac{1}{2\hbar}\lambda_0\alpha_0^2}\, d\alpha_0 = \frac{1}{\sqrt{2\pi\hbar}} \int_{-\infty}^{\infty} d\alpha_0 \to \infty,\ \lambda_0 = 0 \tag{4.24}$$

In order to render this diverging expression finite one has to look at the physical origin of its infinity. The action of a closed orbit is invariant with respect to the choice of the starting and end point, as $\mathbf{x}' = \mathbf{x}'' = \mathbf{x}$. This means that any solution at time τ contributes as much as any other solution at time τ'. It is this continuous translational symmetry in time which leads to an overcounting of the same physical state infinitely many times. This is a familiar problem that appears often in the context of quantum field theories since it is usually not possible in the path integral representation to obtain unambiguous, non-singular solutions when a gauge symmetry is present. In this context it is possible to modify the action by introducing so-called ghost fields that break the gauge symmetry [41]. They are merely a computational tool to preserve unitarity but they do not correspond to any real particle states. Depending on the chosen gauge for a system the formulation of ghosts can vary, yet the same physical results must be obtained with any particular chosen gauge. In this case on can apply a gauge fixing mechanism known as the Faddeev–Popov method [41] to render the expression in Eq. (4.24) finite. This yields the following, well behaved expression [22]

$$\frac{1}{\sqrt{2\pi\hbar}} \int_{-\infty}^{\infty} \mathrm{e}^{-\frac{1}{2\hbar}\lambda_0\alpha_0^2}\, d\alpha_0 = \sqrt{\frac{\mathcal{W}}{2\pi\hbar}} \int_0^{\beta\hbar} d\tau = \sqrt{\frac{\mathcal{W}}{2\pi\hbar}}\beta\hbar\ , \tag{4.25}$$

where $\mathcal{W}$ is the shortened action in mass weighted coordinates $\mathcal{W} = \int \dot{\mathbf{x}}^2 d\tau$. The exact gauge fixing procedure in this particular case can be seen in detail in Ref. 22.

4.2.3 Treatment of the Negative Eigenvalue Mode

Another divergent contribution is caused by a negative eigenvalue. This eigenvalue occurs due to the fact that the instanton solution is a saddle point of the Euclidean

action functional

$$\frac{1}{\sqrt{2\pi\hbar}}\int_{-\infty}^{\infty} \mathrm{e}^{-\frac{1}{2\hbar}\lambda_{-1}\alpha^2}\, d\alpha \to \infty, \quad \lambda_{-1} < 0\ . \tag{4.26}$$

The integral in Eq. (4.26) is clearly divergent, if integrated over the real numbers. However, one can perform an analytical continuation into the complex plane and obtain the following finite expression [14]

$$\frac{1}{\sqrt{2\pi\hbar}}\int_{-\infty}^{\infty} \mathrm{e}^{-\frac{1}{2\hbar}\lambda_{-1}\alpha_0^2}\, d\alpha = \frac{\mathrm{i}}{2}\frac{1}{\sqrt{|\lambda_{-1}|}}\ . \tag{4.27}$$

The factor 1/2 is a consequence of the fact that one is only interested in reactions which propagate in the direction of the product region as the backward reaction does not contribute. The proper analytic continuation of the integral in Eq. (4.26) can be seen in full detail in Ref. 22.

4.3 Thermal Rate Calculation

Using the expression in Eq. (4.14) the canonical partition function is

$$\mathcal{Q}_k^{\mathrm{SC}}(\beta) = F_{\mathrm{RS}}\ \mathrm{e}^{-S_{\mathrm{RS}}/\hbar} + \mathrm{i}F_{\mathrm{Inst}}\ \mathrm{e}^{-S_{\mathrm{Inst}}/\hbar}\ , \tag{4.28}$$

where $\mathrm{i}F_{\mathrm{inst}}$ is the fluctuation factor of the instanton. It is entirely imaginary due to the analytic continuation. The term S_{Inst} describes the instanton's Euclidean action, S_{RS} the action of the reactant state and F_{RS} its corresponding fluctuation factor. Using the imaginary F premise of Eq. (4.10) and the above result for the semiclassical approximation for the partition function one obtains for the thermal rate constant

$$k(\beta) = \frac{2}{\hbar\beta}\frac{\mathrm{Im}\mathcal{Q}}{\mathrm{Re}\mathcal{Q}} = \frac{2}{\hbar\beta}\frac{F_{\mathrm{Inst}}\ \mathrm{e}^{-S_{\mathrm{Inst}}/\hbar}}{F_{\mathrm{RS}}\ \mathrm{e}^{-S_{\mathrm{RS}}/\hbar}}\ . \tag{4.29}$$

For the final expression one simply has to plug in the expression for F_{SC}^i from Eq. (4.23) including the finite expression for the instanton's divergent contributions in Eq. (4.24) and Eq. (4.26). One obtains for a D-dimensional system the following

final expression for the rate constant

$$k(\beta) = \sqrt{\frac{\mathcal{W}P}{2\pi\beta\hbar^2}} \frac{1}{\sqrt{|\lambda_{-1}^{\mathrm{Inst}}|}} \frac{\left[\prod_{i=1}^{DP-2} \frac{1}{\sqrt{|\lambda_i^{\mathrm{Inst}}|}}\right]}{\left[\prod_{j=1}^{DP} \frac{1}{\sqrt{|\lambda_j^{\mathrm{RS}}|}}\right]} \mathrm{e}^{\frac{1}{\hbar}(-S_{\mathrm{Inst}}+S_{\mathrm{RS}})} \ , \tag{4.30}$$

where P is the number of discrete points at which the instanton is evaluated. In this context P is often referred to as the number of images as every coordinate of the instanton in configuration space corresponds to a certain configuration of the system's nuclei. In principle the instanton can be found by integrating the classical equations of motion with the right initial conditions.

In practice, however, it is located by searching stationary points of the discretized Euclidean action functional for the periodic instanton orbit

$$S_E = \sum_{i=1}^{P} \frac{1}{2} \frac{(\mathbf{x}_i - \mathbf{x}_{i-1})^2}{\Delta\tau} + V(\mathbf{x}_i)\Delta\tau \tag{4.31}$$

$$= F(x_{1,1}, \ldots x_{1,D}, x_{2,1}, \ldots, x_{i,j}, \ldots x_{P,D}) \tag{4.32}$$

whereby S_E is in mass weighted coordinates, $\Delta\tau = \beta\hbar/P$, $\mathbf{x}_i = (x_{i,1}, \ldots, x_{i,P})^T$ and $i \in [1, \ldots, P]$ and $j \in [1, \ldots, D]$. In D dimensions and with P discretized points the discretized action functional therefore becomes a function of DP variables. The instanton is then located by finding the roots of

$$\mathbf{0} = \nabla_\mu F \ , \quad \mu \in [1, \ldots, PD] \tag{4.33}$$

$$= (2\mathbf{x}_i - \mathbf{x}_{i-1} - \mathbf{x}_{i+1}) \frac{1}{\Delta\tau} + \frac{\partial V}{\partial \mathbf{x}_i} \Delta\tau \quad , \ i \in [1, \ldots, P] \tag{4.34}$$

Finding the zeros of Eq. (4.34) can nowadays efficiently be done by using a truncated Newton search [18] which is available in the DL-FIND software package [42] and which is used in all subsequent instanton calculations. The eigenvalues for the calculation of the fluctuation factor are then calculated by diagonalizing the

discretized operator

$$\left(-\partial_\tau^2 + V''[\mathbf{x}(\tau)]\right) \Rightarrow \begin{pmatrix} \mathbf{K}_1 & -\mathbf{I} & 0 & \cdots & \cdots & -\mathbf{I} \\ -\mathbf{I} & \ddots & -\mathbf{I} & \ddots & \cdots & 0 \\ 0 & -\mathbf{I} & \mathbf{K}_i & \ddots & \ddots & \vdots \\ \vdots & \ddots & \ddots & \mathbf{K}_{i+1} & -\mathbf{I} & \vdots \\ \vdots & \ddots & \ddots & \ddots & \ddots & -\mathbf{I} \\ -\mathbf{I} & 0 & \cdots & \cdots & -\mathbf{I} & \mathbf{K}_P \end{pmatrix}, \tag{4.35}$$

where $\mathbf{K}_i = 2\mathbf{I} + \Delta\tau^2 \mathbf{V}''(\mathbf{x}_i)$ and $\mathbf{I}$ is a D-dimensional unit matrix. Thus in order to calculate the rate constant one first has to locate the instanton by finding the roots of Eq. (4.34) and afterwards diagonalizing the discretized matrix representation of the operator in Eq. (4.35). This requires Hessians of each image. Figure 4.2 shows schematically the expected result of the rate constant calculation using canonical instanton theory. At first it is important to notice that canonical instanton theory is only applicable for temperatures below the so-called crossover temperature T_c. This is due to the fact that the instanton's period becomes shorter and shorter with increasing temperature until it collapses to a point at T_c. At high temperatures the pseudoparticle is essentially moving in a harmonic oscillator with the curvature ω_{TS}^2 given by the negative eigenmode at the transition state structure. Since the period of an harmonic oscillator is given by $\frac{2\pi}{\omega}$ this gives for the crossover temperature

$$\beta_c \hbar = \frac{2\pi}{\omega_{\mathrm{TS}}}, \tag{4.36}$$

$$T_c = \frac{\hbar \omega_{\mathrm{TS}}}{2\pi k_B} \, . \tag{4.37}$$

The crossover temperature can be seen as indication at which temperature tunneling contributions start to become important. Furthermore, Figure 4.2 shows an overestimation of the thermal rate constant of the instanton calculation when compared to the exact result close to T_c. The exact reasons for this overestimation are discussed in greater detail in chapter 5 as they become obvious when the expression for the canonical rate constant is derived via a stationary phase approximation of the corresponding expression in the microcanonical ensemble.

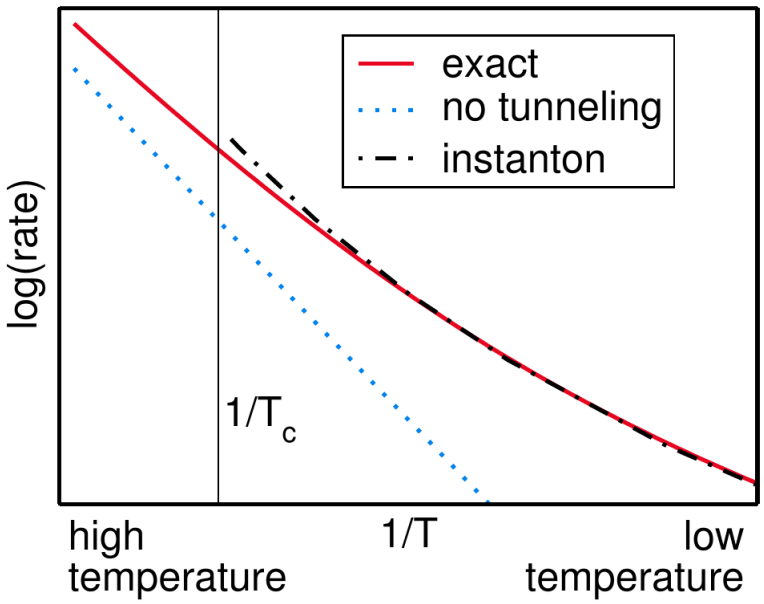

Figure 4.2: Schematic Arrhenius plot of the rate constant calculation for an Eckart barrier using canonical instanton theory. The dotted blue line represents the classical TST result which does not include tunneling. The dashed black line is the result of the instanton calculation. The red line represents the exact quantum solution.

4.4 Summary

In order to determine the thermal rate constant one first has to locate the instanton, a periodic orbit on the upside-down potential energy surface. This is done via a truncated Newton search [18] in order to find a saddle point of the discretized Euclidean action functional. Once the instanton has been found the fluctuation factor, which represents the contributions from second order quantum corrections, is calculated by diagonalizing the discrete representation of the operator in Eq. (4.35). The obtained eigenvalue spectrum contains one negative eigenvalue and and a zero eigenvalue due to the instanton's time translational symmetry. Thus, making the fluctuation factor appear divergent. However, these divergent terms can be handled in a physically sensible manner and be rendered finite by means of analytic continuation and use of the Faddeev Popov method [41]. The calculation of $k(\beta)$ via canonical instanton theory is fundamentally limited to temperatures below the crossover temperature T_c which marks the temperature below which tunneling contributions become dominant. The accuracy of the calculation that one might hope to achieve at best, using this semiclassical approach, is to obtain a rate constant which is in the right order of magnitude compared to a full quantum mechanical calculation.

5 Microcanonical Instanton Theory

While canonical instanton theory is nowadays a widespread approach to calculate thermal rate constants below T_c it has also limitations which make its use impractical in a variety of different reactions. For example in the case of bi-molecular reactions that take place in the gas phase, the assumption of thermal equilibrium is sometimes not justified. In these circumstances one might be interested in a reaction rate constant $k(E)$ which describes the rate of a reaction dependent on the (collision)-energy of the system rather than the temperature. This corresponds to a formulation of instanton theory in the microcanonical ensemble. Furthermore, it is possible to obtain thermal rate constants from microcanonical rate constants via a Laplace transform and subsequently obtain rate constants at all temperatures above and below T_c naturally [43]. Lastly, it is possible to remedy the overestimation of the thermal rate constant close to T_c caused by the direct canonical calculation, if one calculates microcanonical rate constants first and thermally averages them afterwards. In this chapter the basic concept of microcanonical instanton theory is introduced and its current formulation, which heavily relies on the calculation of so-called stability parameters, is reviewed. Like the previous chapter 4 this chapter is meant to be an overview of the current formulation of microcanonical instanton theory.

5.1 Decay of the False Ground State

As mentioned before in section 4.1 the decay of a metastable state can be described by an imaginary part of its energy E. If one defines the energy to be $E = E_{\mathrm{Re}} + \mathrm{i}E_{\mathrm{Im}}$, one obtains for the wave function of the metastable state

$$\Psi_0(\mathbf{x})\mathrm{e}^{-\mathrm{i}\frac{E}{\hbar}t} = \Psi_0(\mathbf{x})\mathrm{e}^{-\mathrm{i}\frac{E_{\mathrm{Re}}}{\hbar}t}\mathrm{e}^{\frac{E_{\mathrm{Im}}}{\hbar}t} = \Psi_0(\mathbf{x})\mathrm{e}^{-\mathrm{i}\frac{E_{\mathrm{Re}}}{\hbar}t}\mathrm{e}^{-\frac{\gamma}{2}t} \tag{5.1}$$

such that γ describes the decay rate of the state

$$\int |\Psi_0(\mathbf{x})|^2 \, d\mathbf{x} = \mathrm{e}^{-\gamma t} \ . \tag{5.2}$$

Let's take the simple example of a one-dimensional potential as depicted in Figure 5.1 and estimate the complex energy. This can simply be done by looking at the

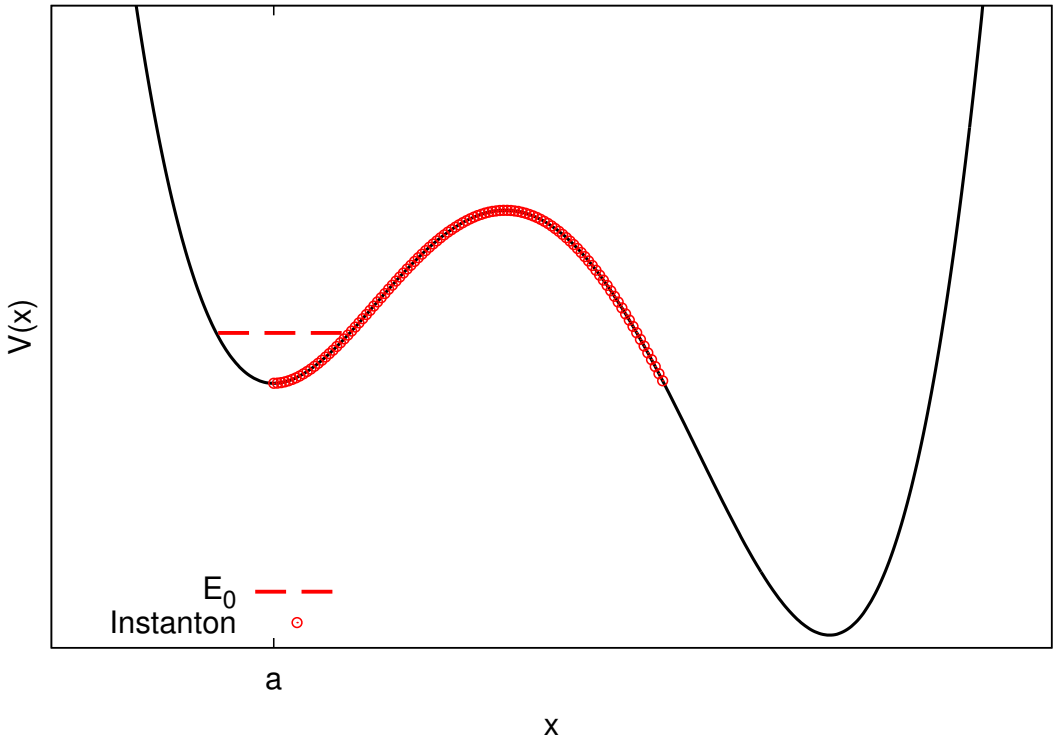

Figure 5.1: Schematic plot of a quartic potential with the ground state energy E_0 marked by the dashed line and the corresponding instanton solution by the dotted line.

transmission amplitude of a particle localized at $x = a$ for a very large time interval $T = t_\mathrm{f} - t_\mathrm{i} \ggg 1$,

$$\left\langle a, t_\mathrm{f} \middle| \mathrm{e}^{-\frac{\mathrm{i}}{\hbar}\hat{H}(t_\mathrm{f}-t_\mathrm{i})} \middle| a, t_\mathrm{i} \right\rangle \ . \tag{5.3}$$

If one performs a Wick rotation and moves to Euclidean time such that $(t_\mathrm{f} - t_\mathrm{i}) = -\mathrm{i}\tau$, one obtains for large τ

$$\left\langle a \middle| \mathrm{e}^{-\hat{H}\tau/\hbar} \middle| a \right\rangle \sim \Psi_0 \Psi_0^* \mathrm{e}^{-E_\mathrm{Re}\tau/\hbar} \mathrm{e}^{-\mathrm{i}\frac{\gamma}{2}\tau} \ . \tag{5.4}$$

If the amplitude in Eq. (5.4) is then approximated with the instanton solution of the particle going from a to a in an infinitely long time interval $\tau \to \infty$ in the upside-down potential as shown by the red line in Figure 5.1, the semiclassical approximation of the amplitude becomes [22]

$$\left\langle a \middle| \mathrm{e}^{-\hat{H}\tau/\hbar} \middle| a \right\rangle_\mathrm{SC} = \sqrt{\frac{\omega}{\pi\hbar}} \mathrm{e}^{-\frac{\omega}{2}\tau} \exp\left(\sqrt{\frac{\mathcal{W}}{2\pi\hbar}} \sqrt{\frac{\prod_{i=1}^{N} \lambda_i^\mathrm{RS}}{\prod_{i=1}^{N-2} \lambda_i^\mathrm{Inst}}} \frac{\mathrm{i}}{2} \frac{\tau}{\sqrt{|\lambda_{-1}|}} \mathrm{e}^{-\mathcal{W}/\hbar} \right) \ . \tag{5.5}$$

The expression in Eq. (5.5) now enables us to identify the metastable state's energy E_0 by comparing the arguments of the exponential functions in Eq.(5.4) and Eq.(5.5) so that one obtains

$$E_0 = \frac{\hbar\omega}{2} - \mathrm{i}\frac{\hbar}{2} \sqrt{\frac{\mathcal{W}}{2\pi\hbar}} \sqrt{\frac{\prod_{i=1}^{N} \lambda_i^\mathrm{RS}}{\prod_{i=1}^{N-2} \lambda_i^\mathrm{Inst}}} \frac{1}{\sqrt{|\lambda_{-1}|}} \mathrm{e}^{-\mathcal{W}/\hbar} \tag{5.6}$$

with ω^2 being the curvature of the potential at point a. This is a very important result because one can immediately see that the energy of the classical solution that is needed in order to determine the decay rate of the ground state is not equal to the ground state energy itself but equal to $V(a)$. Furthermore, the ground state's decay rate was obtained by taking the low temperature limit of $\beta \to \infty$ of the canonical expression in which only the contribution of the ground state remains. If one was interested in all the decay rates for all possible energies, one would have to find all the poles of the trace of the fixed energy propagator as in Eq. (2.62)

$$G(E) = \mathrm{Tr}\left(\delta(\hat{H} - E) \right) \tag{5.7}$$

$$= \frac{1}{2\pi\hbar} \int \mathrm{e}^{\frac{\mathrm{i}}{\hbar}ET} \int \left\langle \mathbf{x} \middle| \mathrm{e}^{-\frac{\mathrm{i}}{\hbar}\hat{H}T} \middle| \mathbf{x} \right\rangle d\mathbf{x}\, dT \ , \tag{5.8}$$

where $E = E_\mathrm{Re} - \mathrm{i}\hbar\gamma/2$ has a small imaginary part γ such that $\gamma \ll E_\mathrm{Re}$. Unlike in the canonical ensemble in which only closed paths of a fixed time interval T (or in

Euclidean time $iT = \beta\hbar$) but all possible energies are permitted, in this case one has to sum over all closed paths of a fixed energy E, but different time periods T are taken into account. An exact quantum mechanical treatment of $G(E)$ would for example require solving the Schrödinger equation or make use of the path integral formalism for the propagator in Eq. (5.8) and evaluate the path integral. Since neither of these methods allow for an exact solution in the case of more complex multidimensional systems, nor is a numerical treatment feasible for more than a few degrees of freedom, one has to approximate the trace of $G(E)$. Fortunately, the path integral representation of $G(E)$ enables a semiclassical treatment which will be used in the following section and heavily relies on the works of Gutzwiller [44,45] and Miller [19, 31, 46].

5.2 Flux Formalism in the Microcanonical Ensemble

In chapter 4 the formulation of instanton theory in the canonical ensemble was introduced via the imaginary F premise. However, one can equivalently use the flux formalism in which the thermal rate constant would be given by the flux operator as defined in Eq. (3.32).

$$k(\beta) = \langle \mathcal{F} \rangle = \frac{\mathrm{Tr}\left(\hat{\mathcal{F}} \mathrm{e}^{-\beta \hat{H}}\right)}{\mathrm{Tr}\left(\mathrm{e}^{-\beta \hat{H}}\right)} \tag{5.9}$$

One can show that the flux formalism is equivalent to the imaginary F premise [47]. However, in order to get a semiclassical approximation of the rate constant via instanton theory for the microcanonical case, one has to make use of the flux formalism as described earlier in section 3.4.2. The microcanonical rate constant $k(E)$ is given in Eq. (3.40) as

$$k(E) = \langle \mathcal{F} \rangle = \frac{\mathrm{Tr}\left(\mathcal{F}\delta(\hat{H} - E)\right)}{\mathrm{Tr}\left(\delta(\hat{H} - E)\right)} \tag{5.10}$$

$$= \frac{1}{2\pi\hbar} \frac{P(E)}{\nu(E)} \ . \tag{5.11}$$

The cumulative reaction probability $P(E)$ as shown in section 3.5 is given by the trace of the product of the flux operator and the microcanonical density operator.

$$P(E) = 2\pi\hbar \ \mathrm{Tr}\left(\hat{\mathcal{F}}\delta(\hat{H}-E)\right) \tag{5.12}$$

Using the Fourier representation of the delta distribution and the definition of the flux operator $\mathcal{F}$ in Eq. (3.39) one obtains

$$P(E) = \int dT \int d\mathbf{x} \left\langle \mathbf{x}\middle|\hat{\mathcal{F}}\mathrm{e}^{-\frac{\mathrm{i}}{\hbar}(\hat{H}-E)T}\middle|\mathbf{x}\right\rangle \tag{5.13}$$

$$= \int dT \iint d\mathbf{x}d\mathbf{x}' \left\langle \mathbf{x}\middle|\hat{\mathcal{F}}\middle|\mathbf{x}'\right\rangle \left\langle \mathbf{x}'\middle|\mathrm{e}^{-\frac{\mathrm{i}}{\hbar}(\hat{H}-E)T}\middle|\mathbf{x}\right\rangle \tag{5.14}$$

$$= \int dT \iint d\mathbf{x}''d\mathbf{x}' \left\langle \mathbf{x}''\middle|\hat{\mathcal{F}}\middle|\mathbf{x}'\right\rangle \int_{x(0)=x''}^{x(T)=x'} \mathcal{D}x(t)\mathrm{e}^{\frac{\mathrm{i}}{\hbar}(\mathcal{S}+ET)} \ . \tag{5.15}$$

In order to simplify the following results atomic units $\hbar = m_\mathrm{e} = 4\pi\epsilon_0 = 1$, $c = 1/\alpha$ and mass weighted coordinates $x_i \to \sqrt{m_i}x_i$ are used from now on. In the next step one moves from real time to imaginary time $\mathrm{i}T = \beta\hbar$ and a steepest descent integration is peformed. This yields the following semiclassical approximation [19]

$$P_\mathrm{SC}(E) = \sum_{k=1}^{\infty}(-1)^{k-1}\prod_{i=1}^{D-1}\frac{1}{2\sinh(ku_i(E)/2)}\mathrm{e}^{-k\mathcal{W}_\mathrm{Inst}(E)} \tag{5.16}$$

The detailed derivation of Eq. (5.16) can be found in Ref. 19. The expression which is used here for $P_\mathrm{SC}(E)$ is essentially $P(E,J)$ for $J=0$ as the J-shifting approximation [48, 49] in which the rotational motion is assumed to be separable from the internal motion is applied throughout the following calculations. Furthermore, chapter 6 contains a more detailed derivation of the expression for the stability parameters u_i including a different formulation which will later turn out to be the basis for the numerical algorithms presented in this thesis. The result in Eq. (5.16) has a couple of interesting features that are worth mentioning. First, the exponential factor is given by the instanton's shortened action $\mathcal{W}_\mathrm{inst} = \int \dot{\mathbf{x}}^2 d\tau$.

This is a direct consequence of the fact that the energy E is kept constant as

$$S_{\text{Inst}} - E\beta = \int_0^\beta \left(\frac{\dot{\mathbf{x}}^2}{2} + V(\mathbf{x}) - E \right) d\tau \tag{5.17}$$

$$= \int_0^\beta \left(\frac{\dot{\mathbf{x}}^2}{2} + V(\mathbf{x}) + \frac{\dot{\mathbf{x}}^2}{2} - V(\mathbf{x}) \right) d\tau \tag{5.18}$$

$$= \int_0^\beta \dot{\mathbf{x}}^2 d\tau \equiv \mathcal{W} \ , \tag{5.19}$$

and in imaginary time $E = (\mathrm{i}p)^2/2 + V(\mathbf{x})$ is conserved along the orbit. The summation of k in Eq. (5.16) is due to the fact that in principle one has to sum over all classical solutions with the same energy E, which also includes solutions that pass the instanton's orbit multiple times. Since the contributions of those trajectories are weighted with $\exp(-k\mathcal{W})$, with k being the multiplicity of the orbit, their contributions decay exponentially and can be neglected at low energies. However, for an instanton, with an energy E close to the transition state's energy E_{TS} this becomes an increasingly bad approximation since close to E_{TS} the shortened action $\mathcal{W}$ gets smaller and ultimately vanishes at $E = E_{\text{TS}}$. This neglect of contributions from repetitions of the instanton's orbit leads to the familiar overestimation of $k(\beta)$ close to the crossover temperature T_c, if canonical instanton theory as described in chapter 4 is applied. The term $\prod_{i=1}^{D-1}(2\sinh(ku_i/2))^{-1}$ represents the second order quantum corrections to the classical solution. The parameters u_i are the so-called stability parameters which were first introduced by Gutzwiller in order to calculate a semiclassical approximation for the density of states [45].

5.3 Stability Parameters and the Monodromy Matrix

In order to obtain the stability parameters, first the monodromy matrix $\mathbf{M}$ has to be determined. It contains information about how significantly a solution to the classical equations of motion deviates from its reference position and momentum under an infinitesimal perturbation of $\delta\mathbf{x}_0$ and $\delta\mathbf{p}_0$ after a time period T_0 has passed. A simple example of such behavior is depicted in Figure 5.2. The

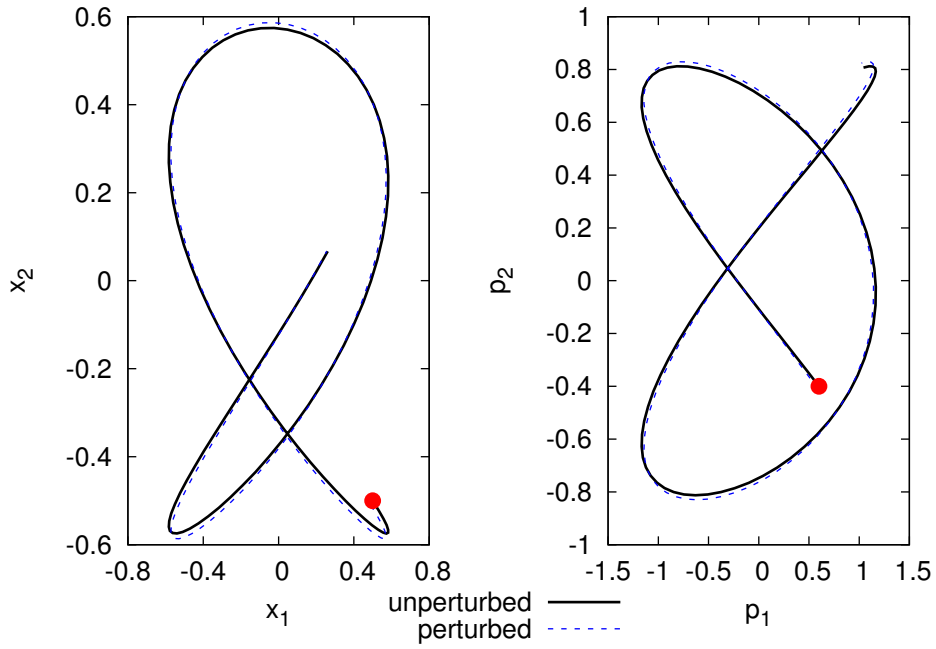

Figure 5.2: The black line shows the position $(x_1, x_2)^T$ and momentum $(p_1, p_2)^T$ of the classical solution of a particle of unit mass moving in the potential $V(x, y) = x^2 + 2y^2$. The dotted blue line shows the behavior of the perturbed solution. The red dot indicates the starting point of the trajectory.

monodromy matrix is defined as [45]

$$\begin{pmatrix} \delta\mathbf{x} \\ \delta\mathbf{p} \end{pmatrix} = \mathbf{M}(T_0) \begin{pmatrix} \delta\mathbf{x}_0 \\ \delta\mathbf{p}_0 \end{pmatrix} , \tag{5.20}$$

where $\mathbf{M}$ is the solution to the linearized equations of motion

$$\frac{d}{dt}\mathbf{M}(t) = \begin{pmatrix} 0 & \mathbf{1} \\ -\mathbf{V}''\left(\left(\mathbf{x}\left(t\right)\right)\right. & 0 \end{pmatrix} \mathbf{M}(t) , \tag{5.21}$$

with the initial condition $\mathbf{M}(0) = \mathbf{I}$ and evaluated at $t = T_0$ [45]. Thus, the eigenvalues of $\mathbf{M}$ inform about the stability of the trajectory. Eigenvalues with an imaginary part and $|\lambda = 1|$ describe a stable deviation whereas real values of

λ are connected to unstable modes. Furthermore, in a conservative system there are two eigenvalues with $\lambda = 1$. These describe a displacement along the path. Additionally, $\mathbf{M}$ is a symplectic matrix meaning that eigenvalues always appear in pairs. If λ_i is an eigenvalue, so is $1/\lambda_i$. The stability parameters u_i from Eq. (5.16) are then defined as $\mathrm{e}^{\pm u_i} = \lambda_i$. Since the instanton solutions in the context of this thesis are always unstable trajectories in a conservative system one always has purely real eigenvalues and at least two eigenvalues which are equal to 1. So in order to obtain the stability parameters one principally needs to determine the instanton solution and its Hessians along the path, plug it in the differential equation in Eq. (5.21) and determine the natural log of the eigenvalues of $M(T_0)$ while excluding the modes along the path with $\lambda = 1$. However, the numerical integration of Eq. (5.21) turns out to be rather tricky, if the available number of discrete points of the instanton trajectory is very low, which is typically the case in real chemical systems. For these reasons new approximate approaches as well as an alternative evaluation method, based on the numerical evaluation of the Van Vleck propagator, are presented in chapter 6.

5.4 Evaluation of $P_{\mathrm{SC}}(E)$ and Summation over Multiple Orbits

If all contributions from multiple instanton orbits ought to be taken into account, the summation over k in Eq. (5.16) has to be performed. In order to achieve this one first uses the series representation of the sinh function,

$$\frac{1}{2\sinh(k\frac{u_i}{2})} = \sum_{n_i=0}^{\infty} \mathrm{e}^{-k\left(\frac{1}{2}+n_i\right)u_i} \ . \tag{5.22}$$

Plugging Eq. (5.22) in Eq. (5.16) results in

$$P_{\mathrm{SC}}(E) = \sum_{k=1}^{\infty}\sum_{n_1=0}^{\infty}\sum_{n_2=0}^{\infty}\cdots\sum_{n_{D-1}=0}^{\infty}(-1)^{k-1}\mathrm{e}^{-k\left(\mathcal{W}(E)+\sum_{i=1}^{D-1}(1/2+n_i)u_i(E)\right)} \ . \tag{5.23}$$

Changing the order of summation and performing the sum over k first gives [19]

$$P_{\mathrm{SC}}(E) = \sum_{n_1=0}^{\infty} \cdots \sum_{n_{D-1}=0}^{\infty} \frac{1}{1 + \mathrm{e}^{\mathcal{W}(E)+\sum_{i=1}^{D-1}(1/2+n_i)u_i(E)}} \ . \tag{5.24}$$

At first one might ask what kind of improvement the series representation in Eq. (5.24) holds. This becomes evident, if one looks at the Eq. (5.24) in the limit in which all orthogonal modes are separable. In this case the stability parameters are given by

$$u_i = \omega_i T_0 = -\frac{d\mathcal{W}}{dE}\omega_i \ , \tag{5.25}$$

with ω_i being the frequency of the i^{th} orthogonal mode and using the fact that $\frac{dW}{dE} = -T_0$. In this particular case one can then approximate the argument in the exponential function as [19]

$$\mathcal{W}(E) + \sum_{i=1}^{D-1}\left(\frac{1}{2}+n_i\right)u_i(E) = \mathcal{W}(E) - \frac{d\mathcal{W}}{dE}\sum_{i=1}^{D-1}\left(\frac{1}{2}+n_i\right)\omega_i \tag{5.26}$$

$$\approx \mathcal{W}\left(E - \sum_{i=1}^{D-1}\left(\frac{1}{2}+n_i\right)\omega_i\right) \ . \tag{5.27}$$

This is a very interesting result since it tells us that if one wants to compute the semiclassically approximated cumulative reaction probability, the energy at which the shortened action needs to be evaluated is reduced by the second order quantum corrections orthogonal to the instanton path. This is due to the same reason which was previously discussed in section 5.1 which treated the semiclassical approximation of the ground state's decay rate. It showed an energy difference between the real part of the ground state's energy and the instanton's energy describing its decay. However, in this formulation it is applicable to energies above the ground state energy. One can generalize the expression in Eq. (5.27) to coupled degrees of freedom by using the following expression [19, 50]

$$W(E - E_n), \text{ with } E_n = E - \sum_{i=1}^{D-1}\left(\frac{1}{2}+n_i\right)\frac{u_i(E-E_n)}{T_0(E-E_n)} \ . \tag{5.28}$$

This yields for the final expression

$$P_{\mathrm{SC}}(E) = \sum_{n_1=0}^{\infty} \cdots \sum_{n_{D-1}=0}^{\infty} \frac{1}{1 + \exp\left[\mathcal{W}\left(E - \sum_{i=1}^{D-1}(\frac{1}{2} + n_i)\frac{u_i(E-E_n)}{T_0(E-E_n)}\right)\right]} \,. \tag{5.29}$$

So in order to compute E_n one has to solve the self-consistent expression on the right in Eq. (5.28), which requires the ability to compute an instanton and its stability parameters iteratively until a solution for a given set of values for $n_1, ..., n_{D-1}$ is obtained. This then needs to be repeated for every combination of n_i in the summation in Eq. (5.29). Nevertheless, in the case of low energies or large values for u_i the summation can be truncated after a few terms as contributions for higher numbers of n_i decay exponentially.

5.5 Summary

Instead of making use of the imaginary F premise, as it is done in the derivation of canonical instanton theory, one has to invoke the flux formalism in which the rate constant can be expressed as the expectation value of the flux operator $\hat{\mathcal{F}}$. In the microcanonical ensemble such a calculation requires in principle the evaluation of the trace of the fixed energy propagator. The expectation value of the flux is then calculated via a steepest descent integration which yields a semiclassical approximation for the cumulative reaction probability $P_{\mathrm{SC}}(E)$. The computation of $P_{\mathrm{SC}}(E)$ then requires the calculation of stability parameters of the instanton's modes which are orthogonal to its path. The stability parameters u_i themselves contain information about the orbit's stability but, in this context, are used to calculate second order quantum corrections to the cumulative reaction probability. These fluctuations have the effect of lowering the classical energy at which the instanton has to be evaluated. For example, in the case of the decay of the ground state the corresponding classical energy equals the reactant state energy and therefore corresponds to an infinitely long orbit. The calculation of stability parameters requires solving the linearized equation of motion in order to obtain the monodromy matrix and its eigenvalues. In essence, the formulation of microcanonical instanton theory presented in this chapter has been around since the

late 1970's [19]. However, it has been rarely used for real chemical systems with a high number of degrees of freedom and in general coupled vibrational modes, in particular coupling to the transition mode. The main reason is the lack of efficient and accurate algorithms to compute the necessary quantities. Therefore, in the second part of this thesis, beginning with chapter 6, new methods to calculate microcanonical and canonical rate constants are presented.

Part II

New Methods and Applications

6 New Methods to Calculate Canonical and Microcanonical Rate Constants

The second part of this thesis focuses on the derivation of new methods and numerical algorithms to calculate the necessary quantities which are needed in order to compute canonical and microcanonical rate constants. In the canonical case the main interest lies in the development of new methods that enable the calculation of thermal rate constants with the same accuracy as the conventional determinant method as described in section 4, yet without the need for diagonalizing large matrices. In the microcanonical case the main task is the computation of the cumulative reaction probability and consequently the calculation of stability parameters. It turns out that in both ensembles an efficient calculation of the rate constant using instanton theory relies on the accurate calculation of stability parameters u_i and additionally in the canonical case the calculation of the rate of change of the instanon's energy with respect to its imaginary time period, $dE/d\beta$. In order to come up with efficient algorithms to calculate these two quantities two principle tools are used. First the method for the calculation of u_i is based on an adaptation of the Van Vleck propagator in imaginary time. The second method to determine $dE/d\beta$ relies only on energy conservation. Additionally, different approximation schemes for the calculation of u_i are suggested which were the product of earlier works for this thesis. In both cases all suggested **methods and results** in this part of the thesis have **already been published** in References 51 and 52.

6.1 Fluctuation Factor for Canonical and Microcanonical Rate Constants

The calculation of the stability parameters is based on the Van Vleck propagator [53] whose final form was derived by Gutzwiller using a stationary phase approximation of the propagator's path integral representation [44]. For a particle moving in real time t from $\mathbf{x}'$ to $\mathbf{x}''$ it is given in atomic units as

$$K_{\mathrm{SC}}(\mathbf{x}'', \mathbf{x}', t) = \sum_{\text{class. paths}} \left(\frac{1}{2\pi \mathrm{i}}\right)^{\frac{D}{2}} \sqrt{\left| -\frac{\partial^2 \mathcal{S}_{\mathrm{cl}}}{\partial \mathbf{x}' \partial \mathbf{x}''} \right|} \, \mathrm{e}^{\mathrm{i}\mathcal{S}_{\mathrm{cl}} - i\nu\frac{\pi}{2}} \ , \tag{6.1}$$

where $\mathcal{S}_{\mathrm{cl}}$ is the action of the classical path going from $\mathbf{x}'$ to $\mathbf{x}''$ in real time. The phase factor ν is called the Maslov–Morse index which counts the number of zeros of the determinant. This is due to the fact that every time the determinant becomes zero or infinite the Fresnel type integrals that appear in the stationary phase approximation are affected by a phase change that adds to the overall phase of K_{SC} [27]. In order to use the expression in Eq. (6.1) for imaginary time trajectories one can perform the same steepest descent approximation for the Wick rotated path integral $t = -\mathrm{i}\tau$ and obtain [54]

$$K_{\mathrm{sc}}(\mathbf{x}'', \mathbf{x}', \tau) = \sum_{\text{class. paths}} \left(\frac{1}{2\pi}\right)^{\frac{D}{2}} \sqrt{\left| -\frac{\partial^2 \mathcal{S}_{\mathrm{E}}}{\partial x_i' \partial x_j''} \right|} e^{-\mathcal{S}_{\mathrm{E}} + i\nu\frac{\pi}{2}} \ , \tag{6.2}$$

with the Euclidean action of the classical solution $\mathcal{S}_E$ replacing the one in real time. In order to obtain a thermal rate constant expression one first has to calculate the semiclassical approximation for the canonical partition function Q^{SC}. The first step is to take the trace of Eq. (6.2)

$$Q^{\mathrm{SC}} = \int K_{\mathrm{sc}}(\mathbf{x}, \mathbf{x}, \beta) d\mathbf{x} \ . \tag{6.3}$$

In order to evaluate the trace, a steepest descent integration is performed. Using that for the classical solution $\frac{\partial \mathcal{S}_\mathrm{E}}{\partial \mathbf{x}} = 0$ and

$$\frac{\partial^2 \mathcal{S}_\mathrm{E}}{\partial \mathbf{x}^2} = \left(\frac{\partial^2 \mathcal{S}_\mathrm{E}}{\partial \mathbf{x}' \mathbf{x}'} + 2\frac{\partial^2 \mathcal{S}_\mathrm{E}}{\partial \mathbf{x}' \mathbf{x}''} + \frac{\partial^2 \mathcal{S}_\mathrm{E}}{\partial \mathbf{x}'' \mathbf{x}''} \right) \Big|_{\mathbf{x}'=\mathbf{x}''=\mathbf{x}} , \tag{6.4}$$

one finally gets

$$Q^\mathrm{SC} = \sum_j Q^{\mathrm{SC},j} \tag{6.5}$$

with

$$\begin{aligned} Q^{\mathrm{SC},j} = & \sqrt{\frac{\left| -\frac{\partial^2 \mathcal{S}_\mathrm{E}^j}{\partial \mathbf{x}' \partial \mathbf{x}''} \right|_{x'=x''=x}}{\left| \frac{\partial^2 \mathcal{S}_\mathrm{E}^j}{\partial \mathbf{x}' \partial \mathbf{x}'} + 2\frac{\partial^2 \mathcal{S}_\mathrm{E}^j}{\partial \mathbf{x}' \partial \mathbf{x}''} + \frac{\partial^2 \mathcal{S}_\mathrm{E}^j}{\partial \mathbf{x}'' \partial \mathbf{x}''} \right|_{x'=x''=x}}} \times \\ & \exp\left(-\mathcal{S}_\mathrm{E}^j - \mathrm{i}\frac{\pi}{2}\nu_j \right) \\ & = F_j \exp\left(-\mathcal{S}_\mathrm{E}^j \right) \exp\left(-\mathrm{i}\frac{\pi}{2}\nu_j \right) \ . \end{aligned} \tag{6.6}$$

The term S_E^j describes the Euclidean action of the j^th classical imaginary time trajectory and the F_j is the corresponding fluctuation factor containing the second order quantum corrections. Since the classical solution that corresponds to the reactant state is simply a particle at rest, it has no turning points, hence $\nu = 0$ and the Euclidean action simply becomes $\mathcal{S}_\mathrm{RS} = \beta V(\mathbf{x}_\mathrm{RS})$. The instanton is a closed orbit and therefore ν depends on how often the particle reaches the turning points. In this case ν can have values of $2k$ where k gives the number of repetitions of the instanton orbit. However, an additional phase factor of $-\mathrm{i}\pi/2$ has to be added in order to account for the fact that the instanton travels only in the classically forbidden region and therefore only contributes to the imaginary part of the partition function. Considering only one orbit of the instanton results in $\nu = 2$ and the fluctuation factor turns imaginary as $\exp(-\mathrm{i}(\nu\frac{\pi}{2} + \frac{\pi}{2})) = \mathrm{i}$. This

gives for the partition function of the reactant and the transition state

$$Q_{\mathrm{RS}} = F_{\mathrm{RS}} \mathrm{e}^{-\mathcal{S}_{\mathrm{RS}}} \ , \tag{6.7}$$

$$Q_{\mathrm{Inst}} = \mathrm{i} F_{\mathrm{Inst}} \mathrm{e}^{-\mathcal{S}_{\mathrm{Inst}}} . \tag{6.8}$$

The term F can in principle be divergent. This is due to symmetries present in the system which lead to an over-counting of real physical states and therefore to a diverging partition function. Since the instanton is a closed orbit the action is invariant with respect to the choice of the starting and end point as $\mathbf{x}' = \mathbf{x}'' = \mathbf{x}$. Furthermore rotation and translational invariance are also symmetries that lead to diverging terms, yet these can easily be handled as those symmetries are also present in the reactant partition function and therefore cancel one another if one is only interested in their ratios. In order to handle the divergent terms, F is expressed in a different representation. First a matrix $\mathbf{M}$ with the following entries is constructed

$$\mathbf{M} = \begin{pmatrix} -\mathbf{b}^{-1}\mathbf{a} & -\mathbf{b}^{-1} \\ \mathbf{b} - \mathbf{c}\mathbf{b}^{-1}\mathbf{a} & -\mathbf{c}\mathbf{b}^{-1} \end{pmatrix} \ , \tag{6.9}$$

whereby $\mathbf{a}, \mathbf{b}$ and $\mathbf{c}$ are defined as

$$\mathbf{a} = \left. \frac{\partial^2 \mathcal{S}_{\mathrm{E}}}{\partial \mathbf{x}' \partial \mathbf{x}'} \right|_{\mathbf{x}'=\mathbf{x}''=\mathbf{x}} \ , \tag{6.10}$$

$$\mathbf{b} = \left. \frac{\partial^2 \mathcal{S}_{\mathrm{E}}}{\partial \mathbf{x}' \partial \mathbf{x}''} \right|_{\mathbf{x}'=\mathbf{x}''=\mathbf{x}} \ , \tag{6.11}$$

$$\mathbf{c} = \left. \frac{\partial^2 \mathcal{S}_{\mathrm{E}}}{\partial \mathbf{x}'' \partial \mathbf{x}''} \right|_{\mathbf{x}'=\mathbf{x}''=\mathbf{x}} \ , \tag{6.12}$$

such that the fluctuation factor in Eq. (6.6) can be written as

$$F = \sqrt{\frac{|-\mathbf{b}|}{|\mathbf{a} + 2\mathbf{b} + \mathbf{c}|}} = \sqrt{\frac{(-1)^D}{|\mathbf{M} - \mathbf{1}|}} \ . \tag{6.13}$$

If $\mathbf{M}$ is represented in its eigenbasis one can immediately see that the right-hand side of Eq. (6.13) diverges as $\mathbf{M}$ has eigenvalues of $\lambda = 1$. These correspond to the symmetries of the system. The matrix $\mathbf{M}$ here is the monodromy matrix as

introduced in section 5.3. With the definition $\lambda_i = e^{\pm u_i}$, one gets for the fluctuation factor

$$F = \sqrt{\prod_{i=1}^{D} \frac{-1}{(e^{u_i} - 1) \cdot (e^{-u_i} - 1)}} \tag{6.14}$$

$$= \sqrt{\prod_{i=1}^{D} \frac{-1}{2 - 2\cosh(u_i)}} \tag{6.15}$$

$$= \prod_{i=1}^{D} \frac{1}{2\sinh\left(u_i/2\right)}. \tag{6.16}$$

The fluctuation factor F including all D degrees of freedom is obviously divergent as it has at least one zero-valued stability parameter $u_i = 0$, in the case of rotational and translational symmetries an additional six, zero-valued stability parameters. For now only the vibrational contributions to the partition function will be considered, such that there is one divergent term remaining due to one zero-valued stability parameter caused by the fluctuations along the path. The fluctuation factor can then be written as

$$F^{\mathrm{Inst}} = F_{\parallel}^{\mathrm{Inst}} \prod_{i=1}^{D_\nu - 1} \frac{1}{2\sinh\left(u_i/2\right)} \tag{6.17}$$

where D_ν describes the number of vibrational degrees of freedom. The parallel fluctuation factor $F_{\parallel}^{\mathrm{Inst}}$, which only appears in the instanton partition function, can not be described by Eq. (6.16) due to u being zero. However, it can be addressed by applying the Faddeev–Popov trick to avoid the over-counting of ghost states in order to render the partition function finite [41]. In this case, however, one can use a much simpler approach to find an expression for $F_{\parallel}^{\mathrm{Inst}}$. The idea is to compare the rate constant obtained by the imaginary F premise with the rate constant obtained by thermally averaging the cumulative reaction probability and from that infer the expression for $F_{\parallel}^{\mathrm{Inst}}$. One starts first by looking at the thermal

rate constant as described in section 4.1. It is given by

$$k(\beta) = \frac{2}{\hbar\beta}\frac{\mathrm{Im}Q_k}{\mathrm{Re}Q_k} \ . \tag{6.18}$$

Using the semiclassical expressions in Eq. (6.8) and Eq. (6.7) and inserting them into Eq. (6.18) yields

$$k(\beta) = \frac{2}{\beta}Q_{\text{t-r}}\frac{2\prod_{j=1}^{D_\nu}\sinh(u_j^{\mathrm{RS}}/2)}{\prod_{i=1}^{D_\nu-1}\sinh(u_i^{\mathrm{Inst}}/2)}F_{\parallel}^{\mathrm{Inst}}\mathrm{e}^{-\mathcal{S}_{\mathrm{Inst}}+\mathcal{S}_{\mathrm{RS}}} \ , \tag{6.19}$$

whereby the term $Q_{\text{t-r}}$ is the ratio of the translational and rotational partition functions of the transition state and the reactant state. Starting in the microcanonical ensemble the thermal rate constant is given by a Laplace transform of $P_{\mathrm{SC}}(E)$ as seen in Eq. (3.29)

$$k(\beta) = \frac{Q_{\text{t-r}}}{2\pi Q_{\mathrm{RS}}}\int_{-\infty}^{\infty}P_{\mathrm{SC}}(E)\exp(-\beta E)dE \ , \tag{6.20}$$

with Q_{RS} being the vibrational partition function of the reactant state. In order to evaluate Eq. (6.20) one performs a steepest descent approximation of the integral using the semiclassical expression for $P_{\mathrm{SC}}(E)$ in Eq. (5.16) for $k = 1$ such that

$$\int_{-\infty}^{\infty}F_{\perp}^{\mathrm{Inst}}(E)\mathrm{e}^{-(\beta E+\mathcal{W})}dE \approx \sqrt{\frac{2\pi}{\frac{d^2\mathcal{W}}{dE^2}}}F_{\perp}^{\mathrm{Inst}}(E_0)\mathrm{e}^{-(\beta E_0+\mathcal{W}(E_0))} \ , \tag{6.21}$$

with $F_{\perp}(E) \equiv \prod_{i=1}^{D_\nu-1}\left(2\sinh(u_i(E)/2)\right)^{-1}$ and E_0 satisfying the condition $\frac{d}{dE}\left(\mathcal{W}+\beta E\right) = 0$. From that the relation $\frac{d\mathcal{W}}{dE} = -\beta$ is obtained which results in

$$k(\beta) = \frac{Q_{\text{t-r}}}{\sqrt{2\pi}Q_{\mathrm{RS}}}\sqrt{-\frac{dE}{d\beta}}\prod_{i=1}^{D_\nu-1}\frac{1}{2\sinh(u_i(E_0)/2)}\mathrm{e}^{-\mathcal{S}_{\mathrm{Inst}}} \ . \tag{6.22}$$

Given the definition $F^{\mathrm{Inst}} \equiv F_{\perp}^{\mathrm{Inst}}F_{\parallel}^{\mathrm{Inst}}$ and comparing Eq. (6.19) with Eq. (6.22)

one gets for the parallel fluctuation factor

$$\begin{aligned}
\frac{2}{\beta}\frac{Q_{\text{t-r}}Q_{\text{Inst}}}{Q_{\text{RS}}} &= \frac{Q_{\text{t-r}}}{\sqrt{2\pi}Q_{\text{RS}}}\sqrt{-\frac{dE}{d\beta}}F_{\perp}^{\text{Inst}}\mathrm{e}^{-\mathcal{S}_{\text{Inst}}}, \\
\frac{2}{\beta}F^{\text{Inst}}\mathrm{e}^{-\mathcal{S}_{\text{Inst}}} &= \frac{1}{\sqrt{2\pi}}\sqrt{-\frac{dE}{d\beta}}F_{\perp}^{\text{Inst}}\mathrm{e}^{-\mathcal{S}_{\text{Inst}}}, \\
F_{\parallel}^{\text{Inst}} &= \sqrt{\frac{\beta^2}{8\pi}}\sqrt{-\frac{dE}{d\beta}}.
\end{aligned} \tag{6.23}$$

The fluctuation factor along the path therefore depends on the time period in imaginary time given by β and the change of the instanton's energy with respect to the change of the period. Thus, in the canonical case one has to locate the instanton at a given β and calculate its stability parameters u_i, as well as $\frac{dE}{d\beta}$. The truncation after $k = 1$ keeps the approach consistent with the direct approach used in the imaginary F premise in which only bounce is considered. Furthermore, for a large number of k, an instanton solution can no longer simply be obtained, as the necessary instanton solution would be above the crossover temperature T_c as $\frac{d\mathcal{W}}{dE} = -\frac{\beta}{k}$. However, at energies close to the transition state energy, where this approximation becomes increasingly bad, one would have to use the summation scheme in Eq. (5.29) and perform the Laplace transform of $P(E)$ numerically, not via the steepest descent approach. In the microcanonical case only the stability parameters u_i have to be determined in order to compute $P(E)$. Thus in either the canonical or microcanonical case, a reliable way has to be found to compute the stability parameters. Additionally if the thermal rate constant is obtained via Eq. (6.22) a reliable method to compute $\frac{dE}{d\beta}$ is needed.

6.2 Calculation of $dE/d\beta$

In order to determine the change of the instanton's energy with respect to β one might be tempted to simply follow a finite difference approach by simply computing two instantons which are a $\Delta\beta$ apart in temperature and calculate $dE/d\beta$ via a difference quotient. While this approach is certainly possible it is rather inefficient as it requires the computation of a least one additional instanton solution.

However, there exits a more elegant approach which works in the following way. Let's first start by looking at the energy conservation of the instanton solution. Since imaginary time is used, the momentum of the pseudoparticle in the classically forbidden region is purely imaginary and therefore the energy E is given by

$$E = \frac{\mathrm{i}^2\mathbf{p}^2}{2} + V(\mathbf{x}) \tag{6.24}$$

$$= -\frac{\mathbf{p}^2}{2} + V(\mathbf{x}). \tag{6.25}$$

The quantity in Eq. (6.25) is conserved along the orbit. In its discretized form it can be written as

$$E = \lim_{P\to\infty}\left(-\frac{(\mathbf{x}_i - \mathbf{x}_{i-1})^2}{2}\left(\frac{P}{\beta}\right)^2 + \frac{1}{2}(V(\mathbf{x}_i) + V(\mathbf{x}_{i-1}))\right) , \tag{6.26}$$

where $\beta/P = \Delta\tau$ is the imaginary time increment for a closed path and P the number of images. The vector $\mathbf{x}_i$ is a D dimensional array that contains the positions for every degree of freedom in mass weighted coordinates at the i^{th} image. Eq. (6.26) implies that $\mathbf{x}_i$ is the position of the pseudoparticle at some time τ' and $\mathbf{x}_{i-1}$ its position at time $\tau' - \Delta\tau$. Since a change in β means that a new instanton solution for a new temperature has to be found one can interpret the points $\mathbf{x}_i$ along the trajectory to be a function of β such that

$$\mathbf{x}_i = \mathbf{x}_i(\beta) \ . \tag{6.27}$$

If Eq. (6.26) is then differentiated with respect to β one obtains

$$\begin{aligned}\frac{dE}{d\beta} = \lim_{P\to\infty}\Bigg(&\frac{P^2}{\beta^3}(\mathbf{x}_i - \mathbf{x}_{i-1})^2 \\ &- \frac{P^2}{\beta^2}(\mathbf{x}_i - \mathbf{x}_{i-1})\left(\frac{d\mathbf{x}_i}{d\beta} - \frac{d\mathbf{x}_{i-1}}{d\beta}\right) \\ &+ \frac{1}{2}\left(\frac{\partial V}{\partial \mathbf{x}_i}\frac{d\mathbf{x}_i}{d\beta} + \frac{\partial V}{\partial \mathbf{x}_{i-1}}\frac{d\mathbf{x}_{i-1}}{d\beta}\right)\Bigg) .\end{aligned} \tag{6.28}$$

In order to evaluate Eq. (6.28) a way is needed to determine the change of an arbitrary point $\mathbf{x}_i$ of the trajectory with respect to β. This can be achieved by first discretizing the classical equation of motion in imaginary time which yields

$$\ddot{\mathbf{x}}(\tau) = \nabla V \ , \tag{6.29}$$

$$(-2\mathbf{x}_i + \mathbf{x}_{i+1} + \mathbf{x}_{i-1}) \frac{1}{\Delta\tau^2} = \nabla V(\mathbf{x}_i) \ , \tag{6.30}$$

$$(2\mathbf{x}_i - \mathbf{x}_{i+1} - \mathbf{x}_{i-1}) + \frac{\beta^2}{P^2}\nabla V(\mathbf{x}_i) = 0 \ . \tag{6.31}$$

Furthermore, it is worth mentioning that the kind of instanton solutions that are used in this context have the property that each image appears exactly twice as the spatial coordinates of the trajectory from the reactant to the product side are the same as on the way back from product to reactant. This leads to $\mathbf{x}_i = \mathbf{x}_{P-i+1}$. However, the following calculations do not use this fact and the algorithms are in general valid for any closed trajectory which may or may not posses turning points. The first step is to differentiate Eq. (6.31) with respect to β. This yields

$$\begin{aligned} \left(2\ \mathbf{I} + \frac{\beta^2}{P^2}\nabla^2 V(\mathbf{x}_i)\right) \frac{d\mathbf{x}_i}{d\beta} - \frac{d\mathbf{x}_{i+1}}{d\beta} - \frac{d\mathbf{x}_{i-1}}{d\beta} &= -\frac{2\beta}{P^2}\nabla V(\mathbf{x}_i) \\ \left(2\ \mathbf{I} + \frac{\beta^2}{P^2}\nabla^2 V(\mathbf{x}_i)\right) \mathbf{q}_i - \mathbf{q}_{i+1} - \mathbf{q}_{i-1} &= -\frac{2\beta}{P^2}\nabla V(\mathbf{x}_i) \ , \end{aligned} \tag{6.32}$$

with $\mathbf{q}_i \equiv \frac{d\mathbf{x}_i}{d\beta}$. Eq. (6.32) is a linear system of equations of the form

$$\mathbf{A}\mathbf{q} = \mathbf{b} \ , \tag{6.33}$$

with $\mathbf{q} = (\mathbf{q}_1, \mathbf{q}_2, \ldots, \mathbf{q}_P)^T$. Alternatively if an index notation is applied one gets

$$\sum_{i'=1}^{P}\sum_{j'=1}^{D} A_{i,j,i',j'}\ q_{i',j'} = b_{i,j}. \tag{6.34}$$

The matrix $\mathbf{A}$ is given by

$$\mathbf{A} = \begin{pmatrix} \mathbf{K}_1 & -\mathbf{I} & 0 & \cdots & 0 & -\mathbf{I} \\ -\mathbf{I} & \ddots & -\mathbf{I} & \ddots & \ddots & 0 \\ 0 & -\mathbf{I} & \mathbf{K}_i & \ddots & \ddots & \vdots \\ \vdots & \ddots & \ddots & \mathbf{K}_{i+1} & -\mathbf{I} & 0 \\ 0 & \ddots & \ddots & -\mathbf{I} & \ddots & -\mathbf{I} \\ -\mathbf{I} & 0 & \cdots & 0 & -\mathbf{I} & \mathbf{K}_P \end{pmatrix} \tag{6.35}$$

where $\mathbf{K}_i = 2\mathbf{I} + \frac{\beta^2}{P^2}\mathbf{V}''(\mathbf{x}_i)$ and $\mathbf{I}$ is a $D \times D$-dimensional unit matrix. The right hand side of Eq. (6.33) is a PD dimensional vector which contains the D-dimensional gradients of each image along the path

$$\mathbf{b} = -\frac{2\beta}{P^2} \begin{pmatrix} \nabla_1 V(\mathbf{x}_1) \\ \vdots \\ \nabla_D V(\mathbf{x}_1) \\ \nabla_1 V(\mathbf{x}_2) \\ \vdots \\ \nabla_j V(\mathbf{x}_i) \\ \vdots \\ \nabla_D V(\mathbf{x}_P) \end{pmatrix}. \tag{6.36}$$

Solving the linear system in Eq. (6.33) requires the knowledge of all Hessians as well as gradients along the instanton path. Furthermore, the matrix $\mathbf{A}$ is a symmetric sparse $(PD \times PD)$ matrix. Having obtained the solution $\frac{d\mathbf{x}_i}{d\beta} = \mathbf{q}_i$ one can now determine $\frac{dE}{d\beta}$ by choosing any arbitrary point $\mathbf{x}_i$ and use it in Eq. (6.28). In practice the value of $\frac{dE}{d\beta}$ will slightly vary along the path due to numerical errors. Therefore, one chooses that point of the trajectory which is closest to its neighboring point. This is usually one of the two turning points. The calculation of $dE/d\beta$ is the bottleneck of the thermal rate constant calculation, as solving Eq. (6.33) scales of the order of $\mathcal{O}(P^3D^3)$ which is equal to the scaling behavior of a matrix diagonalization of a PD-matrix, as used in the determinant method. Nevertheless, solving a sparse linear system of DP equations has a pre-factor in

terms of computational effort which is 1 to 2 orders of magnitude smaller and therefore still allows for a significant improvement in terms of efficiency compared with the determinant method.

6.3 Calculation of Stability Parameters

The calculation of the stability parameters is traditionally done by integrating the linearized equations of motions in Eq. (5.21) and then determining the eigenvalues of the monodromy matrix. However, in this thesis several alternative methods are proposed which appear numerically more stable if only solutions with a relatively low number of discrete points are available. The method presented in 6.3.1 is to make use of Eq. (6.9), which allows for the calculation of the monodromy matrix by using the second derivatives of $\mathcal{S}_\mathrm{E}$ directly. Furthermore in sections 6.3.2, 6.4.1 and 6.4.2, different approximation schemes are introduced to calculate the stability parameters as additional alternatives to integrating Eq. (5.21) and the method presented in section 6.3.1. Chronologically the approximate methods were used first, since at the beginning of this research project the method in section 6.3.1 hadn't been developed yet and so computation in coupled systems relied on those approximate methods which were published in Ref. 51. Nevertheless, they are still useful computational tools and will therefore be included in the following sections.

6.3.1 Numerical Evaluation of Second Derivatives of $\mathcal{S}_E$

Since an analytical treatment of the second derivatives of $\mathcal{S}_\mathrm{E}$ is only possible in the case of a separable potential in which the orthogonal components of the potential have a linear or quadratic form, a way needs to be found to determine these necessary expressions numerically. Based on the previous work by Richardson [55], one starts with the discretized Euclidean action for an instanton that starts at $\tau = 0$ at the point $\mathbf{x}' = \mathbf{x}_0$ and ends at $\tau = \beta$ at the point $\mathbf{x}'' = \mathbf{x}_P$. Furthermore a constant time interval $\Delta\tau = \beta/P$ is used because an arbitrary open path is considered with $P + 1$ images to derive the first and second variations. However, unlike in Ref. 55 the path is then closed by setting $\mathbf{x}' = \mathbf{x}'' = \mathbf{x}$ resulting in P

independent images. The Euclidean action is in this case given by

$$\mathcal{S}_{\mathrm{E}} = \sum_{i=1}^{P} \left[\frac{1}{2} \frac{(\mathbf{x}_i - \mathbf{x}_{i-1})^2}{\Delta\tau} + \frac{\Delta\tau}{2} \left(V(\mathbf{x}_i) + V(\mathbf{x}_{i-1}) \right) \right] . \tag{6.37}$$

The first derivative of Eq. (6.37) is simply the partial derivative with respect to $\mathbf{x}'$ and $\mathbf{x}''$

$$\frac{\partial \mathcal{S}_{\mathrm{E}}}{\partial \mathbf{x}'} = -\frac{(\mathbf{x}_1 - \mathbf{x}_0)}{\Delta\tau} + \frac{\Delta\tau}{2} V'(\mathbf{x}_0) , \tag{6.38}$$

$$\frac{\partial \mathcal{S}_{\mathrm{E}}}{\partial \mathbf{x}''} = \frac{(\mathbf{x}_P - \mathbf{x}_{P-1})}{\Delta\tau} + \frac{\Delta\tau}{2} V'(\mathbf{x}_P) \tag{6.39}$$

In order to calculate the second derivative of Eq. (6.37) one has to keep in mind that while $\mathbf{x}'$ and $\mathbf{x}''$ stay fixed, the points in between can change. In this case $\mathbf{x}_i$ for $i \in [1, ..., P-1]$ is regarded as a function of $\mathbf{x}_0$ and $\mathbf{x}_P$. This results in the second variation

$$\frac{\partial^2 \mathcal{S}_{\mathrm{E}}}{\partial \mathbf{x}' \partial \mathbf{x}''} = -\frac{1}{\Delta\tau} \frac{\partial \mathbf{x}_1}{\partial \mathbf{x}_P} , \tag{6.40}$$

$$\frac{\partial^2 \mathcal{S}_{\mathrm{E}}}{\partial \mathbf{x}' \partial \mathbf{x}'} = \frac{1}{\Delta\tau} \left(\mathbf{I} - \frac{\partial \mathbf{x}_1}{\partial \mathbf{x}_0} \right) + \frac{\Delta\tau}{2} \mathbf{V}''(\mathbf{x}_0) , \tag{6.41}$$

$$\frac{\partial^2 \mathcal{S}_{\mathrm{E}}}{\partial \mathbf{x}'' \partial \mathbf{x}''} = \frac{1}{\Delta\tau} \left(\mathbf{I} - \frac{\partial \mathbf{x}_{P-1}}{\partial \mathbf{x}_P} \right) + \frac{\Delta\tau}{2} \mathbf{V}''(\mathbf{x}_P) . \tag{6.42}$$

If one wants to use these expressions, a method is needed to calculate the terms $\frac{\partial \mathbf{x}_{P-1}}{\partial \mathbf{x}_P}$ and $\frac{\partial \mathbf{x}_2}{\partial \mathbf{x}_1}$. This can be done in the same way as before based on Eq. (6.31). The discretized equation of motions is differentiated with respect to $\mathbf{x}_\alpha$, whereby α can be either 0 or P. This results in

$$2\frac{\partial \mathbf{x}_i}{\partial \mathbf{x}_\alpha} - \frac{\partial \mathbf{x}_{i+1}}{\partial \mathbf{x}_\alpha} - \frac{\partial \mathbf{x}_{i-1}}{\partial \mathbf{x}_\alpha} + \Delta\tau^2 \mathbf{V}''(\mathbf{x_i}) \frac{\partial \mathbf{x}_i}{\partial \mathbf{x}_\alpha} = 0 , \tag{6.43}$$

$$\left(2\mathbf{I} + \Delta\tau^2 \mathbf{V}''(\mathbf{x_i}) \right) \mathbf{J}_i - \mathbf{J}_{i+1} - \mathbf{J}_{i-1} = 0 , \tag{6.44}$$

$$\mathbf{K}_i \mathbf{J}_i - \mathbf{J}_{i+1} - \mathbf{J}_{i-1} = 0 , \tag{6.45}$$

where $i \in [1, ..., P-1]$ and $\mathbf{J}_i \equiv \frac{\partial \mathbf{x}_i}{\partial \mathbf{x}_\alpha}$ is a $D \times D$ matrix with the following boundary conditions for $\alpha = 1$

$$\mathbf{J}_{i=0}^{\alpha=0} = \mathbf{I} \,, \tag{6.46}$$

$$\mathbf{J}_{i=P}^{\alpha=0} = 0 \tag{6.47}$$

and for $\alpha = P$

$$\mathbf{J}_{i=0}^{\alpha=P} = 0 \,, \tag{6.48}$$

$$\mathbf{J}_{i=P}^{\alpha=P} = \mathbf{I} \tag{6.49}$$

In principle what is obtained here is another representation of Eq. (5.21). If one takes Eq. (6.43), which is a second order differential equation of the form $\ddot{\mathbf{J}}(\tau) = -\mathbf{V}''(\mathbf{x}(\tau))\mathbf{J}(\tau)$, and transforms it to first order one gets the familiar matrix differential equation of Eq. (5.21). Instead of integrating Eq. (5.21), one first transforms Eq. (6.43) to a linear system of equations of the form

$$\mathbf{C}\mathbf{q} = \mathbf{d}, \tag{6.50}$$

in which $\mathbf{C}$ is matrix of dimension $D^2(P-1) \times D^2(P-1)$, which is given as

$$\mathbf{C} = \begin{pmatrix} \mathbf{G}_1 & -\mathbf{I} & 0 & \cdots & \cdots & 0 \\ -\mathbf{I} & \ddots & -\mathbf{I} & \ddots & \cdots & 0 \\ 0 & -\mathbf{I} & \mathbf{G}_i & \ddots & \ddots & \vdots \\ \vdots & \ddots & \ddots & \mathbf{G}_{i+1} & \ddots & \vdots \\ \vdots & \ddots & \ddots & \ddots & \ddots & -\mathbf{I} \\ 0 & 0 & \cdots & \cdots & -\mathbf{I} & \mathbf{G}_{P-1} \end{pmatrix} , \tag{6.51}$$

with $\mathbf{I}$ being a $D^2 \times D^2$-dimensional unit matrix and $\mathbf{G}_i$ is a $D^2 \times D^2$ matrix of the form

$$\mathbf{G}_i = \begin{pmatrix} \mathbf{K}_i & & 0 \\ & \ddots & \\ 0 & & \mathbf{K}_i \end{pmatrix} . \tag{6.52}$$

The right hand side of Eq. (6.50) is given by the column vectors of $\mathbf{J}_0$ or $\mathbf{J}_P$ depending on whether $\frac{\partial}{\partial \mathbf{x}_P}$ or $\frac{\partial}{\partial \mathbf{x}_0}$ is calculated. For example in the case of a system with $D = 2$, $\mathbf{d}$ is given by

$$d = \begin{pmatrix} 1 \\ 0 \\ 0 \\ 1 \\ 0 \\ \vdots \\ 0 \end{pmatrix} \text{ for } \frac{\partial}{\partial \mathbf{x}_0}, d = \begin{pmatrix} 0 \\ \vdots \\ 0 \\ 1 \\ 0 \\ 0 \\ 1 \end{pmatrix} \text{ for } \frac{\partial}{\partial \mathbf{x}_P}. \tag{6.53}$$

Correspondingly the solutions are given by

$$\frac{\partial \mathbf{x}_1}{\partial \mathbf{x}_0} = \begin{pmatrix} q_1 & q_3 \\ q_2 & q_4 \end{pmatrix} \qquad \frac{\partial \mathbf{x}_{P-1}}{\partial \mathbf{x}_P} = \begin{pmatrix} q_{D^2(P-1)-3} & q_{D^2(P-1)-1} \\ q_{D^2(P-1)-2} & q_{D^2(P-1)} \end{pmatrix} . \tag{6.54}$$

This scheme works in general for any path whether it is open or closed. In the closed case one just sets $\mathbf{x}_0 = \mathbf{x}_P$ in Eqs. (6.40), (6.41), and (6.42). Instead of calculating the determinant of a $(DP \times DP)$ matrix, one now has to solve a linear system of equations of the form $\mathbf{Cq} = \mathbf{d}$, where $\mathbf{C}$ is a banded matrix of the size $D^2(P-1)$. The computational effort of solving a banded matrix is of the order of $\mathcal{O}(k^2 N)$ where k is the number of diagonals and N the size of the matrix. Since $\mathbf{C}$ has D^2+2 non-zero entries, the overall scaling behavior of this method is $\mathcal{O}(PD^6)$.

6.3.2 Eigenvalue Tracing

If solving the matrix differential equation in Eq. (5.21) becomes unstable due to a low number of images and the eigenvalues of the monodromy matrix $\mathbf{M}$ that correspond to the orthogonal modes can no longer be distinguished from the parallel modes one might use eigenvalue tracing as an approximate alternative. Let's first consider Eq. (5.21) in imaginary time

$$\frac{d}{d\tau}\mathbf{M}(\tau) = \mathbf{F}(\tau)\mathbf{M}(\tau) \ , \tag{6.55}$$

with $\mathbf{F}$ given by

$$\mathbf{F}(\tau) = \begin{pmatrix} 0 & \mathbf{1} \\ \mathbf{V}''(\mathbf{x}(\tau)) & 0 \end{pmatrix} \ . \tag{6.56}$$

The sign change of the Hessian in comparison to Eq. (5.21) is a consequence of the Wick rotation. If $\mathbf{F}$ was a diagonal matrix, the solution for $\mathbf{M}$ would simply be given by $\mathbf{M}(\tau) = \mathbf{M}_0 \exp(\int \mathbf{F}(\tau)d\tau)$. In the next step a transformation matrix $\mathbf{T}$ is introduced which contains the normalized eigenvectors of $\mathbf{F}$ such that Eq. (6.55) can be written as

$$\dot{\mathbf{M}}(\tau) = \mathbf{F}(\tau)\mathbf{T}\mathbf{T}^T\mathbf{M}(\tau) \ , \tag{6.57}$$

$$\mathbf{T}^T\dot{\mathbf{M}}(\tau) = \mathbf{T}^T\mathbf{F}(\tau)\mathbf{T}\ \mathbf{T}^T\mathbf{M}(\tau) \tag{6.58}$$

with the following definitions

$$\mathbf{T}^T\mathbf{F}(\tau)\mathbf{T} \equiv \tilde{\mathbf{F}} \ , \tag{6.59}$$

$$\mathbf{T}^T\mathbf{M}(\tau) \equiv \tilde{\mathbf{M}} \tag{6.60}$$

and using that $\dot{\tilde{\mathbf{M}}} = \dot{\mathbf{T}}^T\mathbf{M} + \mathbf{T}^T\dot{\mathbf{M}}$ one obtains for transformed differential equation

$$\dot{\tilde{\mathbf{M}}} = \tilde{\mathbf{F}}\tilde{\mathbf{M}} + \dot{\mathbf{T}}^T\mathbf{M} \ . \tag{6.61}$$

Now assuming that the eigenvectors of $\mathbf{F}$ vary slowly with time such that $\dot{\mathbf{T}}^T \approx 0$ one obtains for the final solution at period β

$$\tilde{\mathbf{M}}(\beta) = \mathrm{e}^{\int_0^\beta \tilde{\mathbf{F}} d\tau} \ . \tag{6.62}$$

Since $\tilde{\mathbf{F}}$ is a diagonal matrix with the frequencies $\pm\omega_i^2(\tau)$ of $\mathbf{V}''$ as diagonal entries, the stability parameters can be obtained as

$$u_i = \int_0^\beta \omega_i(\tau) \ d\tau \ . \tag{6.63}$$

In order to use Eq. (6.63) one only takes the orthogonal components of $\mathbf{V}''$ along the trajectory. So at each image a reduced Hessian $\tilde{\mathbf{V}}''$ for which the parallel mode has been projected out needs to be computed. This is done via

$$\tilde{\mathbf{V}}'' = \mathbf{Y}_\perp^T \tilde{\mathbf{V}}'' \mathbf{Y}_\perp \tag{6.64}$$

where the basis $\mathbf{Y}_\perp$ contains all modes perpendicular to the instanton path at a given image and is perpendicular to the translational and rotational eigenvectors. Since the instanton is calculated in configuration space via a Newton search of the discretized Euclidean action functional the momentum at each image is not directly available. The tangent vector v_{tang} of the instanton path can either be approximated by taking a difference quotient of neighboring images or more precisely by determining the eigenvector of the operator $(-\partial_\tau^2 + \mathbf{V}'')$ in Eq. (4.35) which corresponds to the parallel mode. That eigenvector contains all tangent vectors at each image. The basis $\mathbf{Y}_\perp$ does not contain the mode corresponding to v_{tang}, hence its shape is $D \times (D-1)$. In order to perform the integration in Eq. (6.63) one has to keep track of the eigenvalues along the path. This tracing can be achieved if $\mathbf{Y}_\perp$ is constructed on a co-moving coordinate system as depicted in Figure 6.1. At first a basis is created using a Gram–Schmidt process to generate an orthonormal basis at the starting image with an arbitrary initial guess basis. The eigenvectors of $\mathbf{V}''$ are computed and stored. For the neighboring image, the process is repeated with the guess basis now being the set of $D-1$ eigenvectors of the previous image which have the smallest projection on to the instanton path. This approach enables one

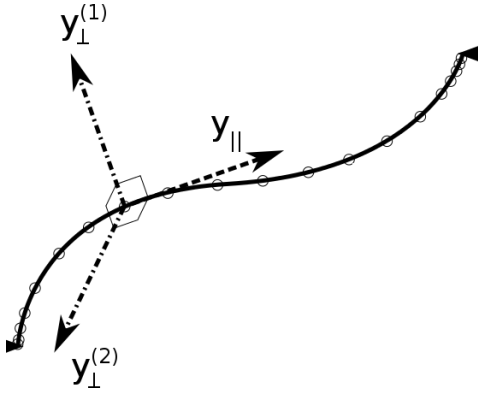

Figure 6.1: Exemplary draft of a co-moving coordinate system in three dimensions. At each image image three basis vectors are created using a Gram-Schmidt process with $\mathbf{y}_\perp^1$ and $\mathbf{y}_\perp^2$ being the basis vectors of $\mathbf{Y}_\perp$ containing the vectors orthogonal to the path and $\mathbf{y}_{||}$ being the basis vector parallel to the path. The guess basis for the Gram-Schmidt process to create $\mathbf{Y}_\perp$ at the i^{th} image is given by $\mathbf{Y}_\perp$ of the previous image.

to create a new coordinate system which is similar to the coordinate system of the previous image and thus allows for eigenvector comparison of two adjacent images. The maximum of the dot-products between eigenvectors of successive images then indicate the connection of the modes along the paths. This process is repeated for all images along the path and the stability parameter can be obtained by using Eq. (6.63).

6.4 Direct Calculation of $F_\perp$

If one is only interested in the value of the orthogonal fluctuation factor $F_\perp$ and not in the individual stability parameters the following approximation methods can be used.

6.4.1 Frequency Averaging

For a low number of images P, the integration of Eq. (5.21) or the tracing of eigenvalues as described in section 6.3.2 might become numerically unstable. If

one is only interested in an approximation to the orthogonal fluctuation factor it is sufficient to simply know the eigenvalues of the reduced Hessians $\tilde{\mathbf{V}}''$ at each image of the instanton path. The approximate expression for $F_\perp$ is derived in the following. One first recalls the expression for $F_\perp$ in Eq. (6.17) and uses exponentials to represent the hyperbolic sine function such that

$$F_\perp = \prod_{i=1}^{D_\nu - 1} \frac{1}{\mathrm{e}^{u_i/2} - \mathrm{e}^{-u_i/2}} \ . \tag{6.65}$$

For large frequencies ω_i or large imaginary time periods β the values for u_i can become relatively large and therefore Eq. (6.65) can be approximated as

$$F_\perp \approx \exp\left(- \sum_{i=1}^{D_\nu - 1} \frac{u_i}{2} \right) \tag{6.66}$$

Using the discretized expression of the integral in Eq. (6.63) and taking into account the fact that the instantons used in this context have the symmetric property of $\mathbf{V}''_i = \mathbf{V}''_{P-i+1}$ one obtains

$$\int_0^\beta \omega_i(\tau)\ d\tau \Rightarrow \sum_{j=1}^{P} \frac{\omega_{j,i} + \omega_{j+1,i}}{2} \Delta\tau = \sum_{j=1}^{P} \omega_{i,j} \frac{\beta}{P} \tag{6.67}$$

where $\omega_{i,j}$ is the i^{th} orthogonal mode of $\tilde{\mathbf{V}}''$ at the j^{th} image. Plugging the result of Eq. (6.67) in Eq. (6.66) one obtains for the final result

$$F_\perp = \exp\left(-\frac{\beta}{2P} \sum_{i=1}^{D_\nu - 1} \sum_{j=1}^{P} \omega_{j,i} \right) \ . \tag{6.68}$$

The expression in Eq. (6.19) is particularly useful as the order of summation can simply be interchanged. In principle one simply has to compute reduced Hessians at each image of the trajectory, calculate the square root of the eigenvalues to obtain the frequencies and sum them all up, thus no individual stability parameters or tracing is required in this approximation. However, as mentioned in the beginning this is only justified as long as the stability parameters are relatively large.

6.4.2 Full Hessians Projection Method

Another method to approximate $F_\perp$ is to calculate the second derivatives of the Euclidean action, including all $3N$ degrees of freedom, first and then afterwards project out the parallel mode as well as the rotational and translational contributions. The relevant eigenvalue equation is then

$$\mathbf{S}''\mathbf{v}_i = \lambda_i \mathbf{v}_i \ , \tag{6.69}$$

where $\mathbf{S}''$ is the discretized operator in Eq. (4.35) of dimension $DP \times DP$, λ_i and $\mathbf{v}_i$ the corresponding eigenvalues and normalized eigenvectors. In the case of no translational and rotational degrees of freedom there is only one zero valued eigenvalue λ_0 corresponding to the parallel mode. The orthogonal fluctuations are then calculated as follows [51]

$$F_\perp = \left(\frac{\beta}{P}\right)^{(D-1)P} \prod_{i=1}^{DP-1} \left(|\lambda_{\mathrm{inst},i}|^{1-\langle \mathbf{v}_i|\mathbf{v}_0\rangle^2}\right)^{1/2} \ , \tag{6.70}$$

where $\mathbf{v}_0$ is the tangent vector corresponding to the parallel displacement along the path. The expression does not stem from a rigorous derivation but is rather motivated by empirical observation. However, in the case of rotational and translational modes Eq. (6.70) needs to be modified in order to take them out of the expression as well. First one defines a quantity A_0 which is the product of the eigenvalues relating to the zero vibrational frequencies

$$A_0 = \prod_{i=1}^{P-1} \lambda_{0,i} \tag{6.71}$$

for which the values of $\lambda_{i,0}$ are given analytically [56] by

$$\lambda_{i,0} = 4\left(\frac{P}{\beta}\right)^2 \sin^2(i\pi/p), \quad i = 1, \ldots, P \ . \tag{6.72}$$

This yields for the final result

$$F_{\perp} = \left(\frac{\beta}{P}\right)^{(D-1)P} \frac{1}{A_0^{D_0}} \prod_{i=1}^{DP-1-D_0} \left(|\lambda_{\mathrm{inst},i}|^{1-\langle \mathbf{v}_i|\mathbf{v}_0\rangle^2}\right)^{1/2} \tag{6.73}$$

with D_0 being the number of zero modes that are left out of Eq. (6.73).

6.5 Summary

The key quantity needed in order to determine microcanonical and canonical rate constants is the fluctuation factor $F_{\perp}$ which contains the orthogonal fluctuations along the instanton path. The indirect approach of first calculating the instanton's individual stability parameters requires the determination of the monodromy matrix. It can be computed by using the algorithm presented in section 6.3.1 which yields a linear system of equations $\mathbf{Cq} = \mathbf{d}$ whereby $\mathbf{C}$ is a banded matrix which enables a very efficient treatment when compared to the determinant method. A different and approximate approach is to use eigenvalue tracing as described in section 6.3.2 which requires the construction of a co-moving coordinate system in order to separate the orthogonal from the parallel modes. If one is not interested in individual stability parameters but only in an approximation to $F_{\perp}$, one can either use the frequency averaging method from section 6.4.1 or the Full Hessians approach in section 6.4.2 which is less based on mathematical rigor but rather on empirical observations for different system which will become apparent in chapter 7. The calculation of canonical rate constants additionally requires the rate at which the instanton's energy changes with respect to β. Rather then relying on a finite difference approach one can use the algorithm presented in section 6.2. Like in the case of $F_{\perp}$ the calculation results in a linear system of equations in which $\mathbf{A}$ is a sparse matrix, yet still has entries on the upper right and lower left corners. While this leads to the same scaling behavior as computing the determinant of $\mathbf{A}$, it enables an acceleration of the rate constant calculation significantly due to much smaller pre-factors of available linear solvers when compared to calculating determinants.

7 Applications

In this chapter the methods proposed in chapter 6 are applied to different chemical systems. These include purely analytical test potentials such as the Müller–Brown system [57] as well as real-life chemical systems for which uni- and bimolecular reaction rate constants are calculated. The neccessary electronic energies are either obtained from a fitted potential energy surface which is available in the literature or from a density functional calculation. The geometry optimization and the subsequent instanton search is done with DL-FIND [42]. For the density functional calculation ChemShell [58] is used as an interface to the Turbomole software package [59].

7.1 Müller–Brown Potential

The Müller–Brown potential is a simple two-dimensional system which can be written in analytic form as

$$V(\mathbf{x}) = \gamma \sum_{i=1}^{4} A_i \exp\left(a_i(x - x_{0,i})^2 + b_i(x - x_{0,i})(y - y_{0,i}) + c_i(y - y_{0,i})^2\right) , \quad (7.1)$$

whereby $\mathbf{x} = (x, y)^T$. The parameters are in this case taken from Ref. 57

$$\gamma = \frac{1}{212} \,, \tag{7.2}$$

$$\begin{aligned}
\mathbf{A} &= (-200, -100, -170, 15)^T \,, \\
\mathbf{a} &= (-1, -1, -6.5, 0.7)^T \,, \\
\mathbf{b} &= (0, 0, 11, 0.6)^T \,, \\
\mathbf{c} &= (-10, -10, -6.5, 0.7)^T \,, \\
\mathbf{x}_0 &= (1, 0, -0.5, -1)^T \,, \\
\mathbf{y}_0 &= (0, 0.5, 1.5, 1)^T \,.
\end{aligned} \tag{7.3}$$

Using this set of parameters for the Müller–Brown potential, the system has one saddle point and three minima. One minimum on the left, one minimum in the middle and a global minimum on the right as shown in Figure 7.1. In this example the reaction from the intermediate minimum at the coordinates $(-0.05001, 0.46669)$ over the barrier with the saddle point at $(-0.822001, 0.624314)$ to the left minimum is studied. Since this is a two-dimensional system without rotational and translational invariance, there is one zero valued stability parameter and another one representing the fluctuations orthogonal to the instanton path. For a particle of the mass of a hydrogen atom the crossover temperature is in this case given by $T_c \approx 2207$ K. Figure 7.2 shows the result of the rate constant calculation in a traditional Arrhenius plot for which the determinant method was used. One can see, starting on the left side in the high-temperature region, that the rate constant drops relatively fast until the decline slows down at around 1600 K and starts to plateau at around 900 K where it converges to a constant rate constant of $k \approx 1.78 \cdot 10^{-15}$ in atomic units. This is due to the fact that at very low temperatures only the ground state is occupied and the rate constant becomes temperature independent since only tunneling of the ground state contributes to the reaction and no longer thermal excitations. This converged behavior is therefore typical for a uni-molecular reaction in which a minimum exists in the reactant well. The determinant method is the computationally least efficient way when compared to the other proposed approaches, yet it has proven to be a stable and reliable method. It is therefore regarded as the benchmark in terms of accuracy

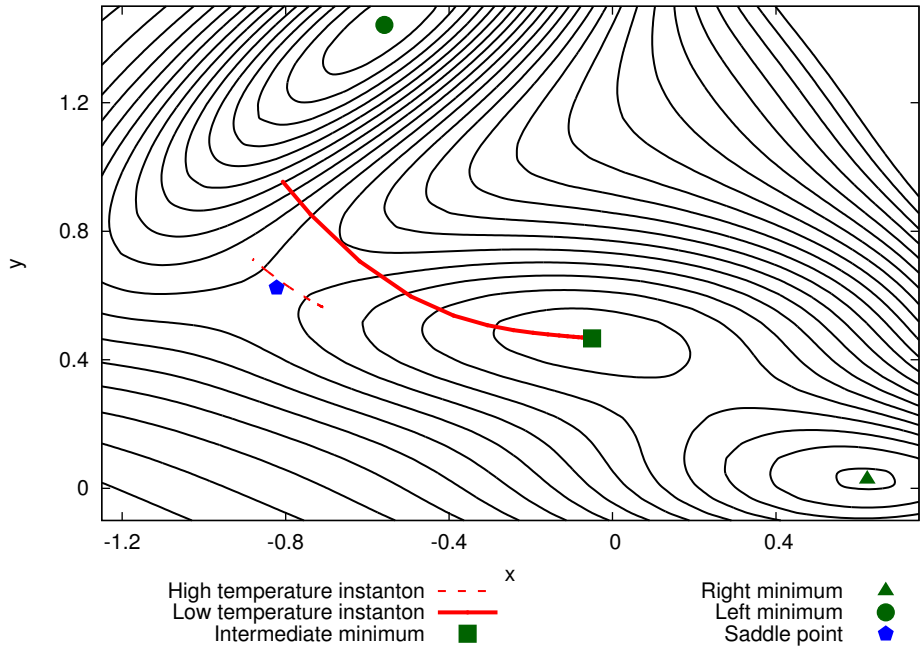

Figure 7.1: Contour plot of the Müller–Brown potential using the parameters from Eq. (7.3). The left minimum is at $(-0.55822, 1.44173)$, the intermediate minimum at $(-0.05001, 0.46669)$ and the right minimum on the right at $(0.62350, 0.02804)$. The saddle point is situated at $(-0.82200, 0.62431)$ resulting in a transition state temperature of $T_c \approx 2207$ K for a hydrogen atom of mass $m = 1822.88\ m_e$. The dotted red line shows the instanton trajectory at a temperature of 2150 K whereas the continuous red line shows the low temperature instanton at 500 K.

to which the other methods are being compared to.

7.1.1 Stability Parameters and $F_\perp$ for the Müller–Brown Potential

Figure 7.3 shows the values for the stability parameters over β for the Müller–Brown potential calculated either by integration Eq. (6.55), solving the linear system $\mathbf{Cq} = \mathbf{d}$ in Eq. (6.50) or approximated by applying eigenvalue tracing. The representation of the stability parameters as u/β signifies the physical inter-

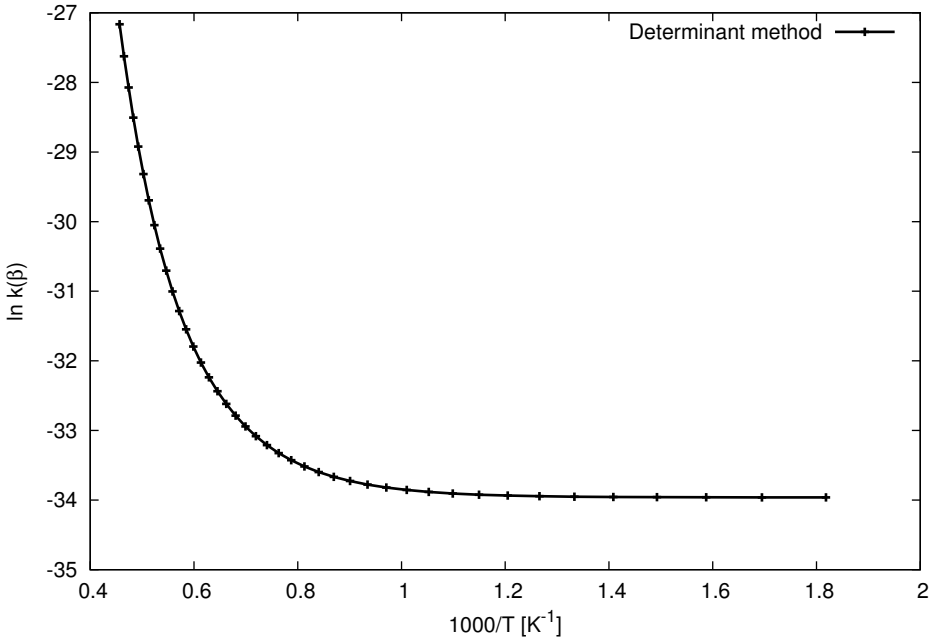

Figure 7.2: Arrhenius plot for the thermal reaction rate constant in atomic units for the reaction going from the middle minimum of the Müller–Brown potential to the left minimum. The results were obtained using the determinant method from Eq. (4.27).

pretation of the stability parameters as frequencies of the molecule's vibrational modes. The number of images with $P = 2048$ is chosen sufficiently high in order to avoid numerical difficulties and enable a comparison of the different methods and examine the consequences of their inherently different approximations. Figure 7.4 shows that the non-approximate algorithms, namely integrating the monodromy matrix in Eq. (6.55) and solving Eq. (6.50) (Cqd), converge to the same value for the stability parameter as one would expect. However, the eigenvalue tracing approximation yields values for $F_\perp$ which are too large across the whole temperature range but are relatively close when compared with the two other methods. These results can then be used to calculate $F_\perp$ using the non-zero stability parameter in Eq. (6.16). Furthermore one can apply the frequency averaging and full Hessian projection approximation to determine $F_\perp$ directly. The results of these calculations are depicted in Figure 7.4. The graph shows the negative natural logarithm of $F_\perp$. Figure 7.5 shows the difference between the value of the natural logarithm of $F_\perp$ using Eq. (6.50) (Cqd) and all other methods. While integrating the monodromy matrix Eq. (6.55) should deliver the same result given the large number of images, the other methods vary depending on the temperature scale. For the most part of the temperature range, the full Hessian projection method seems to be the most reliable as it tends to be closest to the value of Cqd.

7.1.2 Comparison of the Rate Constants

In order to calculate the rate constant one uses Eq. (6.22). Since the Müller–Brown system is a two-dimensional system without translational and rotational degrees of freedom one sets $Q_{\text{t-r}} = 1$. This yields for the final expression

$$k(\beta) = \frac{1}{\sqrt{2\pi}\mathcal{Q}_{\text{RS}}}\sqrt{-\frac{dE}{d\beta}}F_\perp \mathrm{e}^{-\mathcal{S}_{\text{Inst}}} \ . \tag{7.4}$$

For the calculation of $\mathcal{Q}_{\text{RS}}$ one can simply take the analytic expression (see section 9.1) for the canonical partition function of the reactant

$$\mathcal{Q}_{\text{RS}} = \prod_{i=1}^{2} \frac{1}{2\sinh(\omega_i\beta/2)} \mathrm{e}^{-\beta V(\mathbf{x}_{\text{RS}})} \ , \tag{7.5}$$

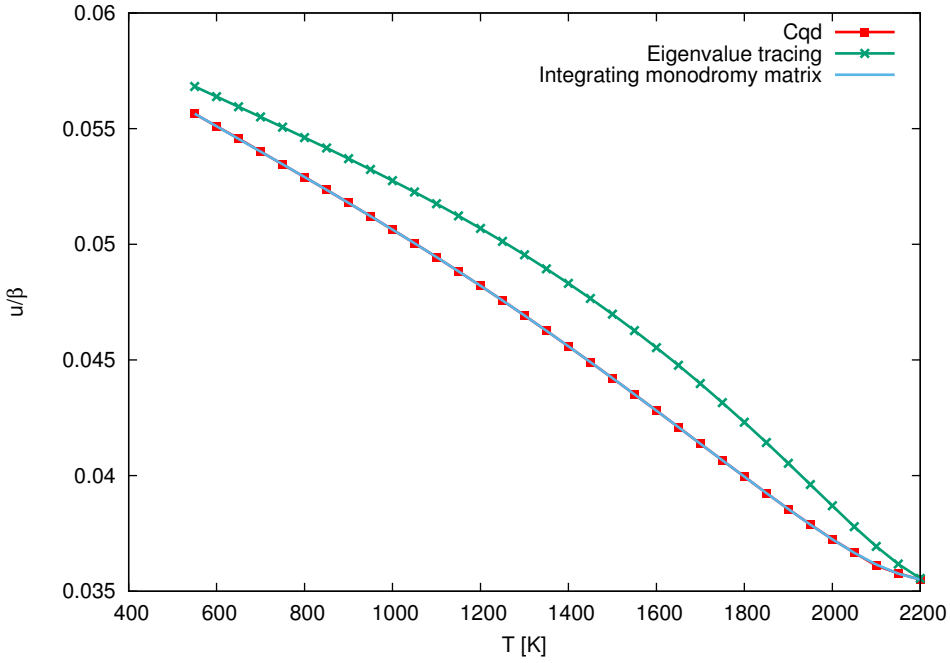

Figure 7.3: Stability parameter over β for the reaction from the intermediate to the left minimum. The red line was obtained by computing the second derivatives of the Euclidean action $\mathcal{S}_E$ by solving the linear system $\mathbf{Cq} = \mathbf{d}$ in Eq. (6.50). The blue line was obtained by integrating the monodromy matrix in Eq. (6.55) via a 4^{th}-order Runga–Kutta method. The green line was obtained via eigenvalue tracing as described in section 6.3.2. All calculations were done for $P = 2048$.

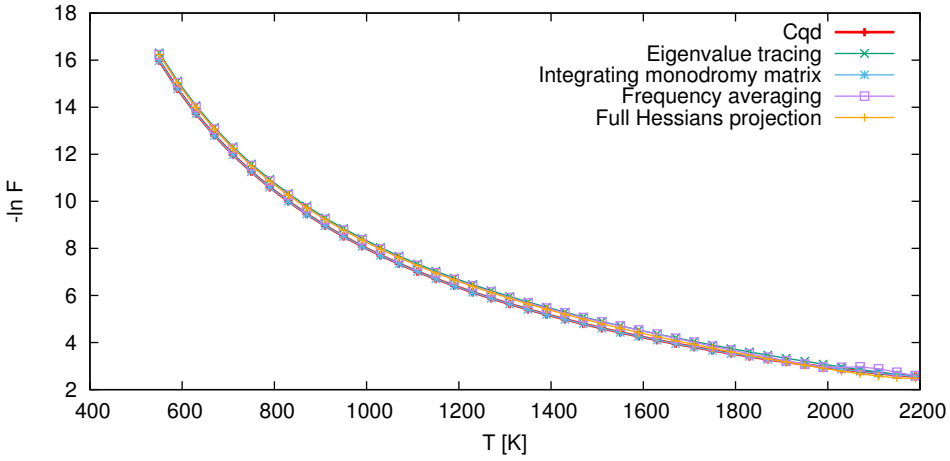

Figure 7.4: Values of $F_\perp$ for the Müller–Brown potential using different methods. The red line labeled Cqd shows the result of solving Eq. (6.50) and the blue line the result of integrating the monodromy matrix in Eq. (6.55). The others represent the results of the different approximation schemes suggested in section 6.3.2, 6.4.1 and 6.4.2. In all calculations 2048 images were used.

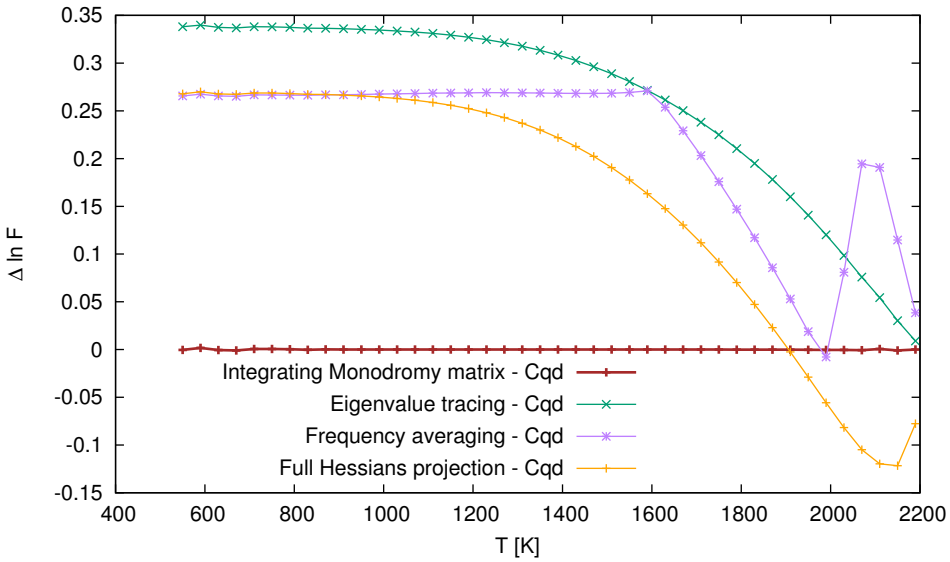

Figure 7.5: Difference between the value of the natural logarithm of $F_\perp$ using Eq. (6.50), labeled Cqd, and all other methods.

with $\omega_1 = 0.02382$ and $\omega_2 = 0.06163$ for the reactant at $(-0.05001, 0.46669)$. The values for $dE/d\beta$ are calculated by using the method proposed in section 6.2. The results are depicted in Figure 7.6 and agree well with the finite difference estimation, yet is considerably faster as only one instanton has to be located. Using the results shown in Figure 7.6 and combining them with the values in Figure 7.5 by plugging them into Eq. (7.4) yields thermal rate constants as depicted in Figure 7.7. Close to T_c all methods result in fairly similar rate constants whereas in the low-temperature region the approximate methods all overestimate the value for the orthogonal fluctuations and therefore lead to a lower rate constant. In this case the approximate methods yield rate constants at 600 K which are approximately 25% to 30% lower than the benchmark rate constant using the determinant method. The approach using Eq. (6.50) (Cqd) performs extremely well and is in very good agreement with the determinant method even at very low temperatures. For example at 600 K Eq. (6.50) results in a rate constant of $k = 1.78026 \cdot 10^{-15}$ a.u. which is only 0.1% lower than the determinant method result of $1.78226 \cdot 10^{-15}$ a.u. .

However, these results were obtained with an extremely high number of images which are usually unattainable, if no analytical potential energy surface is given. Figure 7.8 shows how solving Eq. (6.50) (Cqd) compares with the determinant method if the number of images is reduced. At a small number of images the solutions can start to deteriorate quickly since the imaginary time increment $\Delta\tau = \beta/P$ becomes relatively large. However, in this case, the results in Figure 7.8 show a relatively good agreement of both methods even for a smaller number of images.

Since individual stability parameters have been used by the Cqd-method in order to obtain the canonical rate constants one can easily use them to calculate the cumulative reaction probability $P(E)$ and consequently a microcanonical rate constant $k(E)$. In order to obtain $P_{\mathrm{SC}}(E)$ Eq. (5.28) is applied such that for the Müller–Brown case one obtains

$$P_{\mathrm{SC}}(E) = \sum_{n=0}^{\infty} \frac{1}{1 + \mathrm{e}^{\mathcal{W}(E-E_n)}} \,, \tag{7.6}$$

where E_n is determined by solving a self-consistent equation which is in this case

$$E_n = E - \left(\frac{1}{2} + n\right) \frac{u(E - E_n)}{T_0(E - E_n)} \ . \tag{7.7}$$

In order to solve Eq. (7.7) instantons are first optimized for a given set of imaginary time periods T_0 (or inverse temperatures $\beta = T_0$) which then provide a set of possible values for $\mathcal{W}(E)$, E, and $u(E)$. The required values for $u(E-E_n)/(T_0(E-E_n))$ are then linearly interpolated and Eq. (7.7) is solved iteratively. Afterwards the shortened action $\mathcal{W}$ is linearly interpolated too, in order to obtain $P_{\mathrm{SC}}(E)$ via Eq. (7.6).

At low energies and for large vibrational frequencies, the sum over n in Eq. (7.6) is truncated after a few terms. At high energies, especially when $E > E_{\mathrm{TS,ZPE}}$, many terms must be included. Here $E_{\mathrm{TS,ZPE}}$ denotes the energy of the transition sate including zero-point energy. At high enough energies, $\mathcal{W} = 0$ is assumed to be independent of E_n. The quantization of vibrational energy levels can therefore be neglected, which results in the classical density of states of the transition state as

$$P(E) = \frac{(E - E_{\mathrm{TS}})^{D-1}}{(D-1)!} \prod_{i=1}^{D-1} (\omega_{i,\mathrm{TS}})^{-1} \quad \text{for } E \gg E_{\mathrm{TS}}. \tag{7.8}$$

Eq. (7.8) is used for energies above $E_{\mathrm{TS,ZPE}} + 10 \cdot \omega_{\mathrm{TS,min}}$, where $\omega_{\mathrm{TS,min}}$ is in general the smallest vibrational frequency of the transition state perpendicular to the transition mode. However, in the case of the Müller–Brown potential there is only one perpendicular frequency. Eq. (7.8) means that the first 10 quanta of the vibrations are explicitly taken into account and then the continuous expression in Eq. (7.8) is used. Figure 7.9 shows the results of this calculation for P_{SC} as well as the corresponding microcanonical rate constant $k(E)$ which is obtained by using Eq. (3.27)

$$k_{\mathrm{SC}}(E) = \frac{1}{2\pi\hbar} \frac{P_{\mathrm{SC}}(E)}{\nu_r(E)} \ , \tag{7.9}$$

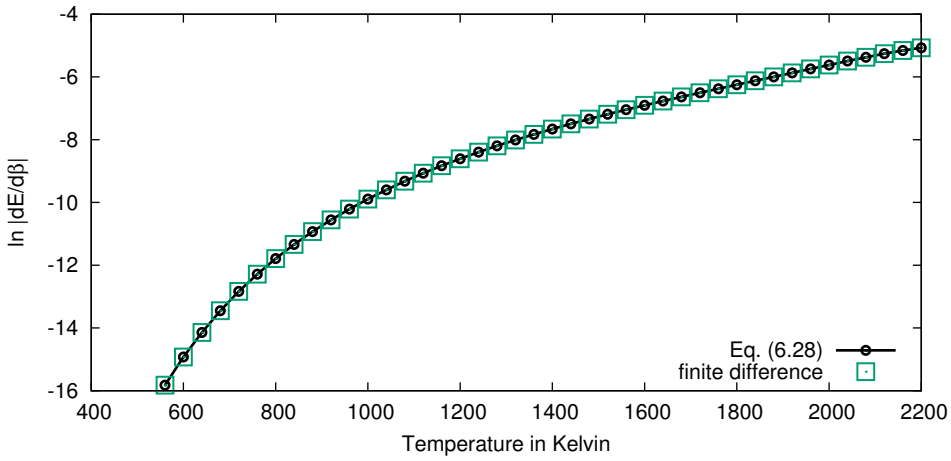

Figure 7.6: Change of the instanton's tunneling energy with respect to β in the Müller–Brown potential calculated at different temperatures. The value of $\frac{dE}{d\beta}$ is negative for all $T < T_c$. The green squares correspond to finite differences between E obtained for instantons at adjacent temperatures. The calculation used $P = 2048$.

whereby here the classical density of states for an harmonic oscillator in the reactant valley is taken to be

$$\nu_r(E) = \frac{E^{D-1}}{(D-1)! \prod_{i=1}^{D} \omega_{i,\mathrm{RS}}} \ . \tag{7.10}$$

However, one has to keep in mind that the semiclassical approximation used here for $k(E)$ is not in the least able to take into account the necessary quantization of the reactant region in the case of a uni-molecular reaction. So $k(E)$ cannot be interpreted as the state specific decay rate of a state at energy E. It can be rather regarded as the mean rate of different states which are averaged over an energy interval ΔE [38]. In order to accurately describe state specific decay rates one would have to invoke a full quantum mechanical treatment which takes into account coupling of the modes in the reactant valley and requires a proper time evolution of those states via a solution of the time-dependent Schrödinger equation.

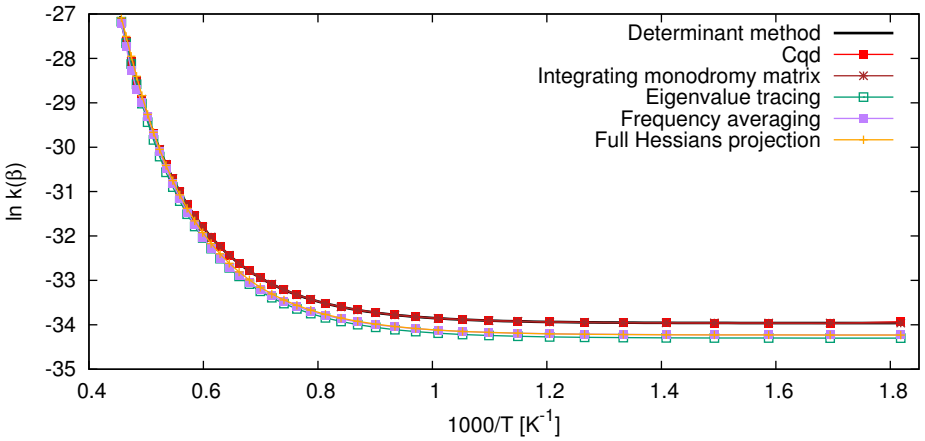

Figure 7.7: Thermal rate constants $k(\beta)$ in atomic units for the Müller–Brown potential, calculated via Eq. (7.4) with the results shown in Figure 7.6 for $dE/d\beta$ and the different values for $F_\perp$ depicted in Figure 7.5.

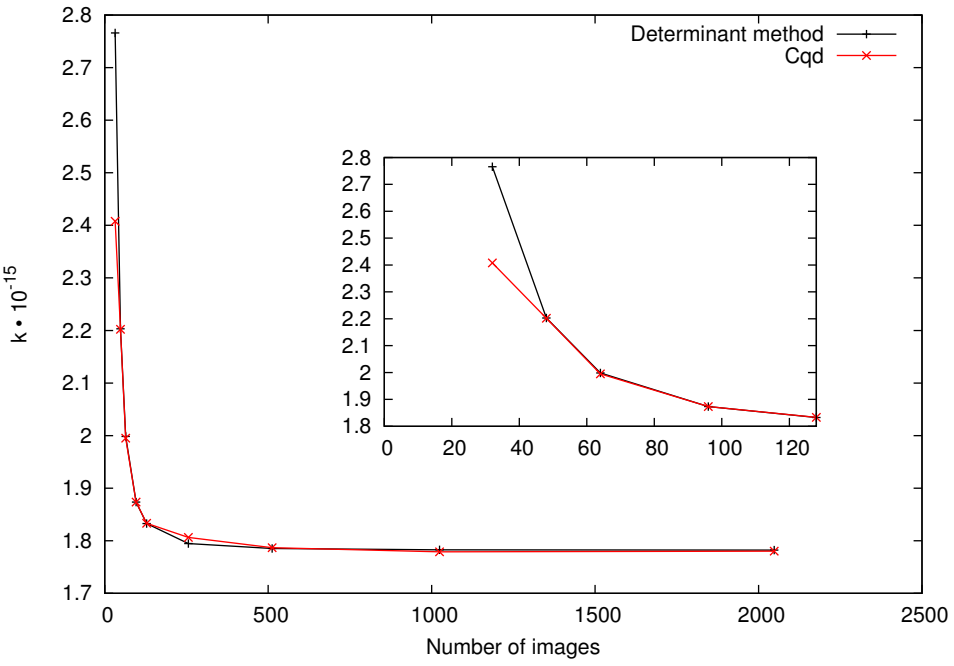

Figure 7.8: Results for the thermal rate constant calculation using the Cqd-method and the determinant method using different number of images at $T = 600$ K.

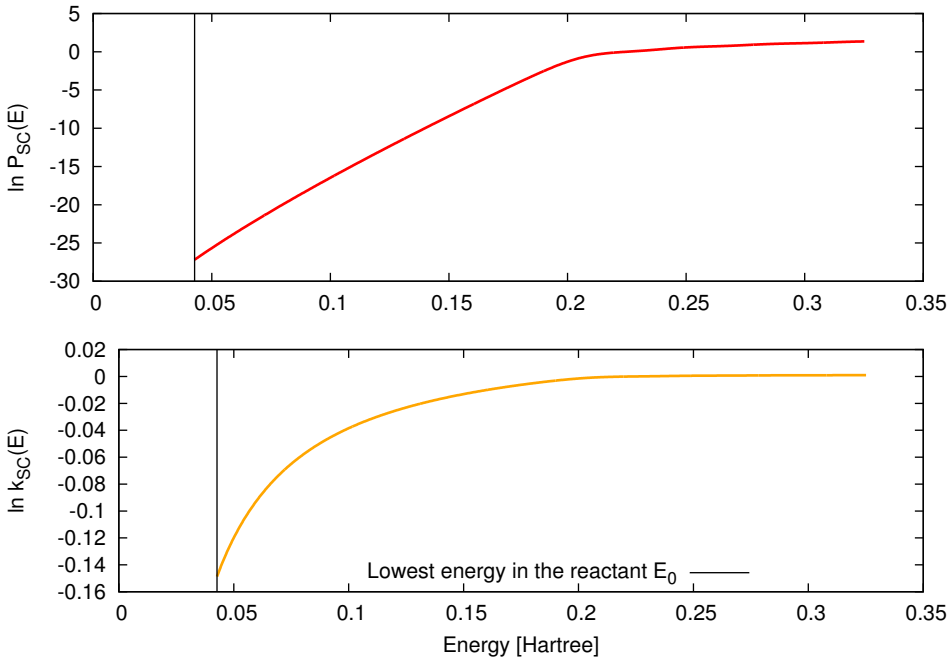

Figure 7.9: Results in atomic units for the cumulative reaction probability $P_{\mathrm{SC}}(E)$ using Eq. (7.6) and the corresponding microcanonical rate constant $k_{\mathrm{SC}}(E)$ which is obtained from Eq. (7.9). The black vertical line marks the ground state energy of the harmonically approximated reactant state.

7.2 Decay of Methylhydroxycarbene

The decay of methylhydroxycarbene to acetaldehyde via tunneling has previously been studied experimentally and computationally [60, 61]. Therefore this reaction is chosen in order to investigate the stability of the Cqd-approach with respect to numerical noise in the gradients and Hessians and to provide data for a system with translational and rotational invariance. The energies and their derivatives are obtained on-the-fly using DFT calculations with the B3LYP hybrid functional [62–67] in combination with the def2-SVP basis set [68]. The calculations are done using Turbomole v 7.0.1. [59]. For the geometry optimizations and and subsequent instanton calculations DL-FIND [42] was used via ChemShell [58] as interface to Turbomole. The focus here is to compare the Cqd-method with the determinant method rather than aiming at high accuracy in comparison to experimental data. Nevertheless, B3LYP (with a different basis set, though) was found to reproduce more accurate calculations quite well [61]. In all subsequent calculations the discretization of the instanton was chosen to be $P = 128$ images. The instantons were optimized such that the largest component of the gradient is smaller than 10^{-9} atomic units. The self consistent field cycles were iterated until the change in energy was less than 10^{-9} Hartree per iteration. Furthermore the $m5$ grid [69] is used. An exemplary instanton of such a calculation is shown in Figure 7.10.

After optimizing the instanton geometries at a series of temperatures below the crossover temperature of $T_c \approx 453$ K, the stability parameters u_i are calculated using Eq. (6.50). For this 7-atom system there are 14 non-zero stability parameters. They can be interpreted as frequencies via $\omega_i = u_i/\beta$, hence wavenumbers in units of cm^{-1} are chosen for this system. The stability parameters are depicted in Figure 7.11. Most of them are almost independent of the temperature. The stability parameter with the strongest temperature dependence corresponds to the movement of the transferred hydrogen atom perpendicular to the instanton path. At high temperatures, the instanton path is short and in the direct vicinity of the saddle point. Correspondingly, the value of the temperature dependent stability parameter is close to 2660.7 cm^{-1}, the wave number of the C–H and O–H stretching mode of the transferred H at the transition state. At lower temperature its

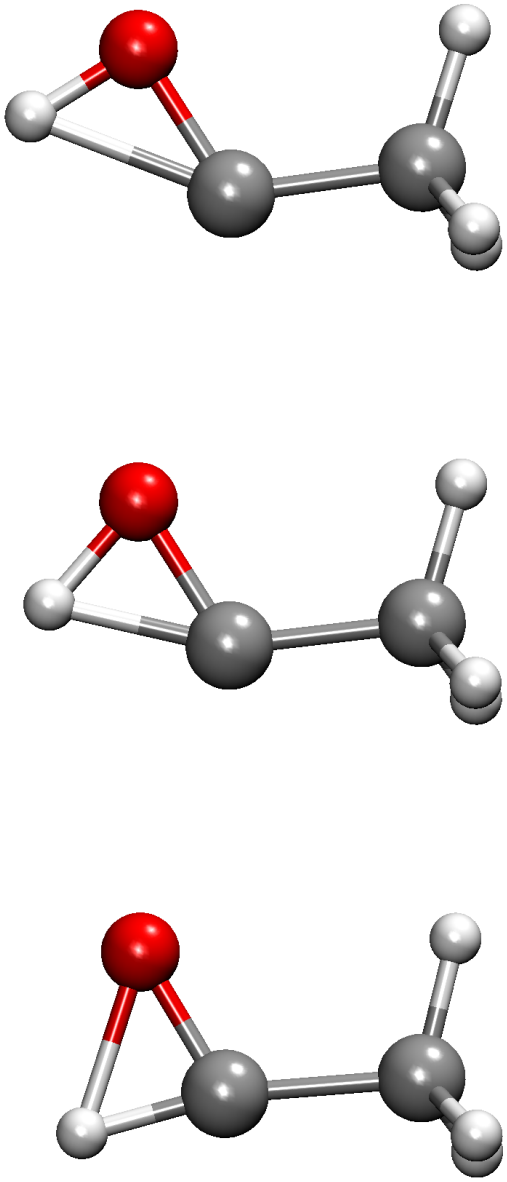

Figure 7.10: Instanton for the decay of methylhydroxycarbene to acetaldehyde at $T = 300$ K from top to bottom. The graph at the top shows the starting image of the instanton in the reactant region, the one in the middle an intermediate stage of the reaction and the one at the bottom shows the configuration of the last image in the product region. The color white is used to label hydrogen, red oxygen and grey carbon atoms.

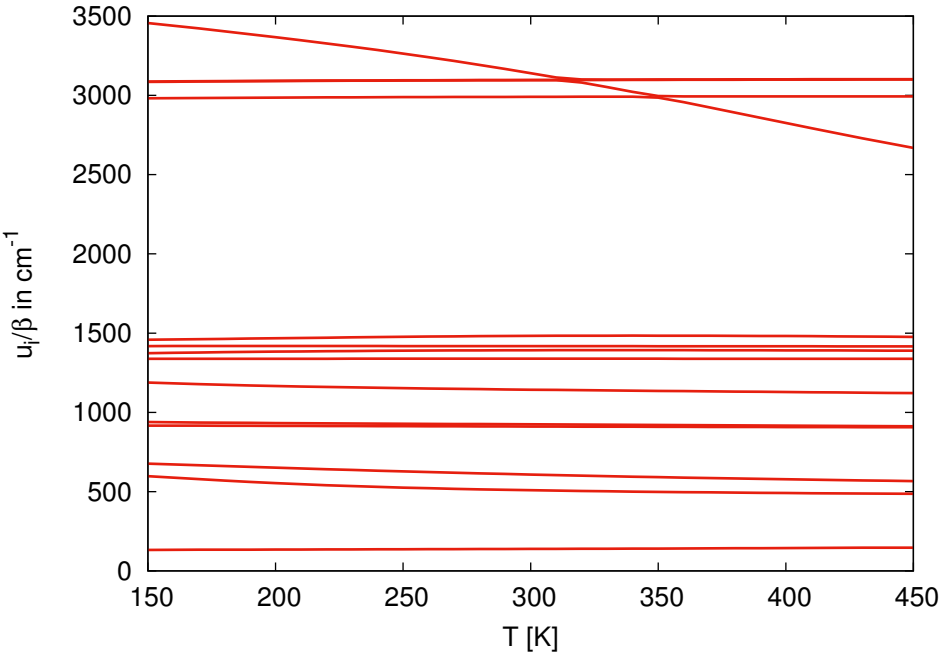

Figure 7.11: The 14 non-zero stability parameters for the decay of methylhydroxycarbene to acetaldehyde using 128 images with the Cqd-method. At high temperatures the value of the temperature dependent stability parameter is close to 2660.7 cm^{-1}, which is the wave number of the C–H and O–H stretching mode of the transferred hydrogen atom at the transition state. At lower temperature its value increases, tending towards the value of 3736.0 cm^{-1}, which corresponds to the O–H stretching mode in the reactant.

value increases, tending towards the value of 3736.0 cm^{-1}, which corresponds to the O–H stretching mode in the reactant, methylhydroxycarbene. The different stages of the reaction are depicted in Figure 7.10. The resulting fluctuation factor F_{Inst} is shown in Figure 7.12. The temperature-dependence of $dE/d\beta$ is shown in Figure 7.13. An approximate method which calculates $dE/d\beta$ with a finite difference approach, using two instantons with adjacent temperatures, is shown for comparison. The new approach using Eq. (6.28) agrees well with the finite difference estimation, yet is considerably faster as only one instanton has to be located. Using the results shown in Figure 7.11, Figure 7.13 and the classical expressions for $Q_{\text{t-r}}$ (see 9.2 and 9.2) one obtains the thermal rate constants depicted in Figure 7.14. One can see clearly a very good agreement between the Cqd-method and the conventional determinant method. The highest deviations between the methods appear at low temperatures with the rate constant determined by solving $\mathbf{Cq} = \mathbf{b}$ being 4.3% larger than the one calculated via the determinant method. The convergece of both methods with respect to the number of images P is shown in Figure 7.15 for two temperatures, $T = 300$ K (top) and $T = 150$ K (bottom). For very few images, both methods are inaccurate, but the determinant method is slightly more stable than the Cqd approach. An instanton path with merely 16 images at a temperature so far below T_{c} results in a rather badly discretized path. At higher numbers of P, it is notable that the Cqd method converges faster to the final result than the determinant method. It is most clearly visible at $T = 150$ K, keeping in mind the different scales of the vertical axes for the two graphs.

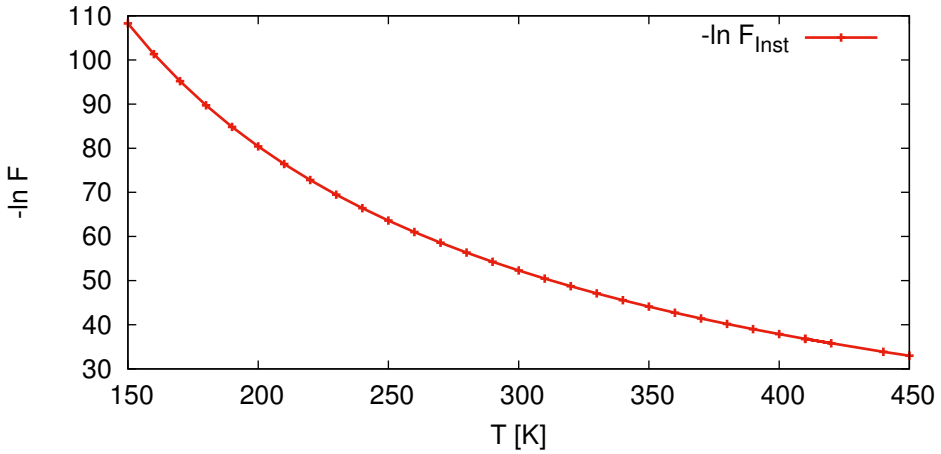

Figure 7.12: Results for the orthogonal fluctuation factor $F_\perp$ in atomic units using Eq. (6.65) with the stability parameters obtained via the Cqd-method from Figure 7.11

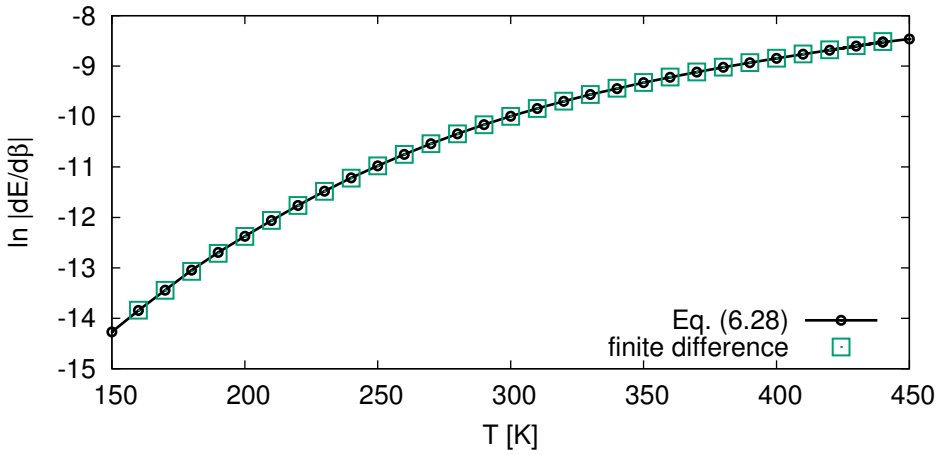

Figure 7.13: Change of the instanton's tunneling energy in atomic units with respect to β for the reaction of methylhydroxycarbene to acetaldehyde calculated with 128 images. The value of $\frac{dE}{d\beta}$ is negative for all $T < T_c$. The green squares correspond to finite differences between E obtained for instantons at adjacent temperatures.

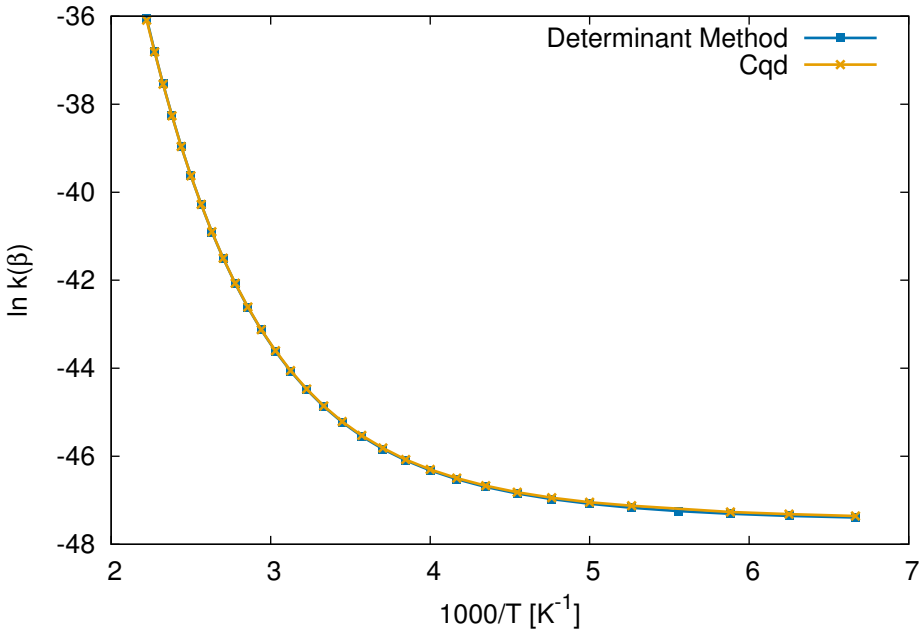

Figure 7.14: Rate constants in atomic units for the reaction of methylhydroxycarbene to acetaldehyde. The orange line was calculated using the Cqd-method and the quantities shown in Figure 7.11 and Figure 7.13. The blue line was calculated with the conventional determinant method.

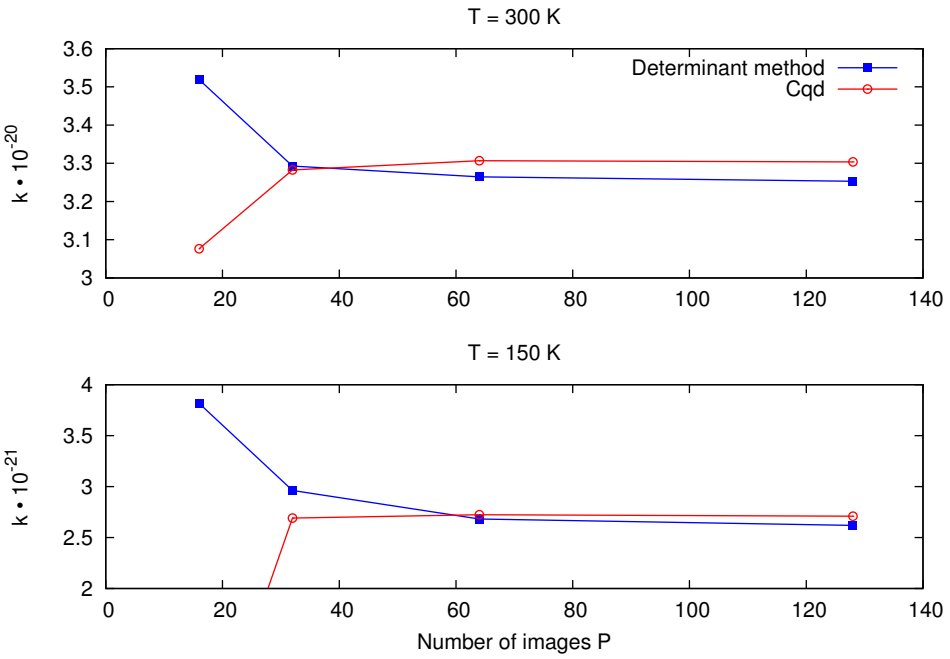

Figure 7.15: Convergence of the rate constants in atomic units with the number of images P at two different temperatures for the reaction of methylhydroxycarbene to acetaldehyde. The red line was calculated using the Cqd-method of Eq. (6.50) and the quantities determined in Figure 7.11. The blue line was calculated with the conventional determinant method.

7.3 Bi-molecular Reaction $H_2 + OH \rightarrow H_2O + H$

So far only uni-molecular reactions have been examined. As test case for a bi-molecular reaction the reaction $H_2 + OH \rightarrow H_2O + H$ is chosen here since it has has been investigated in great detail in the literature [31,70–82]. As a consequence of that there are a set of different fitted potential energy surfaces available. In this case a rather old suface by Schatz and Elgersma [83,84] is used since for this PES reference data for the cumulative reaction probability are available from a quantum dynamics calculation [70,71].
Like in the previous case this system is not chosen in order to gain new physical insights but to compare different methods. All calculations are done in DL-FIND. Like many bi-molecular reactions this system exhibits a pre-reactive energy min-

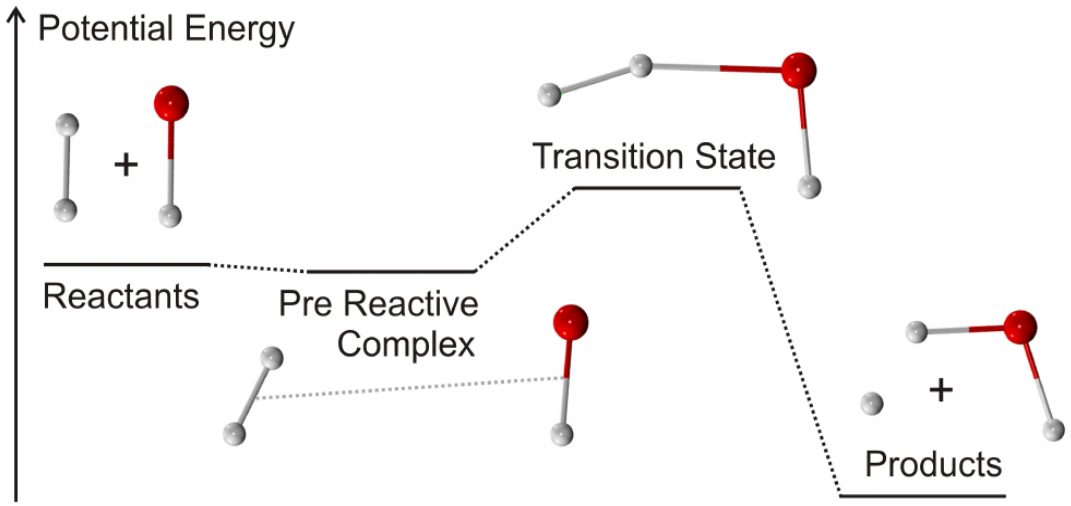

Figure 7.16: Different stages of the reaction $H_2 + OH \rightarrow H_2O + H$, including the weakly bound pre-reactive Van-der-Waals complex . Graph taken from Ref. 85.

imum, a weakly bound Van-der-Waals complex, as depicted in Figure 7.16. At low pressure, such a complex does not thermally equilibrate and either proceeds over the transition state or decays again. This limits the applicability of canonical instanton theory [85,86]. A microcanonical formulation allows the use of the reactant's thermal distribution to calculate thermal rate constants without assuming

thermalization in a pre-reactive minimum. This four-atom system has $12 - 6 = 6$ vibrational degrees of freedom and therefore five non-zero stability parameters. The stability parameters are obtained by integrating Eq. (6.55) and via the approximate eigenvalue tracing approach. Since here the PES is given analytically the calculations are performed with a high number of images $P = 400$ such that integrating Eq. (6.55) yields sufficiently accurate results. Figure 7.17 shows the results for the non-zero stability parameters. The continuous lines were obtained by integrating Eq. (6.55), the dotted lines via eigenvalue tracing. In the eigenvalue tracing approximation the stability parameters are obtained by integrating the traced orthogonal frequencies, shown in Figure 7.18, in imaginary time from 0 to β. From the stability parameters shown in Figure 7.17 one can then obtain $P_{\mathrm{SC}}(E)$ via Eq. (5.29). If no individual stability parameters are available the following approximation is used instead of Eq. (5.29)

$$P(E) = \sum_{n_1} \cdots \sum_{n_5} \frac{1}{1 + \exp[S_0(E - E_{\mathrm{vib},n} - \sigma/T_0)]} \tag{7.11}$$

with

$$E_{\mathrm{vib},n} = \sum_{i=1}^{D-1} \omega_{i,\mathrm{TS}}\ n_i \tag{7.12}$$

where $\sigma = \ln F_\perp$ approximates the zero-point vibrational energy and $E_{\mathrm{vib},n}$ covers vibrational excitations. The results are shown in Figure 7.19. They show a relatively good agreement between the semiclassically approximated $P_{\mathrm{SC}}(E)$ and the probability obtained from the quantum dynamics calculation. The different ground state energy of the quantum calculation compared to $P_{\mathrm{SC}}(E)$ is due to the harmonic approximation which is assumed for the reactant in the semiclassical approximation. Once $P(E)$ is obtained the thermal rate constant can in the bi-molecular case be obtained via a Laplace transformation such that

$$k(\beta) = \frac{Q_{\text{t-r}}}{2\pi Q_{\mathrm{RS}}} \int_{E_{\mathrm{RS}}}^{\infty} P(E) \mathrm{e}^{-\beta E} dE\ , \tag{7.13}$$

where E_{RS} is the ground state energy. For the translational and rotational partition function the classical expression for a bi-molecular reaction is used (see Sec. 9.2 and Sec. 9.2 in the appendix). The result of Eq. (7.13) is shown in Figure 7.20. Even though $P(E)$ obtained from integrating Eq. (6.55) and eigenvalue tracing look very similar, the resulting thermal rate constants are slightly different ($\sim$13%) at low temperature. Obtaining $P_{\mathrm{SC}}(E)$ via frequency averaging or the full Hessians projection method results in pretty good approximations, too. Like in the previous case the approximate methods consistently lead to lower rate constants at all temperatures compared with the determinant method. Using the frequency averaging method also gives very consistent rate constants, even though rather small frequencies perpendicular to the instanton path appear which make the approximation of Eq. (6.63) questionable. However, in this case it seems to work well in practice. The smallest frequency at the reactant side of the instanton (in the pre-reactive minimum) is only 173 cm^{-1} ($\omega = 7.9 \cdot 10^{-4}$ a.u.) on the PES which is used here. If one compares the determinant method with the rate constant obtained from integrating Eq. (7.13) one can see that at high temperature the rate constants do not overestimate the temperatures close to T_c as the determinant approach does. This is a direct consequence of the fact that the used P_{SC} contains multiple instanton orbits since for the derivation of Eq. (5.28) the summation is not truncated after the first orbit $k = 1$ like in the steepest descent approximation, instead the summation over k is performed explicitly.

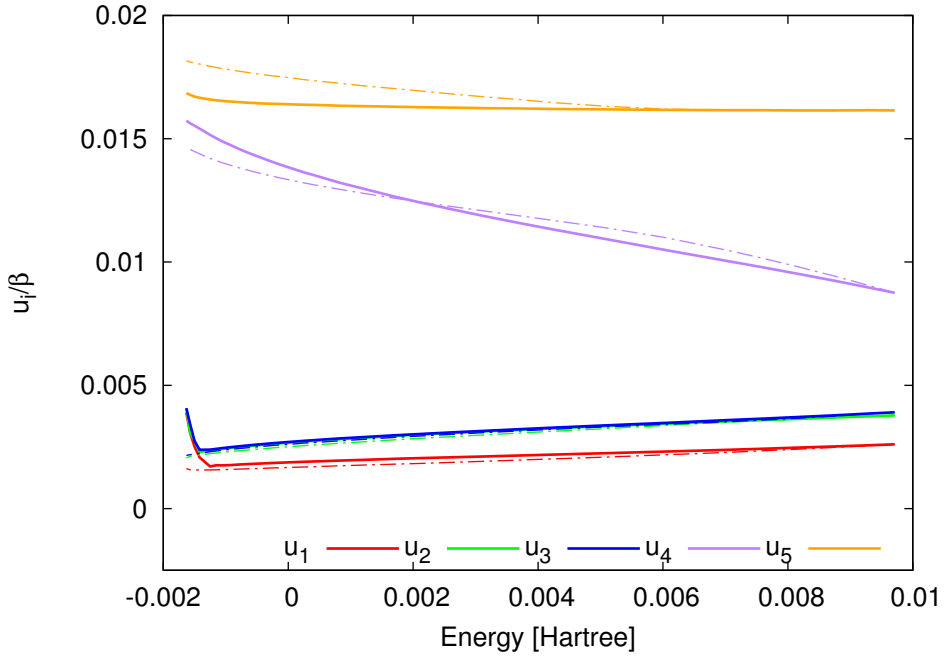

Figure 7.17: Non-zero stability parameters of the reaction $H_2 + OH \rightarrow H_2O$. The continuous lines were obtained by integrating the monodromy matrix in Eq. (6.55), the dotted lines via eigenvalue tracing. All calculation were done with $P = 400$.

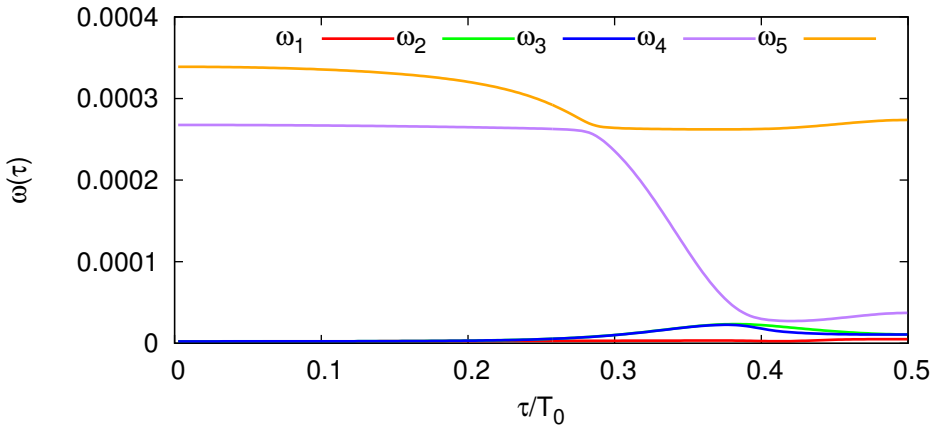

Figure 7.18: Vibrational frequencies of the perpendicular modes in atomic units traced along the instanton path for the reaction H_2 + OH → H_2O + H on Schatz and Elgersma PES [83, 84] at T = 200 K. The time axis is in units of τ/T_0 whereby $T_0 = \beta\hbar$ is the imaginary time period of the instanton solution. The graph stops at $\tau/T_0 = 0.5$ as the path in configuration space from reactant to product is equal to the backwards path.

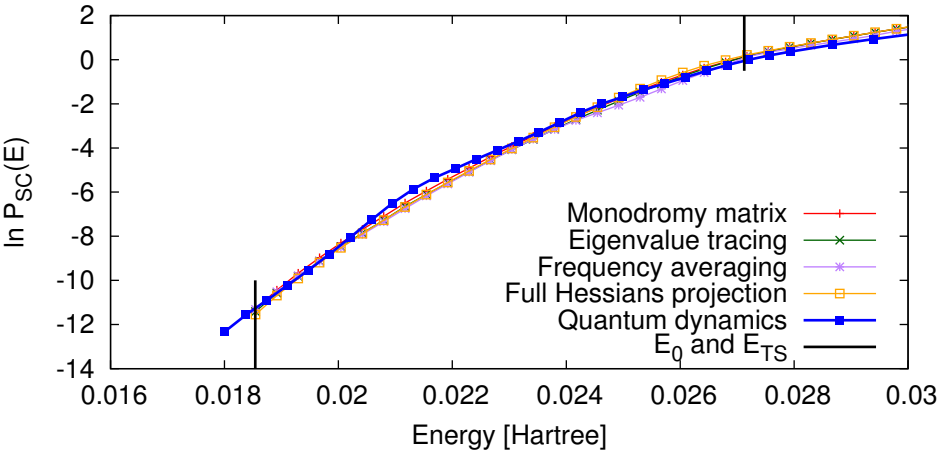

Figure 7.19: $P(E)$ for the reaction H_2+OH on the Schatz–Elgersma PES [83, 84] for the different approximations of $F_\perp$ or $u_i(E)$ discussed in the methods section. Quantum dynamics refers to the reference calculation in Ref. 70, 71. E_0 marks the ground state energy of the harmonically approximated reactant and E_{TS} the energy of the transition state structure.

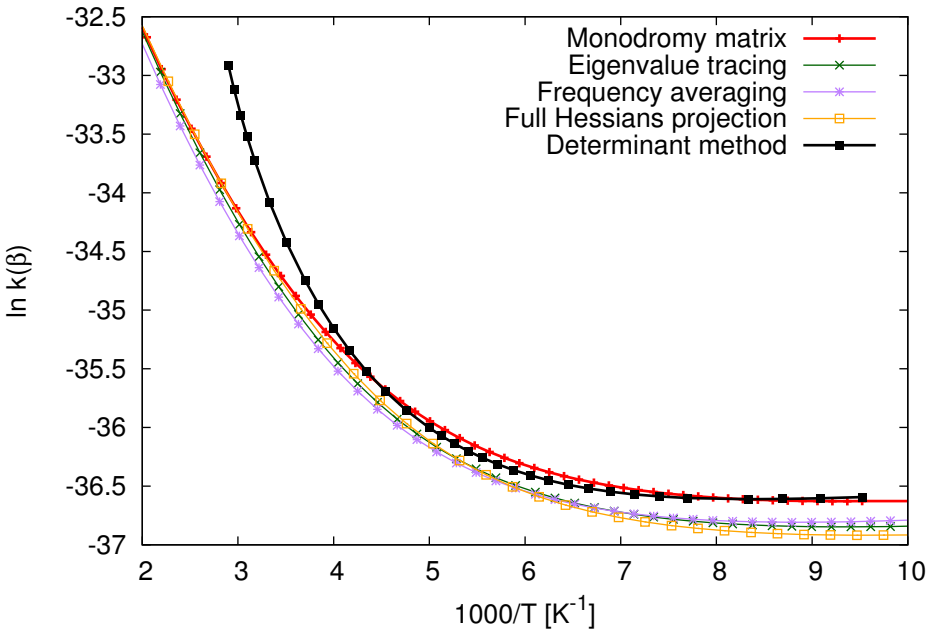

Figure 7.20: Semi-classical thermal rate constants in atomic units obtained via integrating the values of $P_{\mathrm{SC}}(E)$ via Eq. (7.13) in comparison with the determinant method.

8 Conclusion

The calculation of microcanonical and canonical reaction rate constants relies in both cases heavily on adequate methods to compute the fluctuation factor F, which contains second order quantum corrections to the instanton solution. In the microcanonical case one is only interested in the orthogonal contributions $F_\perp$ in order to compute the cumulative reaction probability. In the canonical ensemble one additionally needs to determine the parallel contributions which can be identified with the rate at which the instanton's energy changes with respect to the orbit's imaginary time period as $F_\parallel \propto \sqrt{-dE/d\beta}$.
The conventional determinant method which has been used so far allows for the direct calculation of F in a very reliable fashion, yet it has two profound disadvantages. First it only gives the full fluctuation factor instead of providing the parallel and orthogonal contributions separately, which makes the procedure unsuitable for the calculation of the cumulative reaction probability. Secondly the determinant method as described in chapter 4 requires the diagonalization of a PD-dimensional matrix which is computationally the most demanding approach of all presented methods in this thesis. If, however, $F_\perp$ and $F_\parallel$ are computed separately, a significant speed-up of the rate constant calculation can be achieved.

The methods to calculate the orthogonal fluctuations $F_\perp$ can be divided into two subcategories. Those approaches which require stability parameters from which $F_\perp$ is then obtained or approximate methods which can compute $F_\perp$ directly without the need for individual stability parameters.
If individual stability parameters are needed, two new methods were presented in this thesis. The first is based on the numerical evaluation of the Van Vleck propagator and leads to the linear system of equations $\mathbf{Cq} = \mathbf{d}$ which requires knowledge of all Hessians along the instanton path. Since $\mathbf{C}$ is a banded matrix

the overall scaling behavior is $\mathcal{O}(PD^6)$ which makes this approach particularly useful if the number of images needs to be increased. As was shown in section 7.2, this method is also applicable in the presence of numerical noise in the gradients and Hessians, which is usually the case for any electronic structure calculation in which the energies are not obtained analytically. Therefore solving $\mathbf{Cq} = \mathbf{d}$ provides a rigorously derived and numerically stable way of obtaining stability parameters in multidimensional chemical systems. The second method is to use eigenvalue tracing which allows one to approximate individual stability parameters by tracing the eigenvalues of the Hessians along the path. Whilst being an approximate approach, eigenvalue tracing provides a numerically very stable and reliable method which yields results which are pretty similar to the ones obtained by solving $\mathbf{Cq} = \mathbf{d}$ in the investigated cases.
If only the value for $F_\perp$ is of interest two alternatives have been presented. In the case of frequency averaging $F_\perp$ can be obtained by averaging the orthogonal vibrational frequencies along the path without the need for tracing. While this approach is theoretically only valid for large values of the stability parameters it still gives very consistent rate constants for the investigated systems, even though rather small orthogonal frequencies appeared, e. g. in the reaction $H_2 + OH \rightarrow H_2O + H$. The last approach presented was to use the full Hessians projection approach in which the determinant method is invoked in order to compute the full second derivatives of the Euclidean action first and then project out the parallel vibrational mode as well as the rotational and translational contributions. The method lacks mathematical rigour but appears to give results which are as reliable as frequency averaging or eigenvalue tracing, at least for systems investigated in this thesis.
In summary all mentioned methods provide reliable ways of of obtaining $F_\perp$. However, for cases in which a high number of images can be computed, solving $\mathbf{Cq} = \mathbf{d}$ is the method of choice to calculate $F_\perp$ as it contains no inherent approximations and provides individual stability parameters.

If one is interested in canonical reaction rate constants, additionally the parallel fluctuation factor $F_\parallel$ has to be determined. In order to achieve that the quantity $dE/d\beta$ needs to be computed in an efficient and reliable fashion. Section 6.2 pre-

sented an elegant algorithm based on the energy conservation of the pseudoparticle in the classically forbidden region. The huge advantage in comparison to a finite difference approach is the omission of a second instanton calculation at a temperature adjacent to the first one. The approach presented in section 6.2 only requires solving a linear system of the form $\mathbf{Ax} = \mathbf{b}$ for which the Hessians and gradients along the instanton path are needed. In fact the determinant method does not need gradients, however, they are needed for the instanton optimization, hence no additional effort is required. So if the thermal rate constants for a uni-molecular system are obtained via Eq. (6.22) by using the Cqd-method to obtain $F_\perp$ and the approach from section 6.2 to obtain $dE/d\beta$, one get results which are in excellent agreement with the determinant method, as was shown in sections 7.2 and 7.1 for the analytical and DFT-case, yet the new approach is significantly faster due to different pre-factors for the solvers of linear systems of equations in comparison with the calculation of determinants. While the fundamental bottleneck of any reaction rate constant calculation remains the calculation of energies and Hessians, the new approach might be particularly helpful if one is interested in obtaining thermal rate constants at very low temperature for a system for which a fitted analytic PES is available and therefore a high number of images can be computed. In these cases the rate constant calculation can be speeded up significantly.

Part III

Appendix

9 Auxiliary Calculations

9.1 Analytic Calculation of Q_{RS}

The trajectory of D uncoupled harmonic oscillators in imaginary time is given by

$$\mathbf{X}(\tau) = \frac{x_i'' \sinh(\omega_i \tau) - x_i'' \sinh((\tau - \beta)\omega_i)}{\sinh(\beta\omega_i)} \, \hat{\mathbf{e}}_i \tag{9.1}$$

for $i \in [1, \ldots, D]$. The corresponding Euclidean action is

$$\mathcal{S}_{\mathrm{E}}(\mathbf{x}', \mathbf{x}'', \beta) = \int_0^{\beta\hbar} \left(\frac{1}{2}\dot{\mathbf{X}}^2 + \frac{1}{2}\sum_i^D \omega_i^2 x_i^2(\tau) \right) \, d\tau \tag{9.2}$$

$$= \sum_{i=1}^{D} \frac{(x_i'^2 + x_i''^2)\cosh(\omega_i\beta) - 2x_i'' x_i'}{\sinh(\omega_i\beta)}. \tag{9.3}$$

The evaluation of the second derivatives of $\mathcal{S}_{\mathrm{E}}$ evaluated at the point $\mathbf{x}'' = \mathbf{x}' = \mathbf{x}$ yields

$$\left.\frac{\partial^2 \mathcal{S}_{\mathrm{E}}}{\partial \mathbf{x}_i' \partial \mathbf{x}_j''}\right|_{x'=x''} = -\frac{\omega_i}{\sinh(\omega_i\beta)}\delta_{i,j} \ , \tag{9.4}$$

$$\left.\frac{\partial^2 \mathcal{S}_{\mathrm{E}}}{\partial \mathbf{x}_i' \partial \mathbf{x}_j''}\right|_{x'=x''} = \omega_i \coth(\omega_i\beta)\delta_{i,j} \ , \tag{9.5}$$

$$\left.\frac{\partial^2 \mathcal{S}_{\mathrm{E}}}{\partial \mathbf{x}_i' \partial \mathbf{x}_j''}\right|_{x'=x''} = \omega_i \coth(\omega_i\beta)\delta_{i,j}. \tag{9.6}$$

Using Eq. (6.13) then yields

$$F = \sqrt{\frac{|-\mathbf{b}|}{|\mathbf{a}+2\mathbf{b}+\mathbf{c}|}} = \sqrt{\frac{(-1)^D}{|\mathbf{M}-\mathbf{1}|}} \tag{9.7}$$

$$= \prod_{i=1}^{D} \frac{1}{2\sinh(\frac{\omega_i}{2}\beta)} \tag{9.8}$$

which gives for the $\mathcal{Q}_{\mathrm{RS}}$

$$\mathcal{Q}_{\mathrm{RS}} = \prod_{i=1}^{D} \frac{1}{2\sinh(\frac{\omega_i}{2}\beta)} \mathrm{e}^{-\beta V(\mathbf{x}_{\mathrm{RS}})}, \tag{9.9}$$

i.e. the analytic solution of the partition function of a multidimensional harmonic oscillator.

9.2 Calculation of the Rotational Partition Function

In order to determine the classical expression for the rotational partition function one first invokes the rigid rotor approximation which yields the following quantized energy levels which apply to diatomic molecules such as OH or H_2

$$E_{\mathrm{rot}} = \frac{\mathbf{J}^2}{2I} = \frac{J(J+1)\hbar^2}{2I} \ , \tag{9.10}$$

where I is the moment of inertia and $J \in \mathbb{N}_0$ is the quantum number of the molecule's total rotational angular momentum. Using Eq. (9.10) the canonical rotational partition function gives

$$\mathcal{Q}_{\mathrm{rot}} = \sum_{J=0}^{\infty} g_J \mathrm{e}^{-\beta E_J} = \sum_{J=0}^{\infty} (2J+1)\mathrm{e}^{-\beta \frac{J(J+1)\hbar^2}{2I}} \ , \tag{9.11}$$

where g_J describes the degeneracy of the J^{th}- state. In the case of high temperatures or large I, where $\hbar^2/(2I) \ll \beta$ is fulfilled, the quantum number J in Eq.

(9.11) can approximately be treated as a continuous variable such that

$$\mathcal{Q}_{\text{rot}} \approx \int_0^\infty g_J \mathrm{e}^{-\beta E_J} dJ \tag{9.12}$$

$$= \int_0^\infty (2J+1) \mathrm{e}^{-\beta \frac{J(J+1)\hbar^2}{2I}} dJ \tag{9.13}$$

$$= \frac{\beta 2I}{\hbar^2} \ , \tag{9.14}$$

which results in the classical expression for a rigid rotor. Additionally one introduces a symmetry factor σ

$$\mathcal{Q}_{\text{rot}} = \frac{1}{\sigma} \frac{\beta 2I}{\hbar^2} \ , \tag{9.15}$$

which accounts for the molecule's symmetries and can be calculated from the rotational subgroups of the molecule's point group [87].

9.3 Calculation of the Translational Partition Function

For the classical translational partition function which is used in the gas phase, one starts with the energy levels of a particle in a three-dimensional cubic box of length L. The energy levels here are given as

$$E_{\text{trans}} = \frac{h}{8ML^2} \left(n_x^2 + n_y^2 + n_z^2 \right) \ , \tag{9.16}$$

with M being the mass of the molecule and n_x, n_y, n_z as quantum numbers for each of the possible directions. The canonical partition function is then given by

$$\mathcal{Q}_{\text{trans}} = \sum_{n_x=0}^{\infty} \sum_{n_y=0}^{\infty} \sum_{n_z=0}^{\infty} \mathrm{e}^{-\frac{\beta h}{8ML^2}\left(n_x^2+n_y^2+n_z^2\right)} \ . \tag{9.17}$$

Assuming a narrow spacing between the energy levels and moving from a summation to an integration results in

$$\mathcal{Q}_{\text{trans}} \approx \int_0^\infty \int_0^\infty \int_0^\infty \mathrm{e}^{-\frac{\beta h}{8ML^2}\left(n_x^2+n_y^2+n_z^2\right)} dn_x dn_y dn_z \tag{9.18}$$

$$= V\left(\frac{M}{2\pi\hbar^2\beta}\right)^{\frac{3}{2}}, \tag{9.19}$$

with $V = L^3$ being the volume of the box.

10 Bibliography

[1] G. Binnig and H. Rohrer. Scanning tunneling microscopy—from birth to adolescence. *Rev. Mod. Phys.*, 59:615, 1987.

[2] L. Esaki. New phenomenon in narrow germanium $p-n$ junctions. *Phys. Rev.*, 109:603, 1958.

[3] X. Shan and D. C. Clary. Quantum dynamics of the abstraction reaction of H with cyclopropane. *J. Phys. Chem. A*, 118:10134, 2014.

[4] Q. Cao, S. Berski, Z. Latajka, M. Räsänen, and L. Khriachtchev. Reaction of atomic hydrogen with formic acid. *Phys. Chem. Chem. Phys.*, 16:5993, 2014.

[5] I. Oueslati, B. Kerkeni, W. L. Tchang-Brillet, and N. Feautrier. Quantum scattering study of the abstraction reaction of H atoms from tetramethylsilane. *Chem. Phys. Lett.*, 624:29, 2015.

[6] J. Meisner and J. Kästner. Atom-tunneling in chemistry. *Angew. Chem. Int. Ed.*, 55:5400, 2016.

[7] H. Eyring and M. Polanyi. Über einfache Gasreaktionen. *Z. Phys. Chem.*, 12:279, 1931.

[8] E. P. Wigner. Über das Überschreiten von Potentialschwellen bei chemischen Reaktionen. *Z. Phys. Chem.*, 15:203, 1932.

[9] H. A. Kramers. Brownian motion in a field of force and the diffusion model of chemical reactions. *Physica*, 7:284, 1940.

[10] P. Hänggi, P. Talkner, and M. Borkovec. Reaction-rate theory: fifty years after Kramers. *Rev. Mod. Phys.*, 62:251, 1990.

[11] E. Pollak and P. Talkner. Reaction rate theory: What it was, where is it today, and where is it going? *Chaos*, 15:026116, 2005.

[12] K. J. Laidler and M. C. King. Development of transition-state theory. *J. Phys. Chem.*, 87:2657, 1983.

[13] S. Arrhenius. Über die Reaktionsgeschwindigkeit bei der Inversion von Rohrzucker durch Säuren. *Z. Phys. Chem.*, 4:226, 1889.

[14] J. S. Langer. Theory of the condensation point. *Ann. Phys. (N.Y.)*, 41:108, 1967.

[15] S. Coleman. Fate of the false vacuum: semiclassical theory. *Phys. Rev. D*, 15:2929, 1977.

[16] C. G. Callan Jr. and S. Coleman. Fate of the false vacuum II. First quantum corrections. *Phys. Rev. D*, 16:1762, 1977.

[17] R. P. Feynman and A. R. Hibbs. *Quantum Mechanics and Path Integrals*. McGraw-Hill, 1965.

[18] J. B. Rommel, T. P. M. Goumans, and J. Kästner. Locating instantons in many degrees of freedom. *J. Chem. Theory Comput.*, 7:690, 2011.

[19] W. H. Miller. Semiclassical limit of quantum mechanical transition state theory for nonseparable systems. *J. Chem. Phys.*, 62:1899, 1975.

[20] J. O. Richardson. Derivation of instanton rate theory from first principles. *J. Chem. Phys.*, 144:114106, 2016.

[21] R. P. Feynman. Space-time approach to non-relativistic quantum mechanics. *Rev. Mod. Phys.*, 20:367, 1948.

[22] H. Kleinert. *Path Integrals in Quantum Mechanics, Statistics, Polymer Physics, and Financial Markets*. World Scientific, 5 edition, 2009.

[23] M. Srednicki. *Quantum Field Theory*. Cambridge University Press, 2007.

[24] U. Fano. Description of states in quantum mechanics by density matrix and operator techniques. *Rev. Mod. Phys.*, 29:74, 1957.

[25] G. C. Wick. Properties of Bethe–Salpeter wave functions. *Phys. Rev.*, 96:1124, 1954.

[26] B. C. Hall. *Quantum Theory for Mathematicians*. Springer, 2013.

[27] M. Brack and R. K. Bhaduri. *Semiclassical Physics*. Westview Press, 2003.

[28] M. Feldmaier, M. A. Junginger, J. Main, G. Wunner, and R. Hernandez. Obtaining time-dependent multi-dimensional dividing surfaces using lagrangian descriptors. *Chem. Phys. Lett.*, 687:194, 2017.

[29] K. J. Laidler. Rene marcelin (1885-1914), a short-lived genius of chemical kinetics. *J. Chem. Educ.*, 62:1012, 1985.

[30] M. Born and J. R. Oppenheimer. Zur Quantentheorie der Molekeln. *Ann. Phys.*, 389:457, 1927.

[31] W. H. Miler. Direct and correct calculation of canonical and microcanonical rate constants for chemical reactions. *J. Chem. Phys. A*, 102:793, 1998.

[32] H. Waalkens, R. Schubert, and S. Wiggins. Wigner's dynamical transition state theory in phase space: classical and quantum. *Nonlinearity*, 21:R1, 2008.

[33] M. A. Junginger. *Transition state theory for wave packet dynamics and its application to thermal decay of metastable nonlinear Schrödinger systems*. PhD thesis, University of Stuttgart, 2014.

[34] J. A. Wheeler. On the mathematical description of light nuclei by the method of resonating group structure. *Phys. Rev.*, 52:1107, 1937.

[35] T. Seideman and W. H. Miller. Calculation of the cumulative reaction probability via a discrete variable representation with absorbing boundary conditions. *J. Chem. Phys.*, 96:4412, 1992.

[36] G. A. Voth, D. Chandler, and W. H. Miller. Rigorous formulation of quantum transition state theory and its dynamical corrections. *J. Chem. Phys.*, 91:7749, 1989.

[37] M. A. Shifman. *Instantons in Gauge Theories*. World Scientific, 1994.

[38] W. H. Miller. Tunneling and state specificity in unimolecular reactions. *Chem. Rev.*, 87:19, 1987.

[39] I. Affleck. Quantum-statistical metastability. *Phys. Rev. Lett.*, 46:388, 1981.

[40] V. A. Benderskii, D. E. Makarov, and C. A. Wight. One-dimensional models. *Adv. Chem. Phys.*, 88:55, 1994.

[41] L. D. Faddeev and V. N. Popov. Feynman diagrams for the Yang-Mills field. *Phys. Lett. B*, 25:29, 1967.

[42] J. Kästner, J. M. Carr, T. W. Keal, W. Thiel, A. Wander, and P. Sherwood. DL-FIND: an open-source geometry optimizer for atomistic simulations. *J. Phys. Chem. A*, 113:11856, 2009.

[43] J. O. Richardson. Microcanonical and thermal instanton rate theory for chemical reactions at all temperatures. *Faraday Disc.*, 195:49, 2016.

[44] M. C. Gutzwiller. Phase integral approximation in momentum space and the bound states of an atom. *J. Math. Phys.*, 8:1979, 1967.

[45] M. C. Gutzwiller. Periodic orbits and classical quantization conditions. *J. Math. Phys.*, 12:343, 1971.

[46] W. H. Miller, S. D. Schwartz, and J. W. Tromp. Quantum mechanical rate constants for bimolecular reactions. *J. Chem. Phys.*, 79:4889, 1983.

[47] S. C. Althorpe. On the equivalence of two commonly used forms of semiclassical instanton theory. *J. Chem. Phys.*, 134:114104, 2011.

[48] K. Takayanagi. On the inelastic collision between molecules, II: Rotational transition of H_2-molecule in the collision with another H_2-molecule. *Prog. Theor. Phys.*, 8:497, 1952.

[49] J. M. Bowman. Reduced dimensionality theory of quantum reactive scattering. *J. Phys. Chem.*, 95:4960, 1991.

[50] S. Chapman, B. C. Garrett, and W. H. Miller. Semiclassical transition state theory for nonseparable systems: Application to the collinear H+H_2 reaction. *J. Chem. Phys.*, 63:2710, 1975.

[51] S. R. McConnell, A. Löhle, and J. Kästner. Rate constants from instanton theory via a microcanonical approach. *J. Chem. Phys.*, 146:074105, 2017.

[52] A. Löhle and J. Kästner. Calculation of reaction rate constants in the microcanonical and canonical ensemble. *J. Chem. Theory Comput.*, (in press), 2018.

[53] J. H. Van Vleck. The correspondence principle in the statistical interpretation of quantum mechanics. *Proc. Natl. Acad. Sci. U.S.A.*, 14:178, 1928.

[54] J. O. Richardson, R. Bauer, and M. Thoss. Semiclassical Green's functions and an instanton formulation of electron-transfer rates in the nonadiabatic limit. *J. Chem. Phys.*, 143:134115, 2015.

[55] J. O. Richardson. Ring-polymer instanton theory of electron transfer in the nonadiabatic limit. *J. Chem. Phys.*, 143:134116, 2015.

[56] J. B. Rommel and J. Kästner. Adaptive integration grids in instanton theory improve the numerical accuracy at low temperature. *J. Chem. Phys.*, 134:184107, 2011.

[57] K. Müller and L. D. Brown. Location of saddle points and minimum energy paths by a constrained simplex optimization procedure. *Theor. Chim. Acta*, 53:75, 1979.

[58] S. Metz, J. Kästner, A. A. Sokol, T. W. Keal, and P. Sherwood. Chemshell—a modular software package for QM/MM simulations. *WIREs Comput. Mol. Sci.*, 4:101, 2014.

[59] TURBOMOLE V, a development of University of Karlsruhe and Forschungszentrum Karlsruhe GmbH, 1989-2007, TURBOMOLE GmbH, since 2007; available from `http://www.turbomole.com`.

[60] P. R. Schreiner, H. P. Reisenauer, D. Ley, D. Gerbig, C.-H. Wu, and W. D. Allen. Methylhydroxycarbene: tunneling control of a chemical reaction. *Science*, 332:1300, 2011.

[61] J. Kästner. The path length determines the tunneling decay of substituted carbenes. *Chem. Eur. J.*, 19:8207, 2013.

[62] P. A. M. Dirac. Quantum mechanics of many-electron systems. *Proc. Royal Soc. A*, 123:714, 1929.

[63] J. C. Slater. A simplification of the Hartree–Fock method. *Phys. Rev.*, 81:385, 1951.

[64] S. H. Vosko, L. Wilk, and M. Nusair. Accurate spin-dependent electron liquid correlation energies for local spin density calculations: a critical analysis. *Can. J. Phys.*, 58:1200, 1980.

[65] A. D. Becke. Density-functional exchange-energy approximation with correct asymptotic behavior. *Phys. Rev. A*, 38:3098, 1988.

[66] C. Lee, W. Yang, and R. G. Parr. Development of the Colle–Salvetti correlation-energy formula into a functional of the electron density. *Phys. Rev. B*, 37:785–789, 1988.

[67] A. D. Becke. Density-functional thermochemistry. III. The role of exact exchange. *J. Chem. Phys.*, 98:5648, 1993.

[68] F. Weigend and R. Ahlrichs. Balanced basis sets of split valence, triple zeta valence and quadruple zeta valence quality for H to Rn: Design and assessment of accuracy. *Phys. Chem. Chem. Phys.*, 7:3297, 2005.

[69] K. Eichkorn, F. Weigend, O. Treutler, and R. Ahlrichs. Auxiliary basis sets for main row atoms and transition metals and their use to approximate Coulomb potentials. *Theor. Chem. Acc.*, 97:119, 1997.

[70] U. Manthe, T. Seideman, and W. H. Miller. Full-dimensional quantum mechanical calculation of the rate constant for the $H_2 + OH \rightarrow H_2O + H$ reaction. *J. Chem. Phys.*, 99:10078, 1993.

[71] U. Manthe, T. Seideman, and W. H. Miller. Quantum mechanical calculations of the rate constant for the $H_2 + OH \rightarrow H_2O + H$ reaction: fulldimensional results and comparison to reduced dimensionality models. *J. Chem. Phys.*, 101:4759, 1994.

[72] D. H. Zhang and J. Z. H. Zhang. Accurate quantum calculations for $H_2 + OH \rightarrow H_2O + H$: reaction probabilities, cross sections, and rate constants. *J. Chem. Phys.*, 100:2697, 1994.

[73] U. Manthe and F. Matzkies. Rotational effects in the $H_2 + OH \rightarrow H_2O + H$ reaction rate: full-dimensional close-coupling results. *J. Chem. Phys.*, 113:5725, 2000.

[74] M. Yang, D. H. Zhang, M. A. Collins, and S. Y. Lee. Quantum dynamics on new potential energy surfaces for the $H_2 + OH \rightarrow H_2O + H$ reaction. *J. Chem. Phys.*, 114:4759, 2001.

[75] J. M. Chan, J. A. Bollinger, C. L. Grewell, and D. M. Dooley. Reductively activated nitrous oxide reductase reacts directly with substrate. *J. Am. Chem. Soc.*, 126:3030, 2004.

[76] S. Bhattacharya, A. N. Panda, and H. D. Meyer. Multiconfiguration time-dependent Hartree approach to study the $H_2 + OH$ reaction. *J. Chem. Phys.*, 132:214304, 2010.

[77] B. Fu, E. Kamarchik, and J. M. Bowman. Quasiclassical trajectory study of the postquenching dynamics of OH $A^2\Sigma^+$ by H_2/D_2 on a global potential energy surface. *J. Chem. Phys.*, 133:164306, 2010.

[78] S. Bhattacharya, A. N. Panda, and H. D. Meyer. Cross sections and rate constants for $H_2 + OH$ reaction reaction on three different potential energy surfaces for ro-vibrationally excited reagents. *J. Chem. Phys.*, 135:194302, 2011.

[79] J. Espinosa-Garcia, L. Bonnet, and J. C. Corchado. Classical description in a quantum spirit of the prototype four-atom reaction OH + D_2. *Phys. Chem. Chem. Phys.*, 12:3873, 2010.

[80] T. L. Nguyen, J. F. Stanton, and J. R. Barker. Ab initio reaction rate constants computed using semiclassical transition-state theory: OH + H_2 → H_2O + H and isotopologues. *J. Phys. Chem. A*, 115:5118, 2011.

[81] J. Chen, X. Xu, X. Xu, and D. H. Zhang. A global potential energy surface for the H_2 + OH ↔ H_2O + H reaction using neural networks. *J. Chem. Phys.*, 138:154301, 2013.

[82] B. Fu and D. H. Zhang. A full-dimensional quantum dynamics study of the mode specificity in the H + HOD abstraction reaction. *J. Chem. Phys.*, 142:064314, 2015.

[83] S. P. Walch and T. H. Dunning Jr. A theoretical study of the potential energy surface for H_2 + OH. *J. Chem. Phys.*, 72:1303, 1980.

[84] G. C. Schatz and H. Elgersma. A quasi-classical trajectory study of product vibrational distributions in the H_2 + OH → H_2O + H reaction. *Chem. Phys. Lett.*, 73:21, 1980.

[85] J. Meisner and J. Kästner. Reaction rates and kinetic isotope effects of H_2 + OH → H_2O + H. *J. Chem. Phys.*, 144:174303, 2016.

[86] S. Andersson, G. Nyman, A. Arnaldsson, U. Manthe, and H. Jónsson. Comparison of quantum dynamics and quantum transition state theory estimates of the H + CH_4 reaction rate. *J. Phys. Chem. A*, 113:4468, 2009.

[87] P. R. Bunker. *Molecular Symmetry and Spectroscopy.* PB - NRC Research Press, 1979.

11 List of Figures

Erklärung über die Eigenständigkeit der Dissertation

Ich versichere, dass ich die vorliegende Arbeit mit dem Titel *Calculation of Reaction Rate Constants via Instanton Theory in the Canonical and Microcanonical Ensemble* selbständig verfasst und keine anderen als die angegebenen Quellen und Hilfsmittel benutzt habe; aus fremden Quellen entnommene Passagen und Gedanken sind als solche kenntlich gemacht.

Declaration of Authorship

I hereby affirm that this dissertation titled *Calculation of Reaction Rate Constants via Instanton Theory in the Canonical and Microcanonical Ensemble* is entirely my own work unless otherwise indicated. Passages and ideas from other sources have been clearly referenced.

Name/Name:	Andreas Löhle
Unterschrift/Signature:	_____
Datum/Date:	November 7, 2018